Recent Progress on the Development of Metal-Air Batteries

Lin Li, Zhi-wen Chang, and Xin-Bo Zhang*

The large-scale electrical energy storage using rechargeable batteries buoys any future success in the global efforts to shift energy usage away from fossil fuels to renewable sources. Compared with other battery technologies, such as Li-S and LIBs, the metal-air battery technology holds exceptionally high energy densities and is viewed to be a promising candidate as the energy supplier of the next generation. With the aim to provide easy access to the recent developments of metal-air batteries and advance their development, this review systematically and comprehensively summarizes, compares and discusses the development of all important kinds of aqueous and/or non-aqueous metal-air batteries (all in one), based on metal anodes of Li, Na, Zn, Al, from all important aspects, including oxygen electrochemistry, electrocatalyst, transfer/diffusion and interface, electrode and electrolyte materials, and device configuration. As a benefit, our understanding on metal-air batteries can be deepened and guidance for the development of next generation metal-air batteries can be provided.

1. Introduction

The evolution and development of mankind has been closely related to our utilization of energy. A sustainable energy supply is of vital importance for political stability and the continuous development of economics as our modern society is becoming increasingly energy dependent. Currently, the LIBs are widely used in our society as a powerful energy source, however, its limited energy density ($\approx$400 Wh kg^{-1}, theoretically) has restricted its application as the energy source of next generation.[1–6] As a solution, new batteries with much higher theoretical energy densities than that of LIBs are developed, such as fuel cells and metal-air batteries.[7] Among them, the metal-air battery is viewed as a promising candidate, which can satisfy the ever-growing demand for high energy density, low-cost, environmental friendly power sources for mobile electronics and electric vehicles. In contrast to the closed system of conventional batteries, especially the LIBs, the metal-air batteries feature an open cell structure, in which the cathode active material, oxygen, can be breathed from ambient atmosphere. Accordingly, the weight of the battery can be reduced, thus helping to improve the energy density of metal-air battery. In general, the metal-air battery is composed of porous cathode, electrolyte, metal anode. Metals such as Li, Na, Zn, etc. are appropriate for use as anode materials in metal-air batteries. As for the abundance of these metal, the lithium is widely distributed in the Earth's crust but is not viewed as an abundant element. In light of the report from Carmichel,[8] the relative abundance of lithium in the Earth's crust is limited to be only 20 ppm. Moreover, the lithium resources are unevenly distributed (mainly in South America). In contrast to lithium, sodium resources are unlimited everywhere, and sodium is one of the most abundant elements in the Earth's crust. The infinite sodium resources are also found in the ocean. Additionally, sodium is the second-lightest and -smallest alkali metal next to lithium. When coming to the metallic zinc, it possesses a unique set of attributes including high abundance and low toxicity, and is the negative electrode material for zinc-air battery.[9] Metal-air batteries especially Li-air batteries have a high theoretical energy density, which is also much higher compared with other rechargeable systems such as Li-S and LIBs. As illustrated in **Figure 1**,[20] the theoretical specific energy densities of metal-air batteries are very high. Such high energy output of metal-air batteries, if fully exploited, can serve as next-generation high performance and environmental benign power sources for large-scale energy storage systems, mobile energy fields and aerospace industry.

Metal-air batteries can be divided into three categories based on different metal anode species and rechargeability, which are primary, secondary and mechanically rechargeable batteries. They can also be classified into four types according to different forms of electrolytes and cell configurations including aqueous, nonaqueous aprotic, hybrid and solid-state metal-air batteries. Depending on the use of specific metal, electrolyte and catalytic materials, the involved electrochemistry and reaction products vary largely from each type of metal-air battery. A detailed discussion will be given in the following sections. Generally, metal-air batteries using aqueous electrolytes with neutral or alkaline solvents, for instance, are disposable or mechanically

L. Li, Dr. Z.-w. Chang, Prof. X.-B. Zhang
State Key Laboratory of Rare Earth Resource Utilization
Changchun Institute of Applied Chemistry
Chinese Academy of Sciences
Changchun 130022, P. R. China
E-mail: xbzhang@ciac.ac.cn
L. Li, Dr. Z.-w. Chang, Prof. X.-B. Zhang
Key Laboratory of Automobile Materials
Ministry of Education and College of Materials Science and Engineering
Jilin University
Changchun 130012, China
Dr. Z.-w. Chang
University of Chinese Academy of Sciences
Beijing 100049, P. R. China

The ORCID identification number(s) for the author(s) of this article can be found under https://doi.org/10.1002/adsu.201700036.

rechargeable by replacing the metal anodes or refueling the electrolytes. For example, primary Zn-air batteries are commercialized as hearing-aid batteries; Mg-air and Al-air batteries are also used as power sources for railway and navigation beacons. They can be indirectly "recharged" by mechanically replacing the discharged anodes and slutty electrolytes with fresh metal anodes and electrolytes. Currently, a fully electrically rechargeable metal-air battery remains as a challenge to overcome, among which nonaqueous aprotic Li-air battery have attracted intensive research interests.

It should be noted that metal-air batteries use oxygen as cathode materials, current membrane technology is still inferior to isolate some unfavorable components in air such as CO_2 and H_2O without effectively allow the penetration of oxygen. Considering the high reactivity of metal anodes, these components would interfere the desired electrochemical behavior and reduce the overall performance. At present, the experimental data of most literature reports were obtained under laboratory pure oxygen environment. However, the term "metal-air battery" is widely accepted by researchers as a true metal-air battery is the ultimate goal. In order to be more accurate, the expression of a specific "metal-air" or "metal-oxygen" battery is used to make a distinction of the different testing environments.

In the 1970s, lithium-oxygen (Li-O_2) batteries were firstly proposed as possible power sources for EVs.[10] In 1996, Abraham et al. firstly reported a rechargeable solid-state Li–O_2 battery comprised a thin Li metal foil anode, a Li^+ conductive organic polymer electrolyte membrane and a thin Carbon composite electrode and successfully demonstrated three cycles of charge and discharge.[11] Afterwards, Read studied the effects of electrolyte and air cathode formulation on the discharge capacity, rate capability, and rechargeability of Li-O_2 battery.[12] In 2006, Bruce's group demonstrated the promising electrochemical performance of Li-air batteries.[13] Hence, they began to rapture worldwide research, especially nonaqueous aprotic Li-air battery (**Figure 2**), as evidenced by the explosive growth in published papers and citations on this topic in recent years. The specific energy density of a Li-air battery is 3500 Wh kg^{-1} (based on carbon electrode) and can reach up to 400-800 Wh kg^{-1} if the mass of all battery components are included, which is 2-10 times the energy of the state-of-the-art LIBs. A fully developed Li-air battery is thus expected to exceed current battery technologies with multiplied energy density at much lower cost, with reduced environmental impact. To date, extensive efforts have been made on the exploration of the reaction mechanisms and development of improved battery materials. Although huge progress has been made in recent years, current Li-air battery techniques still fall far behind the increasing demand of environmentally-friendly and petrol-independent power sources. A better fundamental understanding of the electrochemistry, development of more stable and efficient electrolyte and electrode materials, as well as more rational cell design are essential for the future evolvement of Li-air battery.

In comparison, Zn, Al, Mg and Na are known for their abundant reserves in earth and low cost with Al being the most abundant metal element, while Li has a very limited mineable amount of ≈11 million tons. Future shortage of resource is foreseeable if Li were widely used for large-scale energy storage and conversion facilities. It is thus more cost-effective to adopt other

Lin Li was born in 1990. He received his Master degree in Materials Science in 2015 at Jilin University. In 2013–2015, he studied as an exchange student focusing on the design and synthesis of electrode materials for Li-O_2 battery at Changchun Institute of Applied Chemistry, Chinese Academy of Sciences, under the supervision of Prof. Xin-Bo Zhang. He is currently pursuing a PhD in Inorganic Chemistry.
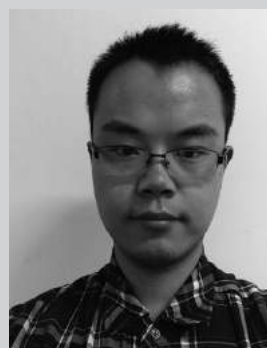
Zhi-wen Chang was born in 1987 and received his BS degree in materials science and engineering from Dalian Maritime University in 2012. He is currently pursuing a PhD under the supervision of Prof. Xin-bo Zhang at Changchun Institute of Applied Chemistry, Chinese Academy of Sciences. His current interests include the synthesis and characterization of nanostructures in lithium–oxygen batteries.
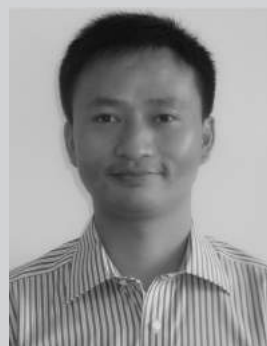
Xinbo Zhang is a Full Professor at Changchun Institute of Applied Chemistry (CIAC), Chinese Academy of Sciences (CAS). He obtained his PhD in inorganic chemistry from CIAC. From 2005–2009, he worked as a Japan Society for the Promotion of Science (JSPS) postdoctoral fellow (2005–2007) and a New Energy and Industrial Technology Development Organization (NEDO) research associate (2007–2009) at National Institute of Advanced Industrial Science and Technology (AIST), Japan. His interests mainly focus on functional inorganic materials for batteries, fuel cells, electrochemical water splitting and carbon dioxide reduction.

metal-air battery systems such as Na-air and Al-air batteries since the gravimetric energy densities are less required compared with portable and mobile electronic devices. The Na-air battery, first introduced in the year of 2011, was considered as a promising alternative to the Li-air battery due to the similar chemical characteristics shared between Na and Li. However, a series of problems concerning the fundamental understanding
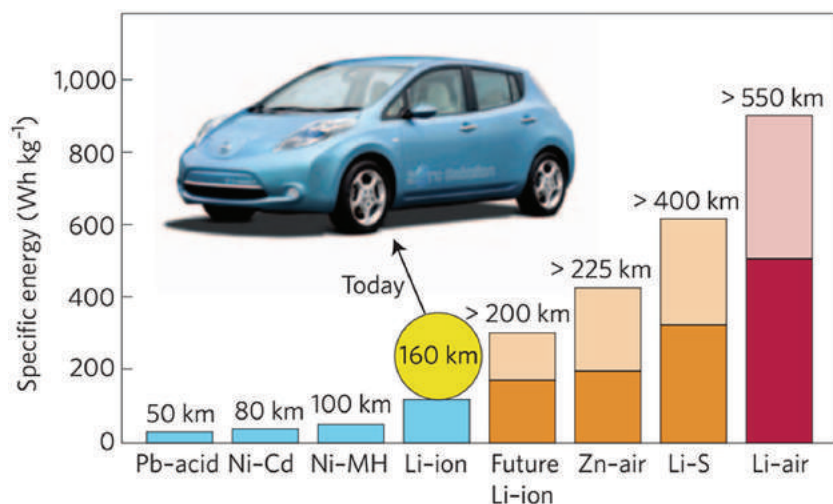
ADVANCED
SCIENCE NEWS
www.advancedsciencenews.com

ADVANCED
SUSTAINABLE
SYSTEMS
www.advsustainsys.com

Figure 1. Practical specific energies for some rechargeable batteries along with estimated driving distances. Reproduced with permission.[20] Copyright 2012, Nature Publishing Group.

of electrochemistry, development of a stable electrolyte and efficient electrode materials remain unsolved. On the other hand, Zn-air, Al-air and Mg-air batteries are confronting the challenge of poor rechargeability and anode corrosion.

Thanks to the rapid development of nanomaterials and modern production technologies in the past decade, metal-air batteries have regained tremendous research activity as they hold a key to the success of the global energy usage shift from fossil fuels to renewable sources. Up to now, remarkable contributions have been made by leading scientists in this important and promising research area. The electrochemistry in metal-air

Figure 2. Schematic presentation of a nonaqueous aprotic Li-air battery composed of a Li metal anode, an aprotic electrolyte, a separator and a porous air cathode.

batteries are widely studied, various novel designs of air cathodes with appropriate materials selection and morphology regulation are presented, the investigation of more favorable electrolytes and electrocatalysts toward more stable and high-performance metal-air batteries are also extensively conducted.[14–55] However, this promising battery technology is still confronted with several scientific and technological challenges before further commercialization. The biggest issue is associated with sluggish kinetics of the air cathode and the low utilization and safety concerns of the metal anode. The electrochemical performance of a metal-air battery depends largely on the physical and electrochemical characteristics of cathode materials. An ideal air cathode for metal-air batteries should exhibit such properties as good conductivity, rational structure design to facilitate the deposition of discharge products (aprotic and solid-state metal-air batteries) and continuous transportation of oxygen and electrolyte, excellent ORR and OER catalytic activity and high structural stability to maintain constant charge and discharge cycles. A well-prepared cathode is thus expected to be the most expensive and complicated part of a metal-air battery. As a matter of fact, the air cathode involves with a series of complicated processes, and by far, there is still a lack of the fundamental understanding of the electrochemistry within. Until now, the most effective electrocatalysts for ORR are noble metals and their alloys. When charging, the poor conductivity of the insoluble discharge products, such as Li_2O_2 in a non-aqueous aprotic Li-air battery, and sluggish kinetics contributes to high polarizations which unfortunately, accelerate the decomposition of electrolytes. A fully rechargeable metal-air battery requires an effective OER catalyst to lower the overpotential and increase the energy efficiency. In this review, a lot of effort is dedicated to the discussion of the electrochemistry, cathode structure design and development of catalysts. The high reactivity of metal anodes can lead to passivation and corrosion in electrolytes, the metal hydroxides, oxides and other byproducts on the anode surface will block the effective mass transportation which will result in the degradation of overall electrochemical performance. In addition, the safety concerns arise from the dramatic reactivity of Li in air especially in humid environment and short circuit caused by dendrite formation during cycling largely hinder the commercialization of Li-air battery. Moreover, effective air-breathing membranes must be developed to block CO_2, H_2O and other gaseous components that might reduce the overall battery performance while allow the penetration of O_2.[56]

Summarizing the development and deepening our understanding of metal-air batteries would provide some guidance for the development of next generation metal-air batteries. However, the very few available reviews are only limited to specific aspects (e.g., electrocatalyst or electrolyte) of one or two kind of metal-air batteries. In addition, most previous reviews are devoted to the discussion of battery materials, rarely concerning theories and basic scientific principles, such as transfer,
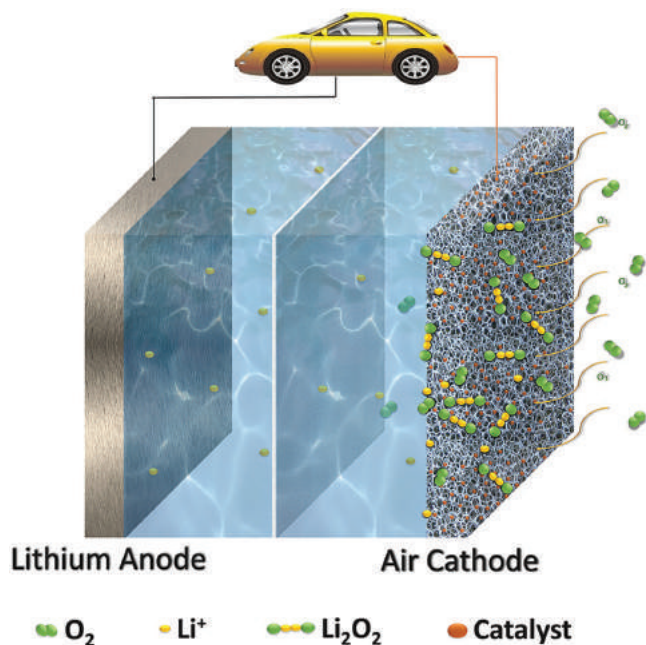
ADVANCED
SCIENCE NEWS
www.advancedsciencenews.com

ADVANCED
SUSTAINABLE
SYSTEMS
www.advsustainsys.com

diffusion, and interface. Since the fundamental features of various metal-air batteries share similarities, learning from one system can promote the development of other systems. Therefore, in this review, we will systematically and comprehensively summarize, compare, and discuss the development of all important types of aqueous and/or nonaqueous metal-air batteries (all in one), based on metal anodes of Li, Na, Zn, Al, Mg, etc. from all important aspects, including oxygen electrochemistry, electrocatalyst, transfer/diffusion and interface, electrode and electrolyte materials, and device configuration. We are certain that this thorough and in depth review could offer better understanding of the scientific and technical issues of metal-air batteries and stimulate some new research in this area, and thus will be of immediate interest to a broad readership of researchers, especially in fields of chemistry, material, energy, catalysis, nanoscience and nanotechnology.

2. Configuration and Oxygen Electrochemistry

Understanding the configuration and oxygen electrochemical reactions within the battery systems is the first step toward building better metal-air batteries. As shown in **Figure 3**, metal-air batteries can be divided into four categories based on the different types of electrolytes and cell configuration, which are aqueous, non-aqueous aprotic, hybrid and solid-state metal-air batteries. The four types of battery systems are all assembled with metal anodes to provide metal sources and porous gas diffusion electrodes as cathodes to obtain oxygen from air. Porous carbon materials were extensively investigated as air cathodes due to their low cost, lightweight, excellent conductivity, good mechanical and chemical stability. The overall reactions for oxygen at the air cathode are ORR and OER at discharge and charge, respectively, while the discharge reaction pathways and the corresponding reverse reactions vary with the different

metal anodes, electrolytes and catalytic materials. For a typical battery electrochemistry, when discharged, the metal anode is oxidized and releases electrons to the external circuitry to produce metal ions, while oxygen diffused in the cathode accepts electrons and reduces to oxygen-containing species. Then the metal cations and oxygen-containing species diffuse across the electrolyte to form discharge products. When charged, the discharge products are decomposed under applied voltage, then metal cations are reduced at the surface of the anode and oxygen evolves at the cathode. Normally, the oxygen electrochemistry kinetics during discharge and charge is rather slow; it is thus essential to introduce oxygen electrocatalysts to promote ORR and OER processes. In this section, the configuration of, and basic oxygen electrochemistry of metal-air batteries is discussed on the basis of different electrolytes.

2.1. Aqueous Systems

Aqueous cells are commonly seen in Zn-air battery system which are composed of zinc metal anodes, porous carbon cathodes and alkaline electrolytes. The greatest advantage of aqueous metal-air systems is that the capacity is not limited by the capability of the cathode because the discharge products are soluble hydroxides which are not stored in the pore structures of the cathode. This can guarantee the continuous gas diffusion through the porous air cathode. Consequently, the mass transportation properties of the electrolyte is the major determinant that determines the performance of aqueous metal-air cells. However, without an effective air selective membrane, a drawback of using alkaline electrolytes is the potential cell failure due to the clogging of electrode pores caused by the accumulation of poor solubility carbonates in alkaline solutions. Acidic electrolytes, on the other hand, do not have such concern, yet the violent reactions and sever corrosion of metal anodes in
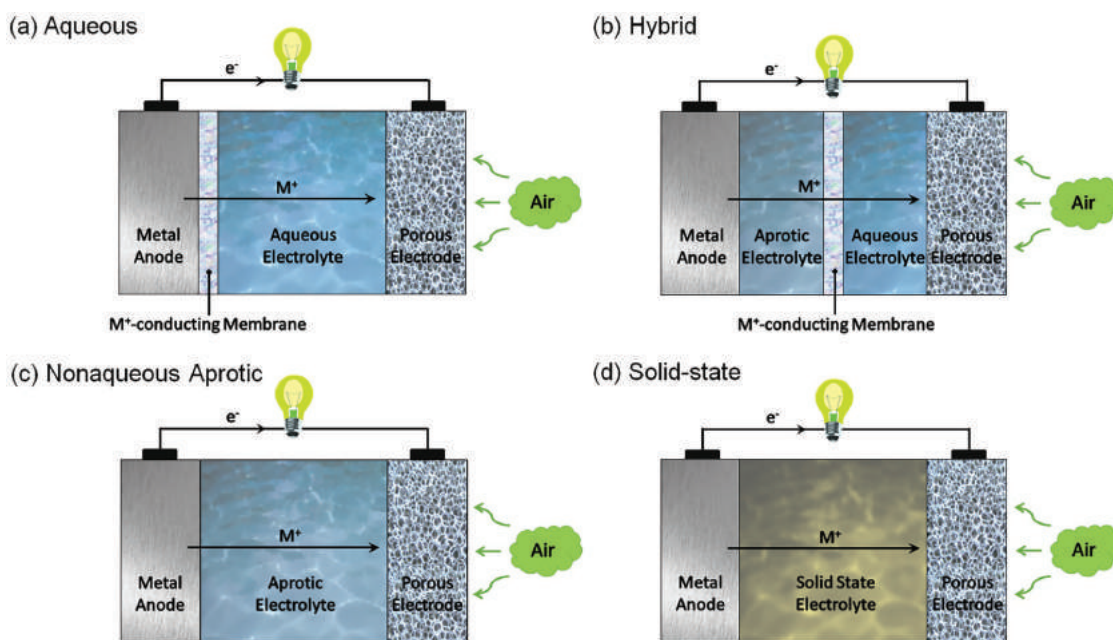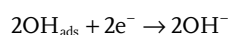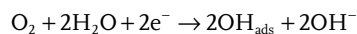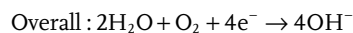

Figure 3. Schematic cell configurations for the four types of metal-air batteries (M^+ represents metal cations).

1700036 (4 of 51)

**ADVANCED
SCIENCE NEWS**

www.advancedsciencenews.com

**ADVANCED
SUSTAINABLE
SYSTEMS**

www.advsustainsys.com

acidic electrolytes can cause serious safety hazard and short shelf-life. Therefore, alkaline electrolytes are generally used because metal anodes are relatively stable. Also, when highly reactive metals such as Li, Na and Mg are used as anodes, as shown in Figure 3a, a protective metal ion-conducting membrane is needed to prevent the vigorous reactions of metal anodes with water. For example, a lithium super-ionic conductor glass electrolyte film (LISICON) $Li_{1+x+y}Al_xTi_{2-x}Si_yP_{3-y}O_{12}$ (LATP) provided by Ohara Inc. showed good Li^+ conductivity ($\approx 3 \times 10^{-4}$ S/cm at 25 °C) and water impermeability which can be potentially used in hybrid Li-air batteries. However, an additional solid-state protective layer is needed to be pre-deposited on the Li anode because the LATP glass film decomposes when in direct contact with lithium metal.[57] Moreover, there's little evidence showing the anode and cathode reactions are reversible for aqueous Li-air batteries. Comparatively, primary and mechanically rechargeable Zn-air cells are much more cost-effective owing to the low cost and simple fabrication of zinc anode.
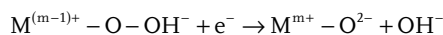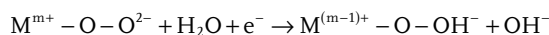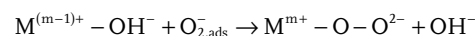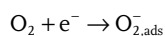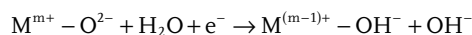
The kinetics of the oxygen electrochemistry in aqueous systems is rather slow, where electrocatalysts are needed to promote and accelerate ORR and OER processes. Depending on different electrocatalysts, the corresponding reaction mechanisms are not identical. For example, two different ORR mechanisms have been intensively studied on metal electrocatalysts, which are, a four-electron and a two electron pathway based on two oxygen adsorption types. The bidentate O_2 adsorption with two O atoms coordinated on the catalyst surface corresponds to the four-electron pathway reduction, the reactions can be represented as follows:

$$\text{Overall}: 2H_2O + O_2 + 4e^- \rightarrow 4OH^-$$

$$O_2 + 2H_2O + 2e^- \rightarrow 2OH_{ads} + 2OH^-$$

$$2OH_{ads} + 2e^- \rightarrow 2OH^-$$

For the end-on type, only one O atom of the oxygen molecule is adsorbed on the surface which favors the two-electron pathway, the reactions are as follows:

$$\text{Overall}: O_2 + H_2O + 2e^- \rightarrow OH^- + OH_2^-$$

$$O_2 + H_2O + e^- \rightarrow OH_{2,ads} + OH^-$$
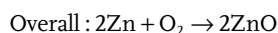
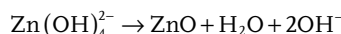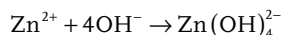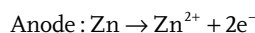$$OH_{2,ads} + e^- \rightarrow OH_2^-$$
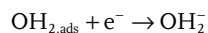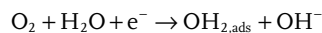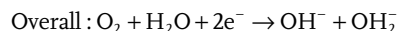
The oxygen electrochemistry at the surface of metal oxides follow the same principle, but is different from that of metal catalysts in surface charge distribution. Anion coordination is completed by the oxygen in H_2O molecule rather than oxygen fully coordinated with surface cations of stoichiometric oxides. Surface cation reduction is thus charge-compensated by protonation of a surface oxygen ligand. For example, a four-step ORR pathway mechanism is proposed blow:

$$M^{m+} - O^{2-} + H_2O + e^- \rightarrow M^{(m-1)+} - OH^- + OH^-$$

$$O_2 + e^- \rightarrow O_{2,ads}^-$$

$$M^{(m-1)+} - OH^- + O_{2,ads}^- \rightarrow M^{m+} - O - O^{2-} + OH^-$$

$$M^{m+} - O - O^{2-} + H_2O + e^- \rightarrow M^{(m-1)+} - O - OH^- + OH^-$$

$$M^{(m-1)+} - O - OH^- + e^- \rightarrow M^{m+} - O^{2-} + OH^-$$

The ORR pathways and mechanisms may vary with different electrocatalysts and electronic structure. Both the two- and four-electron reaction pathway may occur simultaneously and compete with each other.[58] It was also found that a four-electron reduction is dominating in high potential intervals, while the reduction reaction switches to the peroxide-mediated pathway at low potential.[59] It should be noted that the four-electron reduction pathway is more favorable owing to its high energy efficiency and is generally believed to predominates the reduction process on noble metals. The two-electron reduction, on the other hand, is undesirable due to the corrosive peroxide species produced during this process which can cause premature degradation of the battery. This reduction pathway was found to primarily participate on Carbonaceous materials. For other electrocatalysts such as metal macrocycles and transition metal oxides, various ORR pathways coexist depending on different electronic structure, molecular composition, experimental parameter, and so on. The ORR mechanisms in aqueous metal-air systems have been well acknowledged thanks to the numerous investigation on fuel cells in the past decades. However, how to determine explicitly an ORR mechanism remains as a challenge if a series reduction and decomposition of intermediate species can proceed at an extremely fast rate, the overall reaction process can thus be described as a four-electron reduction pathway. In addition, due to the limitation of current analytical techniques, the true surface reactions might be still unclear and more underlying reaction pathways might be undiscovered.

As a typical example, Zn-air batteries have been widely studied as an aqueous type metal-air battery. When discharge, oxygen from the cathode is reduced to hydroxyl ions with electrons released from zinc metal. The hydroxyl ions then migrate to the anode to combine with Zn ions generated from zinc metal to form zincate ions ($Zn(OH)_4^{2-}$), which may further decompose to form ZnO. The electrochemical reactions of Zn-air battery with alkaline electrolytes during discharge can be described as follows:

$$\text{Anode}: Zn \rightarrow Zn^{2+} + 2e^-$$

$$Zn^{2+} + 4OH^- \rightarrow Zn(OH)_4^{2-}$$

$$Zn(OH)_4^{2-} \rightarrow ZnO + H_2O + 2OH^-$$

$$\text{Cathode}: O_2 + 2H_2O + 4e^- \rightarrow 4OH^-$$

$$\text{Overall}: 2Zn + O_2 \rightarrow 2ZnO$$

The equilibrium potential of a Zn-air battery is 1.65 V, but the practical voltage is usually less than 1.65 V due to the Ohmic and concentration loss and internal loss from activation. The hydrogen evolution reaction (HER) can also lead to zinc corrosion according to the reaction: $Zn + 2H_2O \rightarrow Zn(OH)_2 + H_2$. The major challenge for Zn-air battery, however, is the limited lifetime and poor rechargeability. When charging, the zinc metal anode suffers from shape change such as the formation

**ADVANCED
SCIENCE NEWS**

www.advancedsciencenews.com

**ADVANCED
SUSTAINABLE
SYSTEMS**

www.advsustainsys.com

of zinc dendrites, which leading to short circuits. The white solid ZnO powder at the surface of the anode also acts as an insulator, further weakening the rechargeability. Accordingly, mechanically rechargeable Zn-air battery is widely accepted for the application in military and civilian areas. To develop a fully rechargeable Zn-air battery, one must improve the understanding of the electrochemical behavior of Zn anode in alkaline solutions.

For another example, magnesium-air battery is composed with a magnesium anode, an alkaline electrolyte, and a porous Carbon cathode supported with catalysts. The electrochemical reactions of Mg-air battery with an alkaline electrolyte during discharge can be described as follows:

$$Anode: Mg \rightarrow Mg^{2+} + 2e^-$$

$$Mg^{2+} + 2OH^- \rightarrow Mg(OH)_2$$

$$Cathode: O_2 + 2H_2O + 4e^- \rightarrow 4OH^-$$

$$Overall: 2Mg + O_2 + 2H_2O \rightarrow 2Mg(OH)_2$$
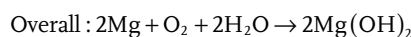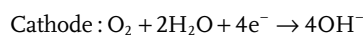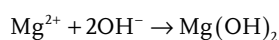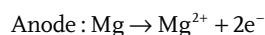
In a similar case, iron-air battery is composed with a iron anode, an alkaline electrolyte, and a porous cathode supported with catalysts. The electrochemical reactions of iron-air battery with an alkaline electrolyte during discharge can be described as follows.[60]

$$Fe + 2OH^- \rightarrow Fe(OH)_2 + 2e^-, \ E_0 = -0.975 \ V \ vs \ Hg/HgO \tag{1}$$

$$Fe(OH)_2 + OH^- \rightarrow FeOOH + H_2O + e^-, \\ E_0 = -0.658 \ V \ vs \ Hg/HgO \tag{2}$$

and/or

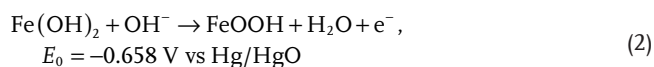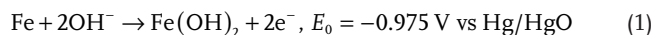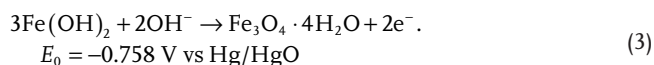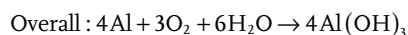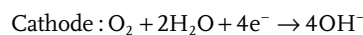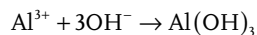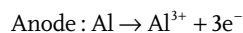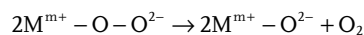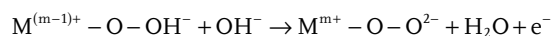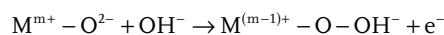$$3Fe(OH)_2 + 2OH^- \rightarrow Fe_3O_4 \cdot 4H_2O + 2e^-. \\ E_0 = -0.758 \ V \ vs \ Hg/HgO \tag{3}$$

Similarly, the electrochemical reactions of an aluminium-air battery can also be expressed as follows:[61]

$$Anode: Al \rightarrow Al^{3+} + 3e^-$$

$$Al^{3+} + 3OH^- \rightarrow Al(OH)_3$$

$$Cathode: O_2 + 2H_2O + 4e^- \rightarrow 4OH^-$$

$$Overall: 4Al + 3O_2 + 6H_2O \rightarrow 4Al(OH)_3$$

It should be noted that aluminium-air battery cannot be recharged; the discharge process will be terminated once the anode is completely consumed. Neutral electrolytes such as NaCl solutions are commonly adopted due to the rapid HER with hydroxide ions in alkaline electrolytes on open circuit. The corrosion of metal anodes is a common issue for aqueous metal-air batteries, which will lead to shortened shelf-life and decrease in capacity and Coulombic efficiency. Some approaches have been proposed to enhance the corrosion resistance of metal anodes such as alloying with other metals or improve the purity of anodes, which will be discussed in section 7.

For the reverse reaction, the reaction pathways can also be complicated since O_2 is generally originated form oxide-state discharge products and the mechanisms may change depending on the electrode materials and their electrochemical structure. Transition metal oxides, especially perovskites are found to exhibit excellent OER performance in alkaline media due to the changeable valence states of the metal cations which can interact with oxygen intermediates to form bonds by changing the valance state. Because of the lacking of efficient catalysts, a large overpotential is needed when charging, leading to huge energy loss and low round-trip efficiency. To realize the fully rechargeability of metal-air battery, developing bifunctional catalysts is of vital importance. The OER process can be described as follows with M^{m+} representing a multi-valence metal cation:

$$M^{m+} - O^{2-} + OH^- \rightarrow M^{(m-1)+} - O - OH^- + e^-$$

$$M^{(m-1)+} - O - OH^- + OH^- \rightarrow M^{m+} - O - O^{2-} + H_2O + e^-$$

$$2M^{m+} - O - O^{2-} \rightarrow 2M^{m+} - O^{2-} + O_2$$

2.2. Nonaqueous Aprotic Systems

Compared with the decades' investigation in aqueous systems, the research in nonaqueous aprotic ones has only been growing up in the last ten years. A nonaqueous aprotic metal-air battery has a similar configuration to that of a conventional LIB which is composed of an anode, a cathode and an aprotic solvent dissolved with metal salt as electrolyte (Figure 3c). The major difference is the porous and open cathode structure of a Li-air cell. Consequently, this battery system is moisture sensitive, thus a selective membrane that only permeable to oxygen is needed. By far, nonaqueous aprotic metal-air batteries can be often seen in the area of Li-air and Na-air batteries. For example, a typical Li-air battery comprises a Li metal anode, an aprotic electrolyte, a separator membrane, and a porous gas cathode. Owing to the ultra-high energy density of Li-air battery, the ORR and OER in Li+ aprotic electrolytes are attracting growing worldwide research interests in recent years. The following discussion on oxygen electrochemistry in nonaqueous electrolyte is thus based on the research in Li-air batteries. Although metal-air batteries using aqueous electrolyte configurations have many advantages including low cost, high ionic conductivity and wide availability, their operating voltage is limited to the range where water is stable against HER or OER rather than the theoretical voltages of metal anodes. A special membrane is also needed between the aqueous electrolyte and highly reactive metal anode such as Li and Na, further rises the cost and complicates the fabrication of a cell. Comparatively, nonaqueous aprotic metal-air battery especially Li-air battery has demonstrated high energy density and good rechargeability, highlighting the advantage over aqueous systems and potential of practical applications. It is thus crucial to understand the oxygen reaction mechanisms in nonaqueous aprotic electrolytes. We will focus on the review of the investigation on the mechanistic understanding of rechargeable Li-air battery system as it has drown particular research interests.

First, we start with a brief overview of the representative works in the early stage of research on aprotic Li-air battery. The first report was in 1996, when a polymer organic electrolyte

ADVANCED
SCIENCE NEWS

www.advancedsciencenews.com

ADVANCED
SUSTAINABLE
SYSTEMS

www.advsustainsys.com

was used to replace the aqueous electrolytes.[11] The discharge reaction was estimated to be $2Li + O_2 \rightarrow Li_2O_2$ by Raman spectroscopy and qualitative analysis, which is different from all aqueous metal-air batteries in that the discharge product Li_2O_2 cannot be observed in aqueous electrolyte and was deposited in the cathode rather than at the anode. The cell was tested in a pure oxygen atmosphere and exhibited an open-circuit voltage of 3 V and rechargeability of three cycles between a voltage range of $2.5 \approx 4.1$ V. A porous Carbon air electrode containing cobalt catalyst was used to lower the charge potential.

Afterwards, Read et al. investigated the effect of organic electrolytes on the performance of Li-air batteries.[12,62–64] They found that the oxygen solubility and diffusion properties depend largely on the formulation of electrolyte, which dramatically influence the discharge capacity and rate capability of Li-air cell. At low oxygen concentrations, the formation of Li_2O was found to prefer over that of Li_2O_2, indicating a substantial improvement in cell performance can be achieved by electrolyte optimization to increase oxygen partial pressure. It was proposed that the oxygen concentration and electrolyte viscosity are the limiting factors of discharge capacity. The discharge products, namely Li_2O and Li_2O_2, and their deposition are also dependent on the type of electrolyte and discharge rate. In addition, these research also imply that the discharge product blow 2.0 V (vs Li/Li^+) is dominated by Li_2O, a thermodynamically stable phase that cannot be easily decomposed upon charging process, leading to high polarizations. A cutoff voltage of 2.0 V is thus widely adopted by researchers when testing the discharge/charge performance of Li-air batteries. Furthermore, the effect of cathode porosity on cell performance was also studied. By comparing the discharge performance of different cathode materials, it was found that a high specific surface area doesn't necessarily correspond to high specific capacity of Carbon. A model of Carbon electrode proposed in **Figure 4**a
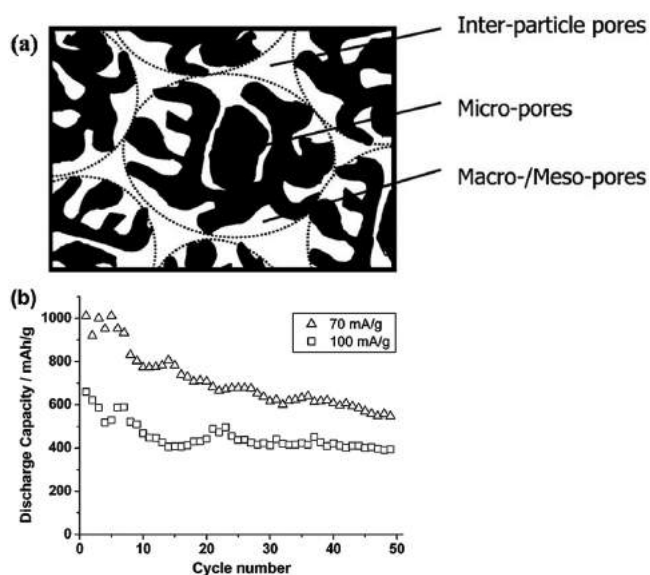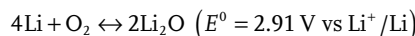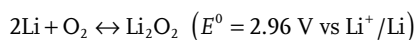

Figure 4. a) A proposed model for carbon air electrode of Li-air battery.[64] b) Variation of discharge capacity with cycle number for the super P-based O_2 cathode (Rates 70 and 100 mAh g^{-1}, capacities are per gram of carbon). Reproduced with permission.[13] Copyright 2006, American Chemical Society.

was used to explain the effect of interparticle micro-, meso-, and macro-size pores on air electrode capacity. The authors claimed that the electrolyte-wetted meso- and macropores are accessible for the dissolved oxygen, but only few parts show catalytic activity to ORR, which mainly contributed to the specific capacity of Carbon. The inter-particle pores, on the other hand, played a major part in the power capability of Li-O_2 cells. The degree of electrolyte-filling thus plays a critical role in the specific capacity and rate capability of Li-O_2 batteries. More specifically, these pores should either be completely wetted with the electrolyte to maintain a maximum reaction area for high specific capacity of Carbon, or not be flooded by the liquid electrolyte to supply sufficient pores for the efficient diffusion of gaseous oxygen to achieve high power capability. This work indicate that substantial improvements in cell performance can be obtained by tailoring the physical properties of air electrode.

In 2006, Bruce and co-workers developed a Li-O_2 cell and successfully tested for more than 50 cycles (Figure 4b).[13] The cell was based on a Swagelok design which comprised of a Li metal anode, 1 M LiPF$_6$ dissolved in propylene carbonate (PC) as electrolyte, a glass fiber separator, and a Carbon cathode containing electrolytic manganese dioxide as catalyst. In situ mass spectrometry was carried out on the gases evolved upon charging, which provided direct evidence that the electrochemical reaction $2Li^+ + 2e^- + O_2 \rightarrow Li_2O_2$ is reversible upon discharge and charge processes. This work provided important proof supporting the feasibility of an O_2 electrode for rechargeable lithium batteries. Although some fundamental and practical issues remain to be settled, such as the role of catalyst in promoting electrode reactions and optimization of cathode structure and electrolyte composition (which will be discussed later), this work opened up an important avenue for further investigation on Li-air batteries.

The above pioneer works on aprotic Li-air battery have presented a great potential in this field, and have attracted tremendous research interests since then. Till now, researchers have gained much more research experiences and better understandings on the Li-O_2 electrochemistry. Despite the great advancements made in this area during the past decade, significant challenges remain in the thorough understanding of the reaction mechanism of the electrochemistry in aprotic electrolytes and development of advanced and high-performance electrodes and electrolytes. As well acknowledged, the cathode reactions of an aprotic Li-air battery are distinct from the intercalation process of a LIB, which allow Li to react directly with oxygen from air at the interface of a porous air electrode. Unlike the ORR process in aqueous electrolytes which undergoes a four- or two-electron reduction pathway corresponding to the formation of H_2O or H_2O_2, the process in nonaqueous electrolytes involve several oxygen-containing species and form insoluble discharge product species that buildup on the cathode surface. Possible net reactions of Li-air battery are listed as follows. Both the reactions have a reversible cell voltage approximates 3.0 V vs Li^+/Li, which suggests they are thermodynamically favored.

$$2Li + O_2 \leftrightarrow Li_2O_2 \quad (E^0 = 2.96 \text{ V vs } Li^+/Li)$$

$$4Li + O_2 \leftrightarrow 2Li_2O \quad (E^0 = 2.91 \text{ V vs } Li^+/Li)$$

**ADVANCED
SCIENCE NEWS**
www.advancedsciencenews.com

**ADVANCED
SUSTAINABLE
SYSTEMS**
www.advsustainsys.com

To Figure out the reaction mechanism, massive effort has been devoted to the investigation of reaction pathways and the impact of external influences of electrolyte, electrocatalyst, surface of electrode, oxygen pressure and so on. Abraham's group studied the role of the electrolyte including the ion conducting salts and solvents on the reversibility and kinetics of oxygen electrochemistry by using cyclic voltammetry (CV) and rotating disk electrode (RDE) techniques.[65–67] For cation effects, it was found that oxygen reaction mechanism is strongly influenced by the cations of conducting salts in acetonitrile-based electrolytes. Larger cations such as tetrabutylammonium (TBA^+) and tetraethylammonium (TEA^+) displayed reversible O_2/O_2^- redox couple, whereas the electrolyte containing smaller Li^+ cations were found to exhibit an irreversible or quasi-reversible one-electron reduction mechanism of O_2 to form O_2^-, O_2^{2-}, and O^{2-} as products. This result suggest potential enhancements in battery's capacity and reversibility if a mixture of Li and/or TBA salts were used as supporting electrolytes to dissolve the oxygen reduction spices. According to Pearson's hard soft acid base (HSAB) theory, hard acids prefer hard bases and soft bases prefer soft acids. TBA^+ as a soft acid can stabilize the soft base O_2^- and prevent further reduction of superoxide to peroxide. On the other hand, alkali metal ions such as Li^+, Na^+, and K^+ are hard Lewis acids, which have a high affinity for hard Lewis bases such as O_2^{2-} and O^{2-}. The soft base O_2^- thus has a low affinity for the hard acid Li^+, which consequently tends either to undergo a second reduction process to form a hard base or to decompose. In other words, the favorable and stable oxygen reduction products in Li^+-containing electrolytes are Li_2O_2 and Li_2O, based on the HSAB theory. More recently, the same group applied HSAB theory to investigate the ORR and OER processes with a series of cations with increasing Lewis acidity (i.e., cation hardness): $TBA^+ < PyR^+ < EMI^+ < K^+ < Na^+ < Li^+$, as shown in **Figure 5**.[67] The O_2^- ions were found to effectively stabilized by TBA^+, PyR^+, EMI^+ and K^+ cations without disproportionate to form O_2^{2-}, which enabled reversible one-electron reactions. In contrast, it was found that hard cations such as Li^+ and Na^+ can promote the disproportionation of metal superoxide to form metal peroxide, emerging an irreversible two-electron (per O_2) process.

It should be noted that a single experimental measurement technique is insufficient to verify the electrochemical mechanism. For example, CV is widely adopted as a simple and effective experimental measurement, but its data only reflect the overall electrochemistry and can be distorted by impurities in the electrolyte at slow scan rates, which can lead to inaccurate results.[68] Thus combining multiple and advanced research tools from experimental to theoretical modeling are needed to study the electrocatalytic processes. For instance, density functional theory (DFT) calculations and other qualitative and quantitative means such as in situ TEM and XRD, Fourier transform infrared spectroscopy (FTIR), X-ray photoelectron spectroscopy (XPS), Raman, nuclear magnetic resonance (NMR), etc. were adopted by researchers as a pair of methods to investigate the reaction mechanisms in nonaqueous aprotic electrolytes during discharge/charge.[69–83] These study also indicated LiO_2 is initially formed in the presence of Li^+ on air electrode by an one-electron reduction process of dioxygen. If not considering the parasitic reactions, the final discharge product in aprotic electrolytes is widely accepted as Li_2O_2. For example, Peng et al. studied oxygen reaction in Li^+-containing CH_3CN electrolyte by means of in situ surface enhanced Raman spectroscopy (SERS) and CV on roughened Au electrode.[70] As shown in **Figure 6**, the reaction of O_2^- with Li^+ was investigated as a function of Li^+ concentration. These results showed distinct reduction peaks in the presence and absence of Li^+ ions. An appearance of a more positive reduction peak can be observed when the concentration of Li^+ is 1 mM, which can be assigned to the reaction between O_2^- and Li^+. The peak potential shifted to lower voltage with lower reduction current as the Li^+ concentration went up. This can be explained by the insulating reduction products which blocked the electrode surface and can be more severe with higher Li^+ concentration. SERS data provided direct spectroscopic evidence that the first step reduction of O_2 in Li^+-containing nonaqueous electrolyte is formation of O_2^-, then binded with Li^+ to form LiO_2 on the electrode surface. The LiO_2 was
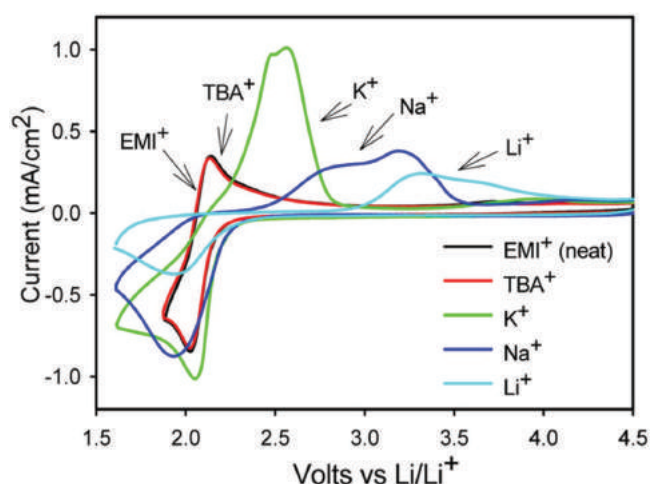
Figure 5. Cyclic voltammogram of neat EMITFSI along with various salts at 0.025 M concentration on a glassy carbon electrode at 100 mV s^{-1}. Reproduced with permission.[67] Copyright 2012, American Chemical Society.
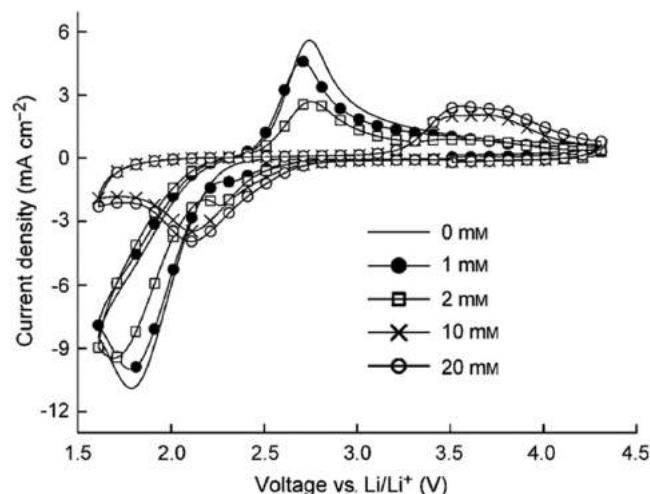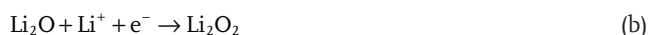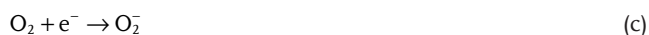

Figure 6. Cyclic voltammetry at an Au electrode in O_2-saturated 0.1 M nBu$_4$NClO$_4$-CH$_3$CN containing various concentrations of LiClO$_4$ as indicated at a scan rate of 1.0 V s^{-1}. Reproduced with permission.[70]

**ADVANCED
SCIENCE NEWS**

www.advancedsciencenews.com

**ADVANCED
SUSTAINABLE
SYSTEMS**

www.advsustainsys.com

found unstable which subsequently disproportionated to the more stable Li_2O_2 following the Equation (2) $Li_2O \rightarrow O_2 + Li_2O_2$, and the first order rate constant for this disproportionation reaction was calculated as k = 2.9 × 10^{-3}/s. The proposed two different possible reaction pathways for Li-O$_2$ couples at the cathode during discharge can be summarized as follows. The first steps of ORR in nonaqueous electrolytes is generally considered to be the formation of lithium superoxide radicals. The further formation of Li_2O_2, if no parasitic reactions are involved, may undergoes a sequential electrochemical route [Eqs. (b)] or disproportionation of LiO_2 species [Eqs. (e)].

$$O_2 + Li^+ + e^- \rightarrow Li_2O \tag{a}$$

$$Li_2O + Li^+ + e^- \rightarrow Li_2O_2 \tag{b}$$

or

$$O_2 + e^- \rightarrow O_2^- \tag{c}$$

$$O_2^- + Li^+ \rightarrow Li_2O \tag{d}$$

$$2Li_2O \rightarrow O_2 + Li_2O_2 \tag{e}$$

To make a Li-air battery rechargeable, the discharge product Li_2O_2 is to be decomposed to lithium ions and oxygen (or referred to as the OER process) during charge.[84–88] Consider the discharge product is pure Li_2O_2, two different mechanisms have been proposed for the oxidation of Li_2O_2 as shown in the following equations:

$$Li_2O_2 \rightarrow 2Li^+ + O_2 + 2e^- \tag{f}$$

or

$$Li_2O_2 \rightarrow LiO_2 + Li^+ + e^- \tag{g}$$

$$LiO_2 \rightarrow Li^+ + O_2 + e^- \tag{h}$$

The core issue of the debate is whether the charging process is a one-step reaction or a two-step process that involves Li_2O as an intermediate. To understand the mechanism of this process, Peng et al. combined in situ SERS and in situ differential electrochemical mass spectroscopy (DEMS) measurements.[69] Experimental data showed no evidence of the existence of Li_2O during charge which indicated a direct one-step decomposition of Li_2O_2 to evolve oxygen. In contrast, a two-stage process was proposed by Shao-Horn's group as illustrated in **Figure 7**.[84] First, three Li-O$_2$ cells with Vulcan Carbon (VC) electrodes were predischarged to a fixed capacity of 200 mAh/g$_c$ at different rates. This process showed relatively fast ORR kinetics where a uniform distribution of Li_2O_2 on the VC surfaces was observed. The charge process was found to be more sluggish and sensitive to rates compared with that of the discharge ORR reaction. Three stages can be observed from the charge profile of a Li-O$_2$ cell in Figure 7, that is, a sloping region between 3.0 V to 3.4 V followed by a relatively flat plateau region at 3.4 V and a second plateau at about 3.6 V. Correspondingly, the first stage can be considered as a delithiation process of the outer shell of Li_2O_2 to form a like species. This stage can be represented as the equation $Li_2O_2 \rightarrow LiO_2 + Li^+ + e^-$, whose kinetics are relatively insensitive to charge rates and catalysts. The second stage which took place at higher overpotentials can be attributed to the oxidation of bulk Li_2O_2 particles to evolve oxygen. Following the equation $LiO_2 + LiO_2 \rightarrow Li_2O_2 + O_2$, kinetics of this stage are sensitive to discharge/charge rates and catalysts. The third stage, which is at the end of discharge can be assigned to the decomposition of electrolyte to evolve CO_2 at high voltages, this phenomenon is in agreement with the studies of McCloskey et al.[89–91] and this issue will be discussed later.

In view of the above proposed mechanisms, the cathode reactions in nonaqueous aprotic Li-air batteries is a series of complicated processes, new perspectives are being continually proposed but the explicit reactions still remain unclear.[92–96]
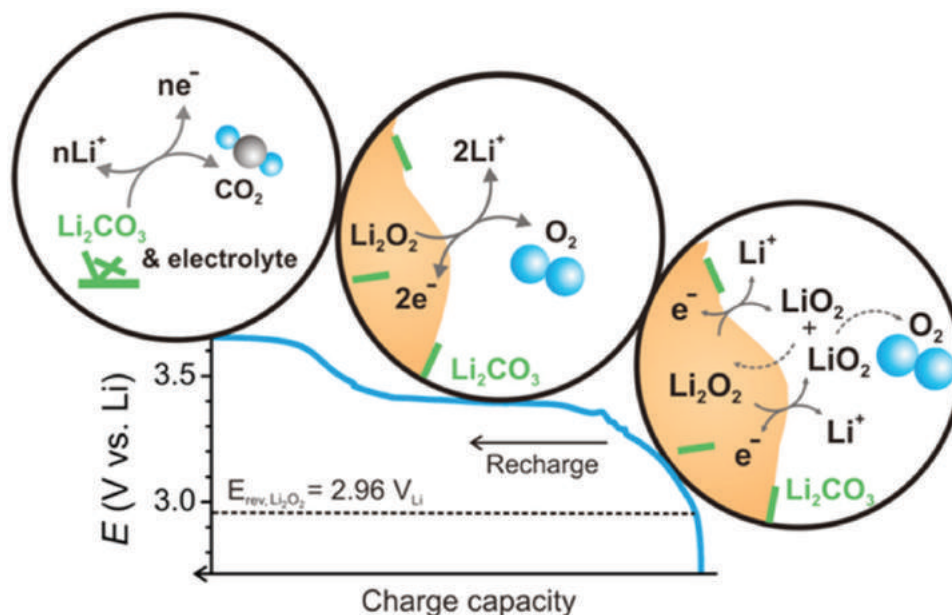

Figure 7. Proposed reaction mechanism during recharge process of Li-air battery. Reproduced with permission.[84] Copyright 2013, American Chemical Society.

**ADVANCED
SCIENCE NEWS**

www.advancedsciencenews.com

**ADVANCED
SUSTAINABLE
SYSTEMS**

www.advsustainsys.com

The practical oxygen electrochemistry can be affected by various factors such as electrocatalysts, electrode materials, electrolytes, oxygen pressure and so on.[97–104] Electrocatalysts have been found effective in lowering the overpotentials during charge, but their mechanic details in this process is under debate.[105,106] The establishment of a thorough understanding of the correlation between electrocatalysts and discharge/charge behaviors is prerequisite for the development of high performance catalysts. The characteristics of an air electrode such as porosity, stability and conductivity also dramatically influences the overall performance of a Li-air cell. Since the intermediates and products during discharge/charge and are less dissolvable in organic electrolytes, the study of their physical and chemical features is thus critical to the further understanding of the limitations in Li-air batteries.[107–132]

Toroid and layer structured Li_2O_2 nanoparticles of hundred nanometers in size were reported by many researchers.[79,107–113] Shao-Horn's group reported that the disc and toroid particles are composed of arrays of plate-like Li_2O_2 crystallites, as highlighted by yellow dashed lines in **Figure 8**a and b.[107] By observing the growth of Li_2O_2 particles at different discharge rates and capacities, Shao-Horn's group proposed that the evolution process can be described as the stack and spray of plate-like Li_2O_2 crystallites. As illustrated in Figure 8c, Li_2O_2 crystals first grow roughly parallel to each other at the center of the discs and then splay apart with increasing disc diameter. With the depth of discharge, additional plates nucleate in the empty space between the splayed plates, resulting in the toroid morphology.

As for the charging process, the same group used in situ TEM as a means to observe the electrochemical oxidation of Li_2O_2.[111] As shown in **Figure 9**, a predischarged solid-state in situ battery consisting of a MWCNT/Li_2O_2 positive electrode and a delithiated Si NW negative electrode coated with solid
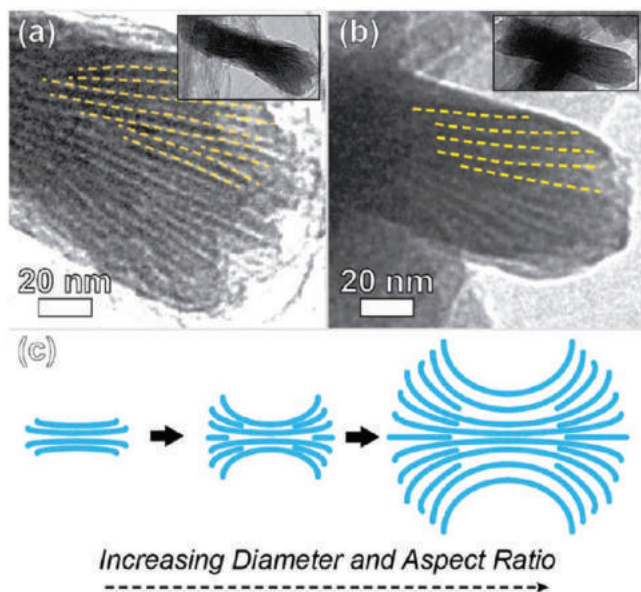
electrolyte was assembled and placed inside a TEM to study the electrochemical oxidation process. A pair of comparative tests were conducted to investigate the limiting factor of the oxidation kinetics. Preferential oxidation at the MWCNT interface was observed whether the Li_2O_2 toroid was in contact with the solid electrolyte or not, suggesting the oxidation process is electron-transport-limited rather than lithium-ion-transport-limited. Later, Hong's group performed an in situ study on the discharge/charge processes of a microscale all-solid-state Li-O$_2$ battery using environmental scanning electron microscope (ESEM).[112] Upon discharge, toroid Li_2O_2 particles were observed with the size already beyond the electron tunneling distance (~5 nm) of insulating Li_2O_2. This suggests electronic and ionic conductivities of the formed Li_2O_2 could be capable to support the growth of the discharge product. Upon charge, the decomposition of Li_2O_2 was found to be initiated from the surface of the particles, which could be associated with the uneven distribution of the ionic and electronic conductivities.

In situ Electrochemical atomic force microscopy (EC-AFM) was also used to provide visual and real-time observations to study the electrochemical reactions during discharge/charge on a highly oriented pyrolytic graphite (HOPG) electrode.[113] At the early stage of discharge, Li_2O_2 nanoplates were found to rapidly grow on the step edges of the HOPG electrode and eventually form a dense Li_2O_2 film. The film then decomposed during OER process and the thickness of the film was also found to be related with the potential upon charge. By-products such as Li_2CO_3, lithium acetate, and fluorine-related species were detected by XPS analysis after five cycles due to the deterioration of HOPG electrode, tetraglyme, and lithium salt. AFM studies also showed sudden death of battery is associated with limited charge transport through the Li_2O_2 film.[114] The thickness of the film is correlated with the discharge currents and the authors found that when film thickness is ~5 to 10 nm, the charge transport is not sufficient to support electrochemistry at the Li_2O_2-electrolyte interface.

Theoretical study based on DFT was also used to predict the surface properties of Li_2O_2 by some researchers.[117–124] As

Figure 8. Side-profile TEM images of disc particles discharged at (a) 50 mA g_c^{-1} to 1000 mAh g_c^{-1} and (b) 90 mA g_c^{-1} to 13000 mAh g_c^{-1}. c) Schematic illustration of the microscale shape evolution of Li_2O_2 particles. Reproduced with permission.[107] Copyright 2013, American Chemical Society.

Figure 9. Schematic illustration of the in situ TEM test of oxidation of Li_2O_2 particles. Reproduced with permission.[111] Copyright 2013, American Chemical Society.

**ADVANCED
SCIENCE NEWS**

www.advancedsciencenews.com

**ADVANCED
SUSTAINABLE
SYSTEMS**

www.advsustainsys.com

Figure 10. Equilibrium shape of Li_2O_2 crystallites based on calculated surface energies and the Wulff construction. Reproduced with permission.[117] Copyright 2012, American Chemical Society.

shown in **Figure 10**, the calculated surface energies were used combined with the Wulff construction to analyze the equilibrium shape of Li_2O_2 crystallites.[117] A low aspect ratio hexagonal prism morphology was predicted of the formed Li_2O_2 with O-rich (0001) being the lowest energy surface and predominate of the surface area. Desp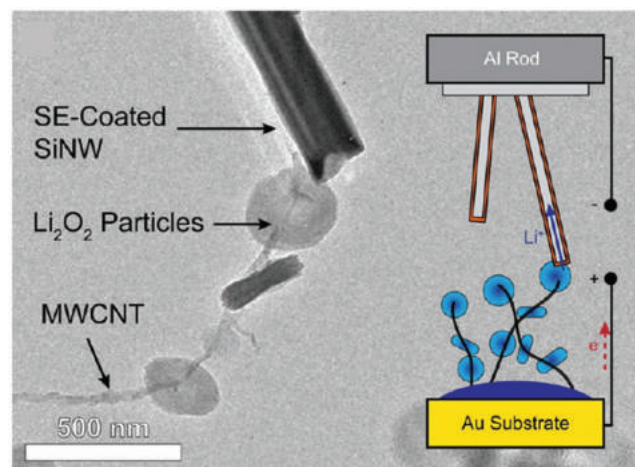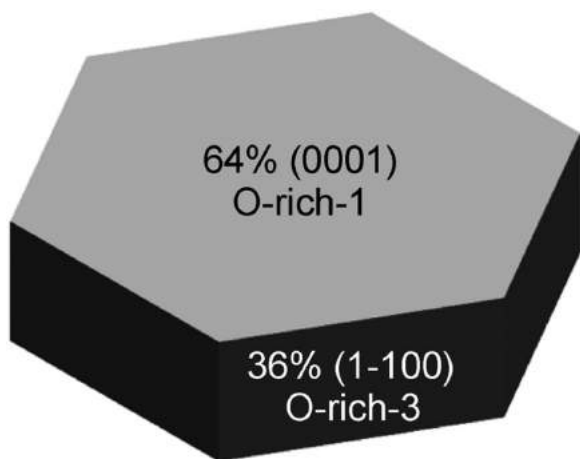ite the fact that Li_2O_2 is a bulk insulator, the calculated results revealed that the stable surfaces of Li_2O_2 were half-metallic and magnetic, while the stable surfaces of Li_2O were quite the opposite. This result offered an explanation of the electrochemical reversibility of Li-air systems with Li_2O_2 being the discharge product and irreversibility of that discharged to Li_2O. Reports by other researchers showed slight different results but most believed the predominance of the stable O-rich (0001) facet with half-metallic and magnetic properties.[118–120]

The above mentioned AFM study suggested that the death of cell is a consequence of electrical passivation of the cathode by the accumulation of discharge products rather than pore clogging or mass transport limitations.[114] This sudden death of Li-air battery is associated with limited charge transport through the thickening Li_2O_2 film to the Li_2O_2-electrolyte interface. When the Li_2O_2 film reaches a critical thickness, the charge transport is thus not capable to support electrochemistry at the Li_2O_2-electrolyte interface. Revealing the mechanisms of charge transport in Li_2O_2 is thus crucial toward better understanding and evolution of the performance of Li-air battery.[121–124] First-principles calculations by Radin et al. revealed that the defect chemistry of Li_2O_2 is affected by the ability of O_2 dimers to change valence state.[121] Lithium vacancies and small hole polarons were observed as the dominant charge carriers, and the charge transport in Li_2O_2 went through a mixture of ionic and polaronic contributions. Further study on the charge transport through Li_2O_2 is needed to understand this major limiting factor of Li-air battery.

2.3. Hybrid and Solid-state Systems

Hybrid and solid-state metal-air batteries are rarely reported, mainly owing to the lack of favorable electrolyte and membrane

materials and the inferior battery performance compared to that of the aqueous and nonaqueous aprotic ones. Based on the anode protection concept, hybrid cells comprising a triple-structured electrolyte (e.g., nonaqueous aprotic/LATP/aqueous) were also developed (Figure 3b).[133–138] For a typical hybrid cell, the anode and cathode is separated by an ionic conductive membrane, a nonaqueous electrolyte is used at the anodic area, while an aqueous electrolyte at the cathodic area. This battery system share the same oxygen electrochemistry with aqueous system but with no need to be concerned about the clogging of air cathode of nonaqueous aprotic systems and the corrosion of metal anodes (especially Li and Na) with electrolytes of aqueous systems. However, the low conductivity and the lack of long-term stability of the membrane, LATP for example, remains as a major challenge, which also increases the difficulty of building hybrid batteries.

Solid-state metal-air batteries share the similar reaction mechanisms with aprotic systems, it introduces an ionically conductive solid electrolyte which can also function as a separator (Figure 3d). Such an electrolyte can be achieved by polymers, glasses, ceramics and their combinations.[139–147] For example, Zhou's group developed a Li-air cell comprising a Li anode, a solid Li-ion conductive electrolyte (LTAP), and a gel cathode which demonstrated a cyclability of 100 cycles with discharge capacity of 2000 mAh/g.[139] Late in 2017, Sun et al. reported the fabrication of solid-state Li-air batteries using garnet (i.e., $Li_{6.4}La_3Zr_{1.4}Ta_{0.6}O_{12}$, LLZTO) ceramic disks with high density and ionic conductivity as the electrolytes, which also demonstrates excellent performances.[147] However, as is the case with hybrid metal-air cells, the poor conductivity and sluggish mass transportation kinetics of electrolyte materials is the major obstacle for the two battery systems, which also explains the rare reports concerning hybrid and solid-state metal-air batteries.

3. Electrolytes and Electrolyte Stability

Electrolyte plays a vital role as a medium to transport metal ions and dissolved oxygen which significantly affects the battery electrochemistry. An ideal electrolyte for metal-air batteries should possess such properties as high oxygen solubility and diffusivity, low moisture absorption, highly stable against reduced oxygen species and metal electrodes, high boiling point, low volatility and viscosity, non-toxic and so on. Each of these properties indirectly affect the battery performance, for example, high volatility can lead to the reduce of electrolyte due to the open cell structure; electrolyte polarity largely determine the wettability of air electrode; ionic conductivity have an impact on the rates of cell electrochemistry; oxygen solubility and viscosity can affect the rate of oxygen transportation and in turn influence the rate capability of cell.[12,63,148–150] In comparison, ionic conductivity of aqueous electrolytes is much higher than nonaqueous aprotic electrolytes. In addition, aqueous electrolytes also possess high boiling point, low volatility and viscosity. However, the operating potential should be limited within a narrow range of potential window where water is stable. The freezing point of aqueous electrolyte is also relatively high, which could affect the battery performance operating at low temperatures.

**ADVANCED
SCIENCE NEWS**

www.advancedsciencenews.com

**ADVANCED
SUSTAINABLE
SYSTEMS**

www.advsustainsys.com

Polymer or solid-state electrolytes are highly safety which are non-flammable, non-volatile and free of the potential electrolyte leakage due to the open cell configuration. The major drawback is their low ionic conductivity owing to the lack of favorable materials which could lead to inferior battery performance to that using aqueous and nonaqueous aprotic electrolytes. However, due to a lack of published works concerning the above two electrolyte systems in metal-air batteries, we mainly focus on the discussion of nonaqueous aprotic electrolytes which are more thoroughly researched in Li-air batteries.

In general, electrolytes for Li-air battery are prepared by dissolving lithium salts in high purity organic solvents at a specific ratio. At the early stages of research on the Li-air battery, Carbonate-based electrolytes such as propylene (PC) and ethylene Carbonate (EC) are widely adopted due to their successful application in lithium-ion batteries owing to the low volatility, wide electrochemical window and liquid temperature range.[13,151,152] However, through experimental and theoretical studies, previous and recent researches have reported the instability of Carbonate-based electrolyte in the presence of highly reactive oxygen-containing species such as O_2^-, O_2^{2-}, LiO_2, LiO_2^-, and Li_2O_2.[153–162] Bruce's group found that alkyl Carbonate electrolyte decomposes on discharge to form CO_2, H_2O and various of Carbonate species (Li propyl bicarbonate, Li formate, Li acetate and lithium Carbonate, as shown in the proposed reaction of **Figure 11**). These Carbonate species were found to be oxidized and release CO_2 on charge and, interestingly, no evidence of the reversible formation and decomposition of Li_2O_2 was found during discharge and charge as evidenced by FTIR, DEMS and isotope labeling tests. As a result, each cycle is associated with the consumption of the electrolyte, and the accumulation of the Carbonate species in the cathode is correlated with capacity fading and cell failure. To further understand the decompose reaction mechanism of PC, EC and dimethyl carbonates

(DMC), DFT coupled with coupled-cluster calculations were conducted by Blanco et al.[154] Theoretical calculation results supported the experimental evidence that cyclic and linear carbonates are unstable against superoxide radicals. Nucleophilic attack of O_2^- was found to account for the decomposition of Carbonate-based electrolytes during ORR. Typically, base-mediated proton transfer from the methyl group of PC was also found to explain the decomposition of PC. In addition to superoxide ions, Laino et al. explicated the degradation process of Carbonate-based electrolyte at the Li_2O_2 surfaces based on DFT calculations.[155] PC was found to spontaneously decompose on the[100] Li_2O_2 surface (which was found to be the most stable surface[71]), where the surface lithium ions played a critical role. Namely, the Li^+ placed the PC molecules into close contact with the O_2^{2-}, which, due to the polarization effect, promoted the nucleophilic addition to the carboxylic carbon, then reduced the activation barrier for ring opening, the stabilization of the negative alkyl carbonate hence resulted in the degradation of PC. It is now well-established that carbonate solvents are not suitable for use in Li-air batteries despite their successful applications in lithium-ion batteries. These studies concerning the stability of electrolytes during discharge and charge have also raised a series of investigation on more reliable aprotic electrolytes.

Learned from the lessons of carbonate-based electrolytes, ether-based electrolytes such as tetraethylene glycol dimethylether (or tetraglyme, TEGDME) and 1,2-dimethoxyethane (DME) were found to be more stable against the attack of reduced oxygen spices.[163–172] Further, they also possess other advantages, for instance, stable to oxidation potentials in excess of 4.5 V (vs Li/Li$^+$), high thermal stability, low volatility for longer chain eithers (such as TEGDME), and low cost. Before the acknowledgement of the instability of Carbonate-based electrolytes, Read firstly reported the use of ether-based electrolyte in Li-air battery, demonstrating good stability and excellent
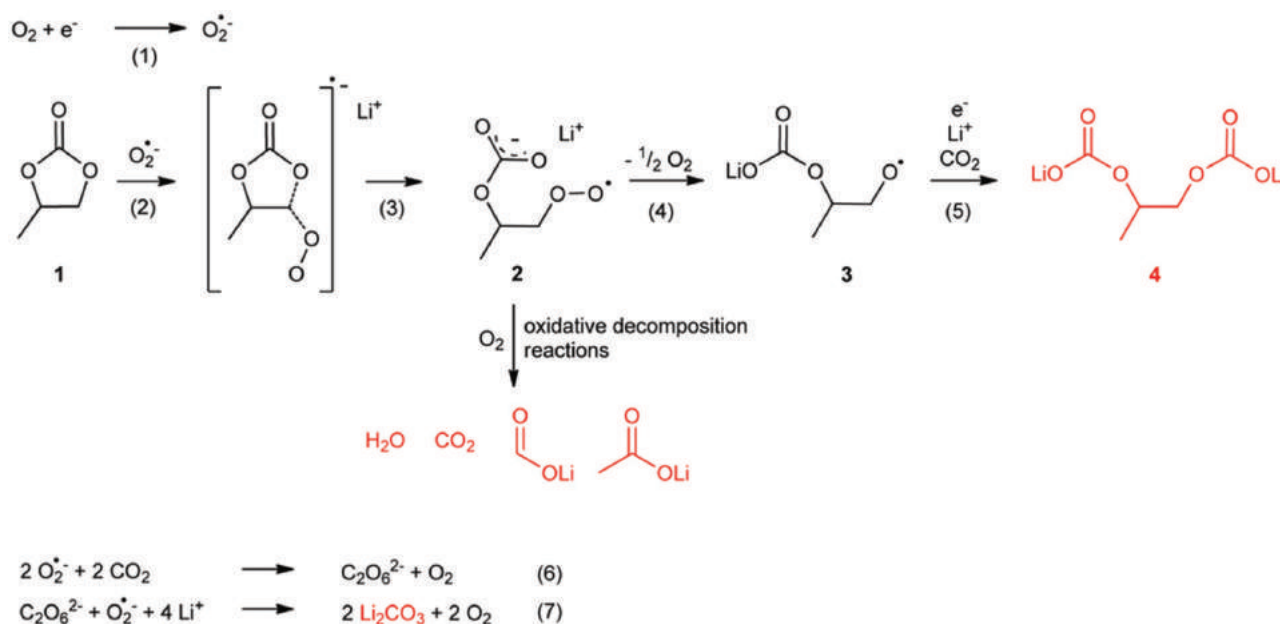

Figure 11. Proposed reaction for the formation of compounds: Li propyl dicarbonate, Li formate, Li acetate, Li_2CO_3, CO_2, and H_2O. Reproduced with permission.[153] Copyright 2011, American Chemical Society.

**ADVANCED
SCIENCE NEWS**

www.advancedsciencenews.com

**ADVANCED
SUSTAINABLE
SYSTEMS**

www.advsustainsys.com

rate capability.[63] In addition, Read also found the ether-based electrolyte outperformed the Carbonate-based electrolyte with lower viscosity while maintained similar oxygen solubility. Experimental and computational study was conducted by Amine and co-workers to compare the stability of Carbonate- and ether-based electrolytes.[163] Electrolyte based on a tri(ethylene glycol)-substituted trimethylsilane (1NM3) was used in a Li-air battery. XPS and FTIR experiments showed direct evidence that only lithium oxides and no carbonates were formed when using 1NM3 electrolyte, while PC was found to decompose to form lithium carbonates during discharge. DFT calculations of the activation barriers of breaking C–O bonds together with hydrogen and proton abstraction of ethers by reduced oxygen species also confirmed the experimental observations. Moreover, this research also found that charge overpotentials of Li-air battery containing Carbonate-based electrolyte was distinctly higher than the counterparts containing ether-based electrolyte, which indicate significant suppress of charge overpotentials and improvement in cyclability can be achieved with the utilization of stable electrolytes.

In spite of the significant advancements in stability of ether solvents, they were also found to decompose during discharge. A research by Bruce et al. qualitatively investigated the stability of ether solvents in Li-O$_2$ cells.[164] By combining electrochemical measurements with XRD, FTIR, NMR and mass spectrometry (MS) analysis, Bruce et al. proposed that both linear and cyclic ethers (e.g., tetraglyme, 1,3-dioxolane, and 2-methyl-THF) all exhibited degradation during discharge. As shown in **Figure 12**, the superoxide ions from reaction (1) can either form Li$_2$O$_2$ following reaction (2) and (3), or abstract a proton from the glyme forming an alkyl radical and further lead to the ether peroxide 2 (reaction (4) and (5)). Such intermediate species can further undergo an oxidative decomposition reaction to form H$_2$O, CO$_2$, lithium formate, and lithium acetate as indicated in reaction (6). Alternatively, these intermediate may undergo rearrangement reactions to form the polyether/ester 3 (reaction (7)). Further, Li$_2$CO$_3$ can be formed following reaction (8) and (9). This research indicated that ether-based electrolytes are still insufficient in resisting the attack of reduced oxygen species which continuously decomposes during each discharge-charge cycle. The accumulation of by-products in the cathode result in the reduction of capacity and limited cycling performance. Nevertheless, ether-based electrolytes, when compared with carbonates, are still much more stable toward the reduced oxygen species as evidenced by the reversible formation and decomposition of Li$_2$O$_2$.

Later, Veith et al. investigated the influence of lithium salts on the discharge Li-O$_2$ electrochemistry using TEGDME as solvent.[165] By analyzing the discharge products of Li-air cells through XPS, Raman and NMR spectrometry, Veith et al. found that a major discharge product in ether-based electrolytes is components of the Li salt. This study show that LiClO$_4$ was least reactive among the Li salts (LiClO$_4$, LiPF$_6$, LiBF$_4$, LiTFSI) investigated. Experimental data showed that Li salts containing F were found to decompose to form halide species up to more than 15% of the discharge products as a highly covalent species, while less than 8% of the products were found containing Cl with LiClO$_4$-based electrolyte. This research further deepened our understanding of electrolyte stability, which the effect of salts should also be taken into account.

In addition to Carbonate- and ether-based electrolytes, our group have firstly introduced a dimethyl sulfoxide (DMSO) based electrolyte in Li-O$_2$ battery.[173] Reversible formation and decomposition of Li$_2$O$_2$ was observed of the battery with superior performances including good rate performance, ultra-high discharge capacity (10600 mAh/g) and low charge potential (≈3.7 V), indicating the sustainability of DMSO-based electrolyte. Later, Bruce's group further demonstrated the advantage and advancements of DMSO in Li-O$_2$ batteries using nanoporous gold and TiC cathodes, respectively.[174,175] The Li-O$_2$ cell composed of a DMSO-based electrolyte and a nanoporous gold electrode demonstrated excellent cycling performance which retained 95% of its capacity after 100 cycles.[174] More importantly, >99% purity of Li$_2$O$_2$ formation at the cathode was observed from FTIR, SERS, NMR, and DEMS experiment data. The discharge/charge of the
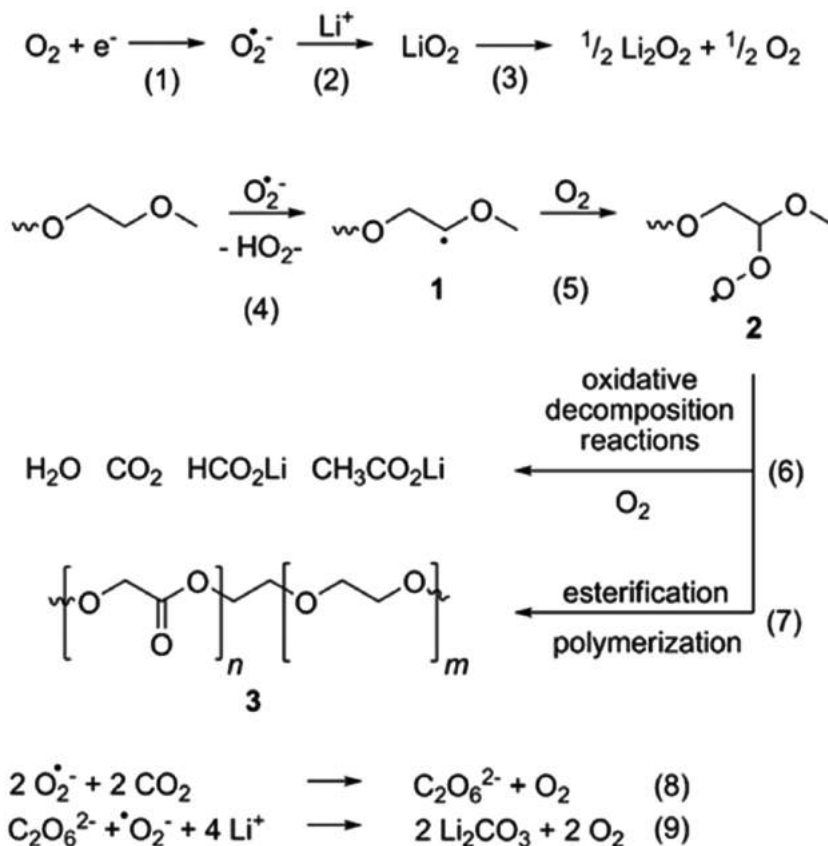

Figure 12. Proposed reaction mechanisms of Li-O$_2$ cells containing ether-based electrolytes during discharge. Reproduced with permission.[164]
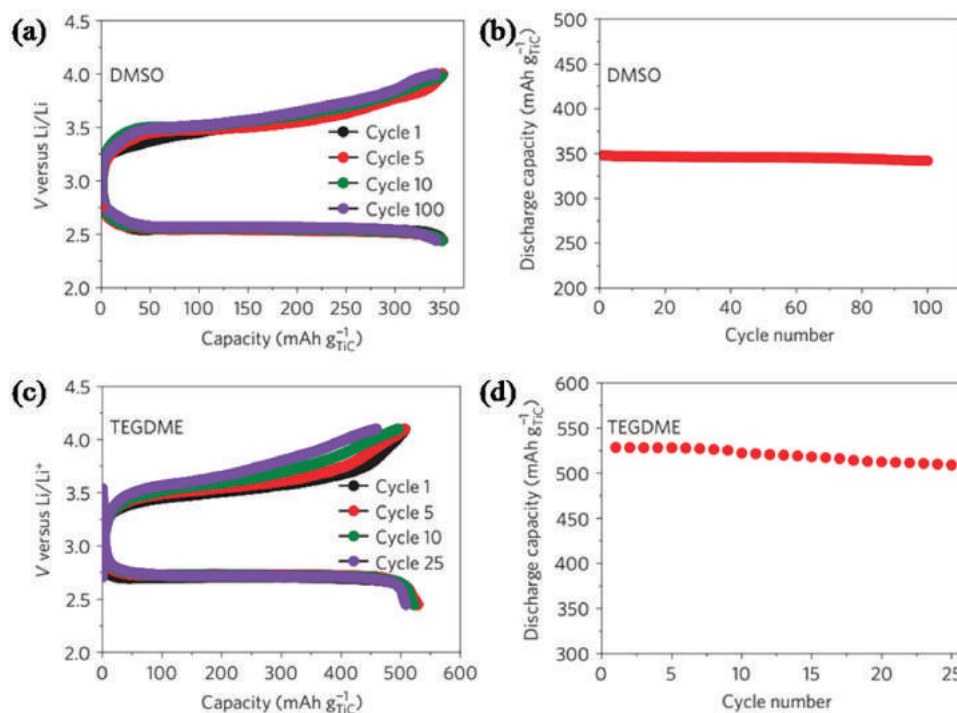
Figure 13. Galvanostatic discharge/charge cycles of Li-O_2 cells containing (a) 0.5 M LiClO$_4$ in DMSO (current density: 1 mA/cm^2) and (c) 0.5 M LiPF$_6$ in TEGDME (current density: 0.5 mA/cm^2). b, d) Capacity retention for the same cell as in (a) and (c), respectively. Reproduced with permission.[175] Copyright 2013, Nature Publishing Group.

cell was associated with almost entirely reversible formation/decomposition of Li$_2$O$_2$, while previously reported Li-O$_2$ batteries were partial Li$_2$O$_2$ formation/decomposition and limited cycling. An in-depth comparative investigation of the performance of Li-O$_2$ batteries using TEGDME- and DMSO-based electrolytes was carried by the same group.[175] The use of a nonCarbon TiC electrode and a DMSO-based electrolyte greatly reduced side reactions arising from electrolyte and electrode degradation. As shown in **Figure 13**, the battery demonstrated >98% capacity retention after 100 cycles, which is even better that that based on nanoporous gold electrode. Moreover, the battery achieved >99.5% purity of Li$_2$O$_2$ formation on each discharge and its complete oxidation on charge as evidenced by FTIR, NMR, XRD and DEMS analysis. In distinct contrast, the battery using TEGDME-based electrolyte showed much significant polarization with increasing cycle number and inferior capacity retention than that with DMSO-based electrolyte. Analysis on the formation of byproducts and ratios of the number of electrons to oxygen molecules during charge and discharge also confirm that DMSO was much more stable than TEGDME, highlighting its superiority in the application in Li-air battery.

Although DMSO-based electrolytes demonstrated promising performance for Li-air battery, a recent study by Shao-Horn's group showed that DMSO is still insufficiently stable against reduce oxygen species that spontaneously form LiOH.[176] In this study, Li$_2$O$_2$ was observed as the only species immediately after discharge, then gradually decomposed completely to form LiOH when prolonged exposed to the DMSO-based electrolyte. Furthermore, this study also showed that Li$_2$O$_2$ can decompose DMSO to DMSO$_2$, even worse,

the addition of KO$_2$ (act as a superoxide species) was found to accelerate the decomposition of DMSO and the conversion from Li$_2$O$_2$ to LiOH which indicated that DMSO is reactive to superoxide and peroxide species. These findings suggest that DMSO is still not sufficiently stable as a solvent for Li-air battery with long cycle life.

Several other organic electrolyte solvent based and mixed-solvent electrolytes and their application in Li-air battery have also been investigated.[157,177,178] Chen et al. reported a 0.1 M LiClO$_4$/dimethylformamide (DMF) electrolyte and studied its stability in Li-O$_2$ electrochemistry.[177] Formation and decomposition of Li$_2$O$_2$ was observed as the dominant reactions at the first cycle. Unfortunately, electrolyte degradation was observed with increasing cycle number, leading to the formation of byproducts including Li$_2$CO$_3$, HCO$_2$Li, CH$_3$CO$_2$Li, NO, H$_2$O, and CO$_2$. The accumulation of such byproducts during each cycle inevitably result in the fade in capacity and cyclability which indicate the insufficient use of DMF-based electrolytes in rechargeable Li-air batteries. Recently, Bardé et al. investigated the performance of three sulfones: ethyl vinyl sulfone (EVS), tetra methylene sulfone (or sulfolane, TMS), and ethyl methyl sulfone (EMS) as electrolyte solvents in Li-O$_2$ batteries.[178] A combined analysis of PXRD, FTIR, NMR, and MS was used to qualitatively and quantitatively study the electrolyte stability. Electrolyte degradation of electrolyte was observed for the three sulfone-based electrolytes, TMS and EMS were found to exhibit more stable cycling performance, whereas EVS, a liquid at room temperature was found least stable in the presence of oxygen species.

The charging process is associated with the oxidation of solid discharge product Li$_2$O$_2$ which is deposited on the surface

ADVANCED
SCIENCE NEWS
www.advancedsciencenews.com

ADVANCED
SUSTAINABLE
SYSTEMS
www.advsustainsys.com

of porous structured air cathode. The weak charge transport between solid Li_2O_2 particles and the cathode interface is a significant problem accounting for the large overpotential during charge. Incorporation of OER catalyst in the cathode has been considered as an effective approach to solve this problem. Note that the cathode catalysts can only facilitate the oxidation kinetics of Li_2O_2 at the interface of the cathode but non-functioning for that at the electrolyte-Li_2O_2 interface, leading to high overpotentials even at low rates. Recently, there's a trend of using dissolvable redox mediators in rechargeable nonaqueous aprotic Li-air batteries to facilitate the ORR and OER kinetics and lower the electrochemical overpotentials upon charge.[179–184] A redox mediator is a diffusible electrocatalyst and electrolyte additive that can be initially oxidized at the electrode surface then oxidize the Li_2O_2 particles to form Li^+ and O_2 gas while itself is reduced. Therefore, a redox mediator should meet several requirements, that is, highly dissolvable in the electrolyte, the redox potential should be slightly higher than that of Li_2O_2 (2.96 vs Li/Li^+), capable of efficiently decomposing Li_2O_2 at its oxidized form, and not reactive toward lithium metal and electrolyte. Chen et al. successfully introduced a redox mediator and effectively alleviated the problem of polarization during charge and greatly enhanced cycling performance of rechargeable Li-O_2 battery.[179] The reported cell was composed of a 1 M $LiClO_4$/DMSO dissolving tetrathiafulvalene (TTF), a nanoporous gold cathode, and $LiFePO_4$-based anode. Upon charge, the TTF was oxidized to TTF^+ at the cathode surface, which in turn oxidized the solid Li_2O_2 and lead to the regeneration of TTF. Experimental observation also showed that after the incorporation of the redox mediator, the cell was able to cycle at a high rate of 1 mA/cm², which was not possible for the cell in the absence of the mediator. As shown in **Figure 14**, with the increase of current density, the discharge/charge curves of the cell showed a slight raise in charge overpotential demonstrating

a stable reversible formation and decomposition of Li_2O_2 in the presence of TTF upon discharge/charge.

Later, the interest in the researches concerning redox mediator (RM) has been surging, various kinds of RM including LiI,[180] 2,2,6,6-tetramethylpiperidinyloxyl (TEMPO),[181] FePc,[182] LiBr,[183] DBBQ[184] etc. have been reported. To be specific, Bergner et al. have recently proposed that 2,2,6,6-tetramethylpiperidinyloxyl (TEMPO) can serve as a highly stable and efficient redox mediator for OER in Li-air batteries.[181] The use of TEMPO in a Li-O_2 cell lead to a distinct reduction of charge voltage and enhancement in cycle life and round-trip efficiency. Bergner et al. also studied the reaction mechanism with the addition of charge transfer mediators and found that a preliminary oxidation of Li_2O_2 without a direct electric contact to the current collector upon charge by the $TEMPO^+$ as evidenced by a huge gas evolution at the early stage of charging process and XRD analysis. Later in 2016, Liang reported the application of LiBr. With the help of the incorporated redox mediator, the charge reactions are transformed from electrochemical pathways to chemical pathways, which unexpectedly bypass the formation of highly reactive intermediates upon electro-oxidation of lithium peroxide. Such transformation reduces self-amplifying degradation reactions of electrode and electrolyte in the Li-O_2 cells. As a benefit, the Li-O_2 battery with this redox mediator exhibits much improved stability at higher charging rates and such research can provide insights for further relevant researches.

To briefly summarize, the development of electrolyte for metal-air batteries is a process that associated with the discovery of more rational solvents and metal salts. Among numerous relevant research in recent years, the majority was on the investigation of more stable and efficient electrolytes for nonaqueous aprotic Li-air battery system. Note that the electrochemistry in a nonaqueous environment is a rather complicated process
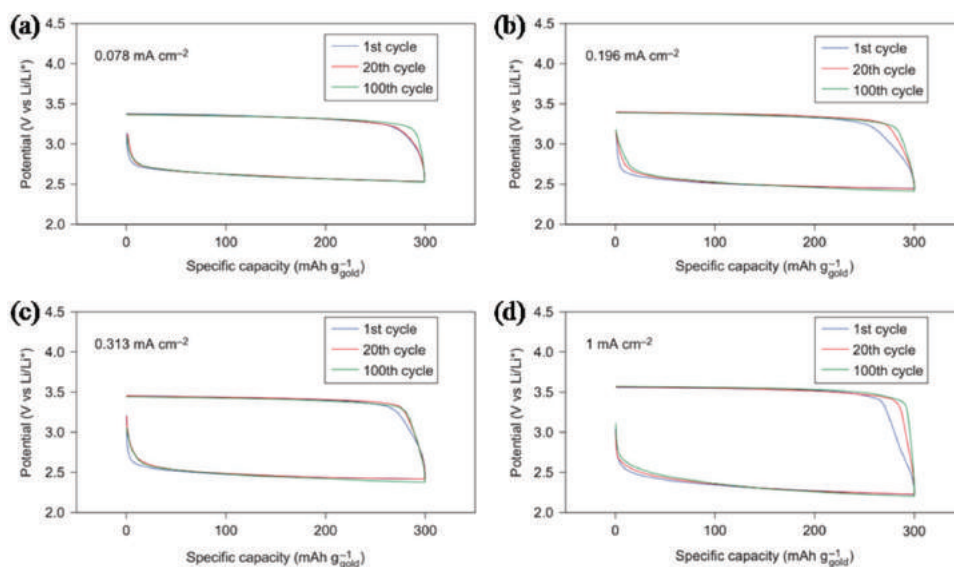
Figure 14. Cycling stability of Li-O_2 cathodes employ TTF as a redox mediator. a–d) Load curves (constant-current discharge/charge) for the first, 20th and 100th cycle of a cell with 1 M $LiClO_4$/DMSO contained 10 mM TTF at a nanoporous gold electrode under O_2, with rates increased from 0.078 mA cm⁻² (a) to 0.196 mA cm⁻² (b), to 0.313 mA cm⁻² (c) and to 1 mA cm⁻² (d). Reproduced with permission.[179] Copyright 2013, Nature Publishing Group.

**ADVANCED
SCIENCE NEWS**
www.advancedsciencenews.com

**ADVANCED
SUSTAINABLE
SYSTEMS**
www.advsustainsys.com

which may be concerned with a series of parasitic reaction of the solvents, salts, and air cathode (which will be discussed in section 4.2), which makes it difficult to develop a Li-air battery with satisfactory overall performances. For nonaqueous Na-air batteries, we don't consider this aspect due to a lack of systemic report on the investigation of electrochemical mechanisms and electrolytes. Other solutions and designs for the stability and performance issue of aprotic electrolytes have also been proposed, but the problems remained unsolved. Currently, developing a fully stable while efficient electrolytes lies as one of the priorities as they play a critical role in determining the electrochemical performance of metal-air batteries.

4. Cathodes

The cathode is also an important part of a metal-air battery where the ORR and OER (rechargeable metal-air battery) take place at its solid interfaces. An ideal air cathode should possess such properties as high electric conductivity, rational structural design, high catalytic activity, high electrochemical stability and structural integrity, and low-cost. Since the cathode reactive material is oxygen, the air electrode should have a porous structure to facilitate the dissolution diffusion of oxygen and electrolyte. The reaction kinetics at the cathode plays a critical role in determine the electrochemical performance of a battery such as rate capability, capacity, and cycling performance, which also requires the air electrode to have favorable catalytic activity for ORR and OER. Note that for metal-air batteries that utilize aqueous electrolytes (e.g., Zn-air, Al-air, Mg-air battery), the discharge products are dissolvable in the electrolytes, whereas the discharge products in Li-air and Na-air batteries that use nonaqueous aprotic electrolytes have little solubility in the electrolytes, deposit in the porous structure of the cathode, as discussed in section 2. On this account, the structural requirements of an air cathode for nonaqueous aprotic metal-air battery systems is much more rigorous, that is to say, the cathode should provide sufficient pore volume for the deposition of solid discharge products and at the same time prevent the clogging of diffusion paths for oxygen and electrolyte diffusion. In fact, the cathode is a substrate where the electrochemical processes occur. For both primary and secondary metal-air batteries, an ideal cathode can be used repeatedly in principle, which further highlight the significance of the research in this field.

4.1. Structural Design

Among the numerous literature reports concerning the field of metal-air batteries, plenty were dedicated to the study of the modification of cathode structure to achieve higher capacity, better rate capability and cycling performances.[185] A highly porous structure can provide diffusion paths and also function as a substrate for ORR and OER catalysts. As stated above, the insoluble discharge products of nonaqueous Li-air and Na-air battery may clog the diffusion path of oxygen, thus making the development of an air cathode is more complicated. In this section, we discuss the rational structural designs for metal-air

batteries with a highlight on the design of nonaqueous aprotic Li-air battery system as it has attracted considerable research interests.

Generally, an air cathode is composed of porous carbon, an electrocatalyst and a polymer organic binder. Different ratios of these compositions can have a great impact on the electrochemical and physical properties of a cathode including electric conductivity, porosity, catalytic activity, and wettability of electrolyte. During discharge process, the ORR takes place at the triple phase interfaces comprised of a solid (cathode), a liquid (electrolyte), and a gas (air/oxygen). On this aspect, a porous structure with high specific surface area can provide sufficient catalytic active sites as well as effective diffusion path for mass transport which is beneficial for the advance of rate capability and specific capacity. Carbon materials were mostly used in air cathodes owing to their excellent electric conductivity, good electrochemical stability, easy control of morphology, favorable ORR activity, and low cost, as evidenced by numerous related reports. Commercial carbon such as Ketjen Black (KB) and Super P (SP) Carbon were widely used in air cathodes at the early studies of metal-air batteries, these materials can also be seen in some commercial devices such as Zn-air battery. Other nanoporous Carbonaceous materials such as Carbon nanotubes (CNTs), graphene and their derivatives are also found to exhibit favorable performances. In order to accelerate the electrochemical kinetics, ORR and/or OER catalysts were also introduced into the porous structure of the air cathode (see section 5).

However, for metal-air batteries that use organic electrolytes, a porous cathode should not only provide diffusion paths for effective mass transport, but also accommodate the accumulation of solid discharge products, which sets a higher requirement to construct an air cathode. To date, it is well acknowledged that the meso-and macro-pores have the greatest contribution to the capacity of nonaqueous aprotic Li-air batteries, which can provide effective space for the deposition of discharge products (e.g., Li_2O_2, NaO_2, Na_2O_2, etc). Micro-pores can be effective for oxygen transportation but was also found to be easy clogged by solid discharge products which have little contribution to cell capacity. Thus the pore volume of meso- and macro-pores is considered as a limiting factor of discharge capacity. To this end, our group have proposed an ideal structure model of the air cathode for nonaqueous metal-air batteries, as illustrated in **Figure 15**.[15] The hierarchical porous structure is composed of interconnected macro-, meso-, and micro-pores which effectively facilitates electrolyte wetting, oxygen dissolution, mass transportation of oxygen and electrolyte. Such structure is also favorable for the deposition of solid discharge products and prevent pre-mature death origin from pore clogging of the aggregation of undiscoverable discharge products. Further, electrocatalyst are grown uniformly onto the porous structure to form a three-dimensional catalytic network which can allow a full utilization of the porous structure and better contact with discharge products to effectively enhance ORR and OER kinetics. This proposed cathode model is believed to display excellent physical and electrochemical performance such as good structure integrity and high capacity with fast formation and decomposition of solid discharge products.

Based on this cathode design, our group have recently reported a free-standing honeycomb-like palladium-modified

**ADVANCED
SCIENCE NEWS**

www.advancedsciencenews.com

**ADVANCED
SUSTAINABLE
SYSTEMS**

www.advsustainsys.com
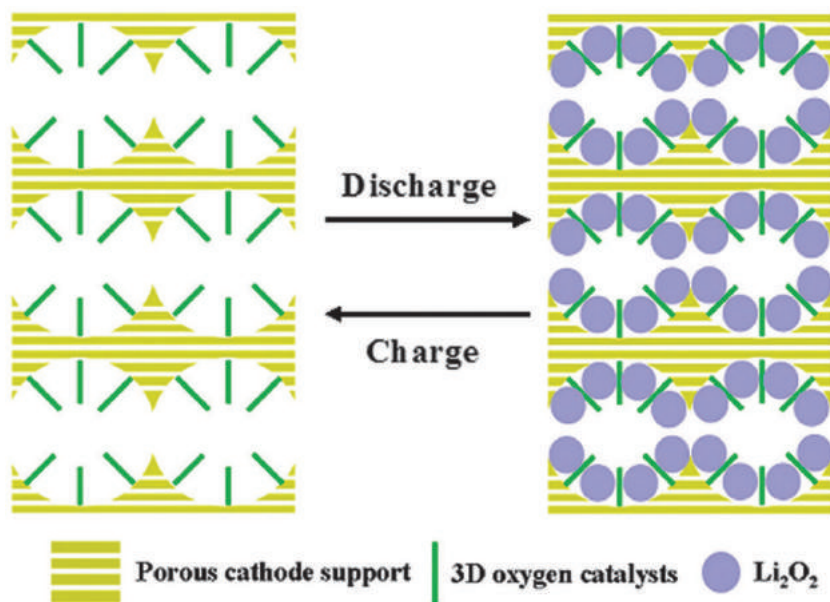
Figure 15. Proposed structure model of the air cathode for rechargeable nonaqueous metal-air batteries. Reproduced with permission.[15] Copyright 2014, The Royal Society of Chemistry.

behavior and morphology of the discharge product, leading to superior performance of high rate capability (5900 mAh/g at a current density of 1.5 A/g) and excellent cycling performance (205 cycles at a current density of 300 mA/g and a specific capacity limit of 1000 mAh/g, as shown in Figure 16c and d). Shao-Horn's group also proposed a design principle of air cathode to improve specific capacity and cycling performance of lithium-oxygen battery through a novel and facile biological method to synthesis structure-controlled metal oxides by using M13 virus as template.[187] This method allowed the formation of high aspect ratio metal oxide nanowires facilitating compositional control that outperforms those made by mechanical mixing. Moreover, the nanowires formed a hierarchical porous network which can maximize the interaction between the catalyst and discharge product, increasing reversibility and generating a stable cycle life of Li-O_2 battery. Furthermore, by incorporating only 3–5 wt% of Pd nanoparticles in the material, the corresponding Li-O_2 cell displayed a high specific capacity of 13,350 mAh/g at 0.4 A/g and a good cycling performance of 50 cycles (4000 mAh/g at 1 A/g.).

hollow spherical Carbon (P-HSC) deposited onto Carbon paper as a cathode for a Li-O_2 battery.[186] As shown in **Figure 16**a, mercaptopropylsilyl-functionalized silica spheres were firstly deposited onto the framework of Carbon paper using an electrophoretic technique, and then in situ-loaded with Pd NPs and covered with a Carbon shell. Figure 16b is the corresponding FESEM image of the morphology of the P-HSC deposited on carbon paper, showing the successful preparation of the hierarchical porous nanostructure. In addition, the P-HSC was firmly embedded into the framework of the CP without the addition of binder, emerging a free-standing structure and low-resistance pathways for electron transportation. When used as a cathode for Li-O_2 battery, the optimized structural design demonstrated great advantage in tailoring the deposition

4.2. Cathode Stability of Li-air Batteries

Apart from the instability issue of nonaqueous aprotic electrolyte in Li-air battery system, the instability of cathode was also discovered as another major cause of capacity fade, limited cycle number, and sever polarization problems.[188–191] Bruce's group reported that Carbon is relatively stable below 3.5 V (vs Li/Li$^+$) on discharge or charge, but oxidatively decompose to form Li_2CO_3 in the presence of Li_2O_2 when charged above
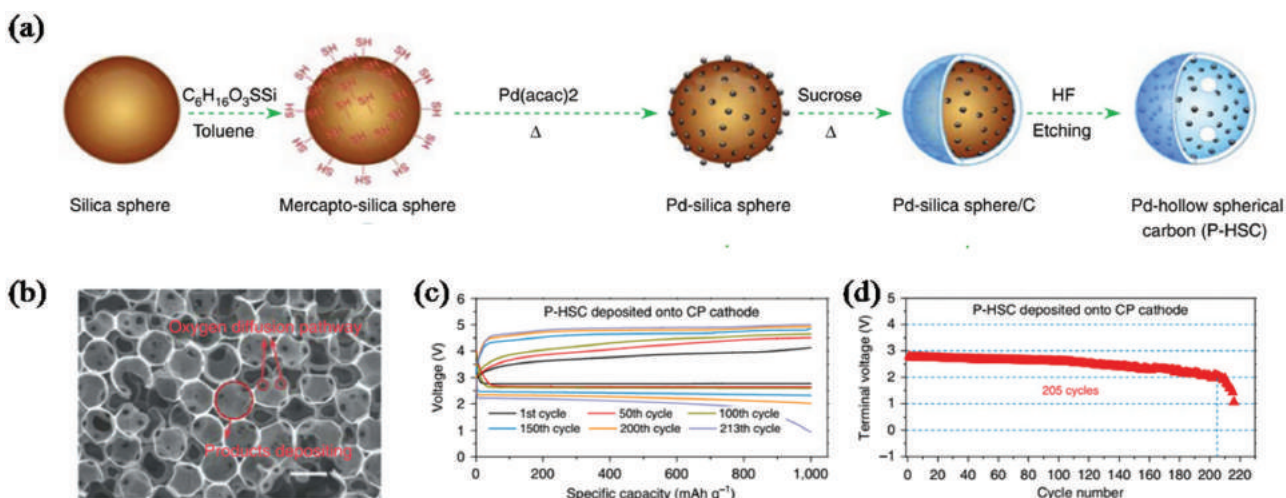
Figure 16. a) Schematic of the preparation of P-HSC. b) FESEM image of the prepared P-HSC deposited onto CP. The red arrows point out the hierarchically porous structure of P-HSC. Scale bar represents 500 nm. c) Discharge-charge curves and (b) variation of voltage on the terminal of discharge of the Li-O_2 cells with the P-HSC deposited onto CP cathode. Reproduced with permission.[186] Copyright 2013, Nature Publishing Group.

**ADVANCED
SCIENCE NEWS**
www.advancedsciencenews.com

**ADVANCED
SUSTAINABLE
SYSTEMS**
www.advsustainsys.com

Figure 17. Schematic illustration of the decomposition process of carbon electrode in Li-air battery during discharge and charge. Reproduced with permission.[188] Copyright 2013, American Chemical Society.
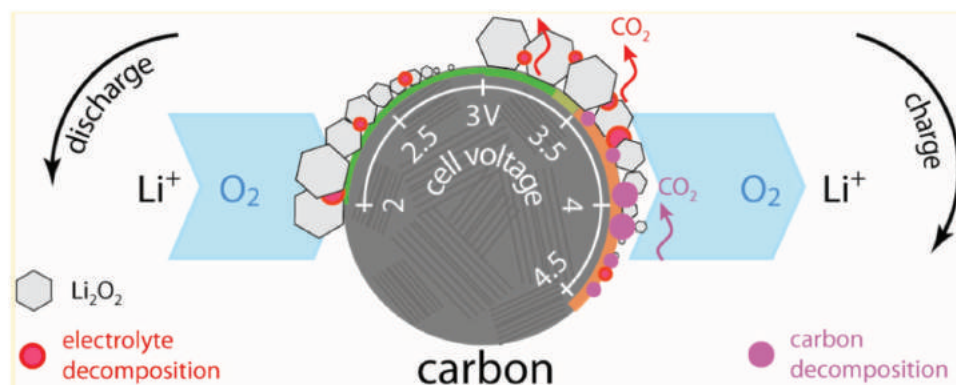
3.5 V (as illustrated in **Figure 17**).[188] It was found that the proportion of Carbon directly reacts with Li_2O_2 is small, however, Carbon can actively promote the decomposition of electrolyte on cycling, giving rise to byproducts such as Li_2CO_3 and Li carboxylates (of DMSO- and TEGDME-based electrolytes). Moreover, hydrophilic Carbon was found more catalytically active toward the degradation of electrolyte while those with a hydrophobic surface is relatively more stable. The formation and decomposition of Li_2CO_3 and Li carboxylates was also observed during discharge and charge, but oxidation of Li_2CO_3 on charging to ~ 4 V is incomplete which accumulates with the increasing cycle number, leading to sever polarization, fade in capacity, and reduce in cycle number. Experimental results also showed that Carbon may be relatively stable if the oxidation of Li_2O_2 can be operated below 3.5 V. This study demonstrates the issue of stable cycling is dependent on synergy between electrolyte and electrode which cannot be considered separately.

Polymer organic binder such as poly(vinylidene difluoride) (PVdF) is widely used in the preparation of air cathodes to ensure the physical structure integrity. Unfortunately, Nazar's group found that PVdF readily reacts with superoxide species to form dehydrofluorination and formation of H_2O_2 which further react with catalysts to the form of H_2O, and finally leading to the formation of LiOH at the presence of Li_2O_2. The hydroxide cannot be oxidized during charge, which accumulates and coats on the porous surface, resulting in the termination of the electrochemical of formation and decomposition of Li_2O_2. Binder-free designs of cathode were then widely investigated by researchers through various synthetic methods such as electrodeposition, hydrothermal, and chemical vapor deposition (CVD) to avoid the use of binder and further enhancing the stability of cathode. Later, Shao-Horn's group pointed out that defects and oxygenated functional groups (activated double bonds or aromatics) of Carbon can function as reactive sites to react with superoxide radicals to form carbonates, as evidenced by XPS results.[190] Superoxide radicals first promote nucleophilic addition or electron transfer reactions on these reactive sites, leading to epoxy-groups, and further converted into carbonates. As has been stated in section 3, the decomposition of electrolytes can also be originated from the defects on carbon surface,[90] indicating the modification of carbon materials by lowering or eliminating surface defects may be an effective approach to improve round-trip efficiency and prolong the cycle life of Li-air battery.

To this end, several approaches to stabilize the air cathode have been proposed by researchers. A cathode material architecture proposed by Lu et al. demonstrated as a possible solution to the instability of Carbon.[192] Through atomic layer deposition (ALD) process, the Carbon surface was firstly passivated by a Al_2O_3 protective layer to prevent the potential catalyzing the decomposition of the electrolyte and Carbon degradation with reduced oxygen species. Then Pd nanoparticles were attached to the surface as an effective OER catalyst to lower charge overpotential thus prevent the decomposition of Carbon and lithium peroxide. Experimental observations showed that a dramatic reduction in charge overpotential (≈0.2 V) was achieved which can be attributed to the high catalytic activity of Pd nanoparticles and efficient electronic transport at the Pd/C interfaces. In addition, the protective layer of Al_2O_3 blocked the reactive sites of Carbon surface which also played a part of contribution on lowering the charge overpotential. Kang et al. recently reported that the reactive sites of Carbon can be deactivated by an ionic solvate of DME and lithium nitrate ($LiNO_3$) through the electrochemical nitrogen doping of Carbon forming pyridinic structure during discharge.[193] This method was simple yet found effective in stabilizing Carbon and eliminating the release of CO_2 during charging. The authors also noted that N-doping process is not a sufficient requirement to eliminate CO_2 evolution given some ex situ processes cannot fully mitigate the reactive sites of Carbon to parasitic reactions. Zhou's group reported that a core-shell structure of CNTs uniformly coated with a RuO_2 shell can effectively prevent direct contact of Carbon with Li_2O_2, thus avoiding the formation of Li_2CO_3 from Carbon decomposition.[194] It was also observed that the RuO_2 coating layer largely preserved the structural properties of CNTs such as high specific surface area and porous structure. Moreover, the RuO_2 shell can also function as efficient bifunctional catalyst for ORR and OER, preventing the parasitic reaction at high charge overpotentials. The similar strategy was also reported by Xie et al., where a thin layer of FeO_x was grown in situ on three dimensionally ordered mesoporous (3DOM) Carbon by ALD technic.[195] In addition to the concept of preventing direct contact between Carbon and reduced oxygen species, Pd nanoparticles were further decorated on the cathode surface to lower the charge potentials. This

**ADVANCED
SCIENCE NEWS**

www.advancedsciencenews.com

**ADVANCED
SUSTAINABLE
SYSTEMS**

www.advsustainsys.com

work adopted a 3DOM structure which can provide unique hierarchical structure to facilitate the mass transportation of reactants as well as the accommodation of the deposition of Li_2O_2. Such design can not only enhance the cathode stability through conceal the Carbon surface and lower the charge overpotentials, but also significantly improved the specific capacity and rate capability of the $Li-O_2$ cell.

The above proposed approaches indicate that the stabilization of Carbon can be achieved by Carbon passivation and/or lowering the charge voltage below 3.5 V. Besides the above two methods, some non-Carbon materials were also found to exhibit excellent electrochemical stability in nonaqueous Li-air system to sustain favorable battery performance.[174,175,196–200] Bruce's group, as stated in section 2, utilized nanoporous gold and TiC as air cathodes to exclude the parasitic reaction associated with cathode stability to study the degradation of electrolytes. In this field, wang's group recently proposed that $TiSi_2$ nanonet can also serve as a stable cathode support with high surface area and conductivity.[196] To promote the ORR and OER kinetics, Ru nanoparticles were homogenously deposited on the surface of $TiSi_2$ nanonet using ALD technic. This cathode design significantly hindered the parasitic reaction correlated with cathode degradation and enable the $Li-O_2$ cell to be operated over 100 cycles with an average round-trip efficiency of more than 70%. Interestingly, the Ru nanoparticles were found to be selectively grown on b planes of the $TiSi_2$ nanonet, which could be resulting from different interface energetics. Since then, several other kinds of carbon-free cathodes have been reported,[197–206] such as mesoporous titanium nitride (m-TiN),[200] Ir/B_4C cathode,[201] and $TiN@Pt_3Cu$ cathode.[204] In the research by Kim,[200] the m-TiN possess a 2D hexagonal structure and large pores (>30 nm). Due to the well-aligned pore structure and decent electric conductivity of TiN, the battery reaction was quite reversible, resulting in robust cycling performance for over 100 cycles under a potential cutoff condition. And according to Luo,[204] a 3D array composed of one-dimensional $TiN@Pt_3Cu$ nanowires was synthesized and employed as a whole porous air electrode in a lithium–oxygen battery. Benefitting from the high electronic conductivity of the TiN nanowires and the highly efficient catalytic activity of Pt_3Cu, the constructed one-dimensional $TiN@Pt_3Cu$ nanowire array cathode demonstrates excellent energy conversion efficiency and rate performance in full discharge and charge modes. The discharge capacity is up to 4600 mAh g^{-1} along with an 84% conversion efficiency at a current density of 0.2 mA cm^{-2}, and when the current density increased to 0.8 mA cm^{-2}, the discharge capacity is still greater than 3500 mAh g^{-1} together with a nearly 70% efficiency. To a considerable extent, these researches associated with the construction of non-carbon cathode have highlighted the importance of rational design and synthesis of cathode in enhancing the performance of rechargeable $Li-O_2$ batteries, providing guideline for further researches in the field of non-carbon electrode. In these aspect,

5. Electrocatalysts

As presented in section 2, the cathode reactions of metal-air batteries are generally electrochemical processes involving oxygen reduction and/or oxygen evolution. Oxygen electrocatalyst in the cathode is thus crucial for the performance of a metal-air battery with respect to rate capacity, power density, cycling stability and capacity retention efficiency. For the past decades, ORR catalysts for fuel cells have been extensive investigated. The similarities shared between fuel cells and metal-air batteries can provide strategic and technic guidance to promote the development of high performance metal-air cathodes. Generally, most of the ORR catalysts for fuel cells are applicable to metal-air batteries, however, the inferior energy conversion efficiency resulting from poor OER activity is the major obstacle hindering the realization of a true rechargeable metal-air battery.[207,208] In recent years, great efforts have been devoted to the investigation of electrocatalysts for rechargeable Li-air batteries, further impelled the development in metal-air areas. A variety of materials have been reported to actively stimulate oxygen reduction and/or evolution, including (1) noble metals, alloys and oxides, (2) transition metal oxides, (3) Carbonaceous materials, (4) metal-nitrogen complex, and (5) conductive polymers. This section will mainly focus on the review of the characteristics of catalysts in direct relation to metal-air batteries, such as structural design, synthesis method, catalytic mechanism and activity, and so on. Considering the similarities and differences between different metal-air battery systems, one can find it inspirational that what is learned from one system can promote the development of other systems.

5.1. Noble Metals

Noble metals (such as Pt, Au, Pd, Ru, Ag, etc.), have been known as the most effective electrocatalyst and they are widely applied in the $Li-O_2$ battery.[209–230] As reported, Arava et al. reported the fabrication of Pt subnanocluster decorated N-doped single-walled carbon nanotube cathodes in 2016.[210] In this research, Pt/N-SWCNTs exhibited high discharge capacities of 7685 and 5907 mAh/g at 100 and 500 mA/g, respectively, and also good capacity retention. Moreover, a stable capacity of 3000 mAh/g with 100% Coulombic efficiency at 500 mA/g was demonstrated under repeated cycling conditions. While Wang et al.[213] reported the synthesis of an effective cathode catalyst of ruthenium nanocrystals supported on carbon black substrate by a surfactant assisting method. The as-prepared ruthenium nanocrystals exhibited an excellent catalytic activity as cathodes in $Li-O_2$ batteries with a high reversible capacity of about 9,800 mAh g^{-1}, a low charge–discharge over-potential (about 0.37 V), and an outstanding cycle performance up to 150 cycles (with a curtaining capacity of 1,000 mAh g^{-1}). The electrochemical testing shows that ruthenium nanocrystals can significantly reduce the charge potential comparing to carbon black catalysts, which demonstrated that ruthenium based nanomaterials could be effective cathode catalysts for high performance $Li-O_2$ batteries. In this aspect, a series of Ru-based researches,[214–220] such as network structured carbonized bacterial cellulose-supported Ru nanoparticles,[214] a three-dimensional (3D) mesoporous graphene-like carbon structure decorated with Ru particles,[215] ruthenium nanocrystal decorated vertical graphene nanosheets@Ni foam,[216] etc. have been published. To be specific, according to Want et al.[216] the Ru-decorated

ADVANCED
SCIENCE NEWS
www.advancedsciencenews.com

ADVANCED
SUSTAINABLE
SYSTEMS
www.advsustainsys.com

VGNS@Ni foam can significantly reduce the charge overpotential via the effects on the OER and achieve high specific capacity, leading to an enhanced electrochemical performance. The Ru-decorated VGNS@Ni foam electrode has demonstrated low charge overpotential of ≈ 0.45 V and high reversible capacity of 23 864 mAh g^{-1} at the current density of 200 mA g^{-1}, which can be maintained for 50 cycles under full charge and discharge testing condition in the voltage range of 2.0–4.2 V. Furthermore, Ru nanocrystal decorated VGNS@Ni foam can be cycled for more than 200 cycles with a low overpotential of 0.23 V under the capacity curtained to be 1000 mAh g^{-1} at a current density of 200 mA g^{-1}. In addition, other kinds of noble metals such as Pd,[221] Pt,[222] Au,[227] are also widely applied in Li-O$_2$ battery, which are not discussed in detail.

Despite the well-established investigation of the oxygen electrochemistry in aqueous systems for the past decades, the study of catalytic mechanisms in nonaqueous systems is relatively rare. In addition, the realization of a rechargeable metal-air battery require the capability of catalysts functioning both excellent ORR and OER activity. Owing to the increasing popularity gained in the nonaqueous aprotic Li-air battery research field in recent years, noble metals were the first to be investigated as cathode catalysts due to their superior activity in aqueous electrolytes.[231–239] A DFT study of ORR by lithium on Au (111) and Pt (111) indicated mechanistic details.[231] Early studies by Shao-Horn's group on the employed rotating disk electrode (RDE) measurements to quantify the activity of catalysts. It was reported that the ORR activity of Au was higher than that of Pt in the presence of lithium ions in aprotic electrolytes.[232] Another study by the same group showed that Au/C had the highest discharge activity, while Pt/C exhibited extraordinarily high charging activity.[233] By combine one catalyst that is highly active for ORR and another for OER can be an effective way to produce bifunctional catalyst. Based on this, PtAu nanoparticles homogenously dispersed on Carbon support were prepared to serve as bifunctional catalysts for nonaqueous aprotic rechargeable Li-O$_2$ batteries.[234] As shown in **Figure 18**a, a CV method was used to obtain the electrochemical surface area of PtAu nanoparticles which was estimated to be 38 ± 4 m^2/g$_{PtAu}$. The Li-O$_2$ battery based on PtAu/C catalyst delivered discharge and charge voltages that were comparable to that of Au/C and Pt/C, respectively. This was attributed to the high kinetics of surface Au and Pt atoms toward ORR and OER, separately. As a result, the overall voltage gap between charge and discharge was greatly reduced, leading to better round trip efficiency. Although subsequent research demonstrated that the electrolyte used in this work (PC/DME) suffer from some parasitic
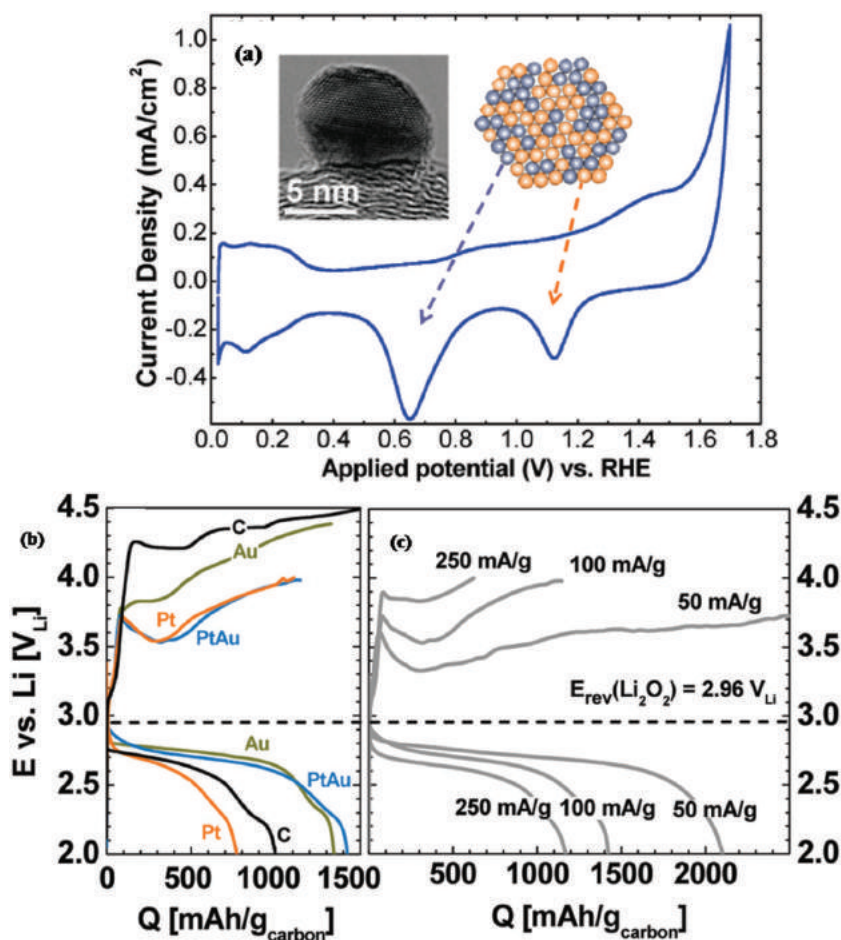
Figure 18. a) Cyclic voltammograms of PtAu/C (room temperature, 50 mV s^{-1}). Insets: (left) HRTEM image of PtAu/C; (right) schematic representation of PtAu, the arrows indicate the CV signatures for Pt (gray) and Au (yellow). b) First discharge/charge profiles of Li-O$_2$ cell with carbon at 85 mA/g$_{carbon}$ and Au/C, Pt/C, and PtAu/C catalysts at 100 mA/g$_{carbon}$. c) Discharge/charge profiles (first cycle) of PtAu/C at 50, 100, and 250 mA/g$_{carbon}$. Reproduced with permission.[234] Copyright 2010, American Chemical Society.

reactions, the concept proposed here is nevertheless enlightening. The impact of electrolytes will be discussed in detail in the following section. Later, the same group further performed a systematic investigation on the intrinsic ORR kinetics of polycrystalline Pd, Pt, Ru, and Au surfaces in a more stable 0.1 M LiClO$_4$ 1,2-dimethoxyethane electrolyte via RDE measurements.[235] It was found that the Li$^+$-ORR activity of these material surfaces was primarily associated with the oxygen adsorption energy, forming a volcano shape trend with Pd exhibiting the highest potential. More importantly, the activity trend of these polycrystalline surfaces was in good agreement with the trend in the discharge voltage of Li-O$_2$ batteries based on the nanoparticle catalysts.

The ability to operate under high rates is critical to the practical application of metal-air batteries, which is highly dependent on the catalyzed formation and deformation of discharge products upon cycling. The discharge rate capability of rechargeable Li-O$_2$ batteries based on Vulcan Carbon (VC) and Au/C were studied in the range of 100 to 2000 mA/g$_{Carbon}$.[236] To eliminate the impact of the parasitic reactions of PC-based

**ADVANCED
SCIENCE NEWS**

www.advancedsciencenews.com

**ADVANCED
SUSTAINABLE
SYSTEMS**

www.advsustainsys.com

Figure 19. Charge–discharge curves (a) and cycling profile (b) of Li-O$_2$ battery with a 0.1 M LiClO$_4$-DMSO electrolyte and a NPG cathode, at a current density of 500 mA g^{-1} (based on the mass of Au). Reproduced with permission.[174] Copyright 2012, American Association for the Advancement of Science.

electrolyte, the rate capability of Li-O$_2$ batteries were tested with 1,2-dimethoxyethane electrolyte. It was found that Li-O$_2$ cells based on Au/C catalyst exhibited higher discharge voltage than that based on VC at both low rates and high rates. This phenomenon can be attributed the higher activity of Au/C for ORR at low rates, while at high rates, the faster lithium transport in nonstoichiometric and defective lithium peroxide formed upon discharge on air cathodes based Au/C could be ascribed to the higher discharge voltage. Later, Bruce et al. demonstrated a higher rate Li-O$_2$ battery based on nanoporous gold (NPG) cathode and a stable dimethyl sulfoxide (DMSO) electrolyte.[174] Considering the high mass density of Au (≈10 fold greater than Carbon), the current density based on Au would, for example 500 mA/g, correspond to ≈5000 mA/g for the same porous cathode based on Carbon. Due to the synergistic effect of the fast kinetics of the formation and decomposition of Li$_2$O$_2$ and e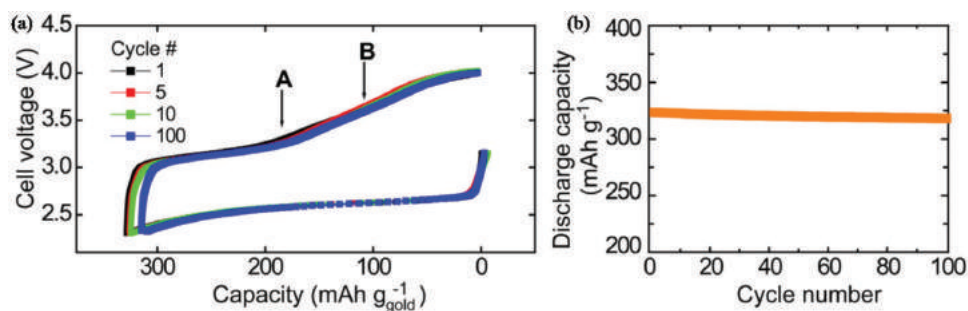ffective mass transportation of reactants on the NPG cathode, the Li-O$_2$ battery exhibited 95% capacity retention after 100 cycles (as shown in **Figure 19**), which is still a high value up to now. However, the fabrication of a NPG cathode is rather complicated which remain as challenge for practical applications Charge profiles (first cycle) of PtAu/C at 50, 100, and 250 mA/g$_{Carbon}$.[234]

Nonaqueous aprotic Li-O$_2$ batteries based on other noble metals are also recently investigated. Recently, Pd nanodendrites with an average size of approximately 14 nm have been strongly anchored on graphene nanoplatelets to produce a catalyst, based on which the Li-O$_2$ battery has exhibited good performance.[237] In other research, Yoon and co-workers exploit two types of double-walled RuO$_2$ and Mn$_2$O$_3$ composite fibers,[238] i.e., (i) phase separated RuO$_2$/Mn$_2$O$_3$ fiber-in-tube (RM-FIT) and (ii) multicomposite RuO$_2$/Mn$_2$O$_3$ tube-in-tube (RM-TIT), by controlling ramping rate during electrospinning process. Both RM-FIT and RM-TIT exhibited excellent bifunctional electrocatalytic activities in alkaline media. The air electrodes using RM-FIT and RM-TIT showed enhanced overpotential characteristics and stable cyclability over 100 cycles in the Li-O$_2$ cells, demonstrating high potential as efficient OER and ORR catalysts.

It should be noted that despite the excellent ORR and OER activity of noble metals, their high cost remains as the biggest challenge that hinders their large-scale application in metal-air batteries. To find alternative low-cost catalysts, researchers have focused on the investigation of transition metals, carbonaceous

materials, and so on. These materials demonstrated promising performances in different metal-air systems, which we will discuss in detail in the following sections.

5.2. Transition Metal Oxides and Nitrides

Non-precious transition metal oxides probably represent the most interesting class of oxygen catalysts. They possess advantages such as abundant reserve in earth, low-cost, easy preparation and environmental friendliness. In addition to the catalytic use, their application in LIBs and SCs are widely investigated owing to their unique tunable structure. In recent years, they are generally accepted as promising substitutes to traditional noble metals for metal-air batteries. To date, various transition metal based electrocatalysts have been reported, which demonstrated preferable oxygen catalytic activity and general stability under alkaline electrolyte.[240,241] To be specific, transition metal oxides can also be divided into mixed metal oxides, such as spinel-type and perovskite-type oxides. Among all the transition metal based oxygen electrocatalysts reported so far, transition metal oxides and nitrides account for a certain proportion, demonstrating promising application in metal-air batteries. Thanks to the rapid development of ORR catalysts for fuel cells, most of these catalysts can be applied to metal-air batteries using alkaline electrolyte with minor modification. However, as discussed in the device configuration section, metal-air batteries such as Li-air battery utilizing nonaqueous electrolytes can improve the energy density compared to those using aqueous electrolytes, by introducing different reaction mechanisms. Thus, the ORR catalysts cannot be directly used in non-aqueous metal-air batteries, owing to the rather different electrochemical mechanisms. In this section, we mainly focus on the discussion of transition metal oxides, including synthetic methods, inherent structure, catalytic activity and mechanism, with respect to the application environment. Other transition-metal-based catalysts, such as carbides, carbonitrides and oxynitrides are also covered.

5.2.1. Single Metal Oxides

Single metal oxides, such as manganese oxides (MnO$_x$) and cobalt oxides (CoO$_x$), have attracted great research interests

ADVANCED
SCIENCE NEWS
www.advancedsciencenews.com

ADVANCED
SUSTAINABLE
SYSTEMS
www.advsustainsys.com

in the field of metal-air batteries due to their excellent oxygen electrochemical catalytic activity and low cost.[242] Notably, manganese oxides have received considerable attention and were widely investigated as one of the most promising candidates as bifunctional catalysts to replace noble metals. The variable valence states of manganese correspond to a variety of oxides, ranging from MnO, Mn_2O_3, Mn_3O_4 and MnO_2, each demonstrating different crystal structures. In addition, they also possess prominent advantages such as low cost, environmental-friendliness and high chemical stability. The unique and interesting properties of MnO_x give rise to rich redox electrochemistry and materials chemistry, which provide plenty of opportunity for the investigation of non-noble electrocatalysts for metal-air batteries. Since the first report of the study of MnO_x for ORR in the early 1970s,[243] many researchers have made great efforts to examine and optimize their electrochemical behavior for high performance air cathodes.[244–264] Their catalytic activity toward ORR and OER was also investigated as functions of chemical composition, crystalline structure, oxidation state, and morphology.[241,262–270] For example, the catalytic activity of MnO_2 toward ORR in alkaline media was reported by Cheng et al. following the sequence of α- > β- > γ-MnO_2.[262] This difference in catalytic activity can be attributed to the different configuration of the basic structural unit of MnO_2 ($[MnO_6]$ octahedron), which is correlated to the tunnel size that influence the insertion and transfer of ions in the lattice framework. The α-MnO_2 structure is that of hollandite and consists of double chains of $[MnO_6]$ octahedron with the tunnel structure of (2×2) and (1×1), which can facilitate the adsorption and accommodation of oxygen and lithium ions. Moreover, it was reported that α-MnO_2 contain more defects and $-$OH groups, which are beneficial to the surface adsorption of O_2 and dissociation of O—O bonds. Ohsaka's group found that the peak current varies greatly depending on the kind of MnO_x species incorporated in the MnO_x/Nafion-modified gold electrode.[265] The activity of MnO_x in alkaline solution was then found to follow the order of $MnOOH > Mn_2O_3 > Mn_3O_4 > Mn_5O_8$.

In addition to the chemical composition and crystal structure, the morphological structure, which relates to surface area and catalytic sites, also plays an important role in oxygen electrochemistry of MnO_x. It was also found that α-MnO_2 nanospheres and nanowires outperform the counterpart microparticles.[262] Benbow et al. also compared the catalytic activity of α-MnO_2 catalysts with different morphologies in both alkaline and nonaqueous electrolytes.[269] Among all the prepared catalysts, nanorod-type α-MnO_2 obtained from a solvent-free method demonstrated the highest ORR activity in both aqueous and nonaqueous media. This can be ascribed to the small crystallite size, low average oxidation state of manganese, high surface area, and large pore volume. Generally speaking, catalytic activity of nanostructures exceed the bulk particles owing to their smaller size and higher surface area. With the decrease in size, the reactivity can be enhanced by larger surface-to-bulk ratio and numerous surface defects. Higher surface area permits more active sites for the contact between reactants and electrolyte. Based on α-MnO_2 nanowires as cathode catalyst, Bruce et al. demonstrated a Li-O_2 cell with a capacity of 3 000 mAh/g and good cycling stability (**Figure 20**).[241] The excellent performance of α-MnO_2 against other closely related manganese oxides can be attributed to the synergistic effect of the unique
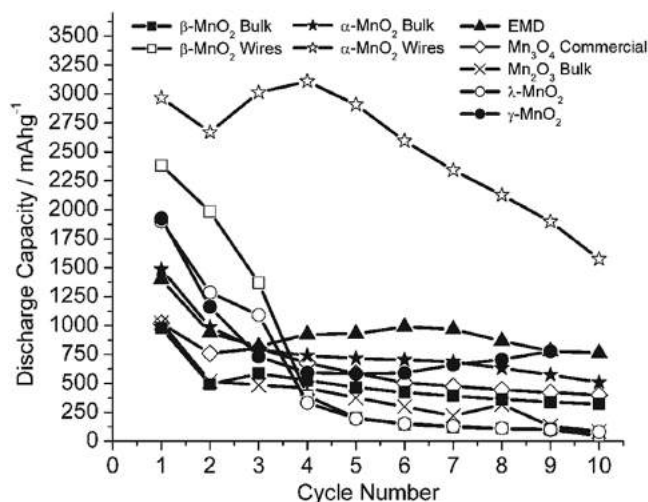
Figure 20. Variation of discharge capacity with cycle number for several porous electrodes containing manganese oxides as catalysts: α-MnO_2 in bulk and nanowire form, β-MnO_2 in bulk and nanowire form, γ-MnO_2, λ-MnO_2, Mn_2O_3, and Mn_3O_4. Cycling was carried out at a rate of 70 mA g^{-1} in 1 atm of O_2. Reproduced with permission.[241]

crustal structure and the porous morphology character. This is a very early report of the catalytic performance of MnO_x in nonaqueous Li-O_2 battery systems, and inspired significant investigation of the catalytic activity of MnO_x in this area. Our group also reported γ-MnOOH nanowires synthesized by a simple one-step hydrothermal method as cathode catalysts for rechargeable nonaqueous Li-O_2 battery.[260] The loose and porous structure provided excess void space, which is beneficial for the storage of discharge products, flow of gases, and soak of the electrolyte. In accordance with that reported by Bruce et al., great improvements in discharge capacity, cycle stability, and rate retention were obtained. By using atomic layer deposition (ALD), Katie et al. investigated the ORR and OER performances of MnO_x deposited on glassy carbon.[244] This method can achieve complex nanostructured designs and allow conformal deposition of catalytic thin films onto complex substrates. Results showed that the catalytic activity of catalysts synthesized though ALD is comparable to the best MnO_x catalysts in the literature, demonstrating a viable way to produce highly active and conformal thin film catalysts. Compared with noble metal catalysts, however, manganese oxides are generally less active, especially in terms of overpotentials and the capability to catalyze 4-electron reduction. In order to enhance the catalytic performance, strategies such as doping with cations, coating with metals, and integrating conductive nanostructures were reported by researchers.[262,271–276] Roche et al. proposed that a four-electron ORR mechanism can be observed from doped MnO_x/C.[272] The ORR process can be concluded as follows:

$$MnO_2 + H_2O + e^- \leftrightarrow MnOOH + OH^-$$

$$2MnOOH + O_2 \leftrightarrow (MnOOH)_2 \cdots O_{2,ads}$$

$$(MnOOH)_2 \cdots O_{2,ads} + e^- \rightarrow MnOOH \cdots O_{ads} + OH^- + MnO_2 \, (rds)$$

$$MnOOH \cdots O_{ads} + e^- \leftrightarrow MnO_2 + OH^-$$

**ADVANCED
SCIENCE NEWS**
www.advancedsciencenews.com

**ADVANCED
SUSTAINABLE
SYSTEMS**
www.advsustainsys.com
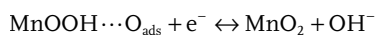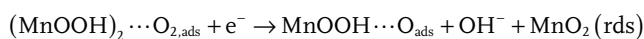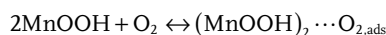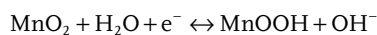
The first step of the proposed mechanism is probably the quasiequilibrium proton insertion process into MnO_2 leading to the formation of MnOOH. The second step is the adsorption of O_2 onto tow MnOOH surface sites while the third step is the electrosplitting process of the $O_{2,ads}$ species which is the rate determining step. The final step is electrochemical reduction of O_{ads} to OH^-. The coexistence of Mn^{3+} and Mn^{4+} redox species are believed to act as oxygen acceptor and donor mediator, respectively, which assist electron transfer to molecular oxygen, thus facilitate the ORR. Doping of divalent cations, such as nickel and magnesium, can stabilize the Mn^{3+} and Mn^{4+} species and enhance the ORR activity. Recently, Chen's group reported a simple and economic strategy to enhance the activity of rutile-type β-MnO_2 by introducing native oxygen defects without modification by foreign additives, as shown in **Figure 21**a.[264] Oxygen deficiencies were introduced into manganese oxides by simple heat treatment under different condition. XRD patterns in Figure 21b indicate that heat treatment in Ar and air lead to oxygen non-stoichiometry, which is compensated by the reduction of Mn^{4+} to Mn^{3+}. In Figure 21d, two domains can be observed after heat treatment in Ar, which indicate the formation of a typical pyrolusite lattice and a new structure that corresponds to a different fast Fourier transformation (FFT) pattern. The new lattice fringes and FFT profile can be attributed to phase reconstruction and transformation, which correspond to oxygen-vacancy-induced structural variations of MnO_2. Both experimental and DFT computational studies showed that MnO_2 catalyst with a modest concentration of oxygen vacancies renders more prominent improvement in currents, potentials, and electron transfer toward ORR.

In addition to the widely investigated manganese oxides, cobalt oxide (Co_3O_4) is another important and promising candidate to replace noble metal catalysts. The bifunctional catalytic of Co_3O_4 in alkaline electrolyte and tunable composition have been reported by some researchers.[277–288] Co_3O_4 can be shown to be $Co^{2+}[Co_2^{3+}]O_4^{2-}$ with a spinel crystal structure based on a close-packed face centered cubic configuration of O^{2-} ions, in which Co^{2+} ions occupy the one-eighth of the tetrahedral A sites while Co^{3+} ions occupy one half of the octahedral B sites.[277] Since the ORR is a surface-structure sensitive reaction and the catalytic activity is largely associated with the cations in a higher oxidation state on the surface, so the exposed Co^{3+} sites play predominant roles for ORR. Based on this, an effective approach is to increase the exposed Co^{3+} cations through nanoengineering of the structure of Co_3O_4. Recently, Xu et al. reported carbon-supported Co_3O_4 nanoparticles with rod and spherical structures prepared in the mixed water and dimethyl-formamide (DMF) solvent and tailored the morphology to increase the ratio of surface-exposed Co^{3+} cations.[278] The Co_3O_4 with the nanorod structure prepared with a moderate ratio of water to DMF exhibited the highest catalytic activity, even exceeded that of noble Pd catalyst at the low potential region. This facile optimization method of Co_3O_4 catalyst provides an effective way to enhance catalytic activity for ORR. It should be noted that Co_3O_4 is a p-type semiconductor, thus the use of conductive additives is necessary. Zhao and co-workers

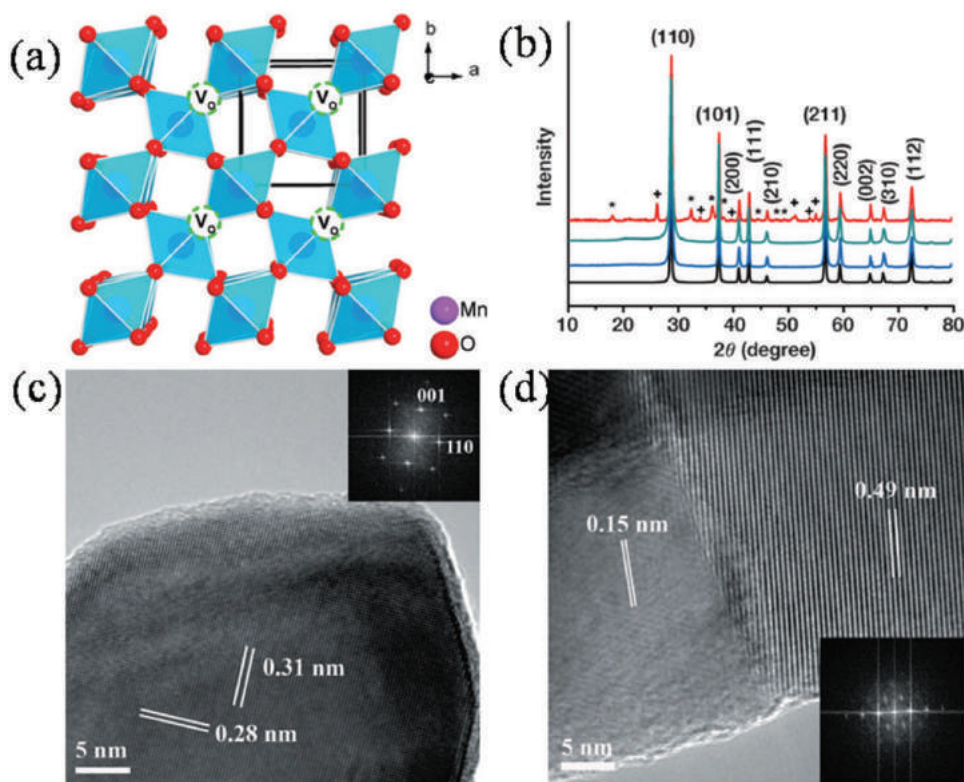**Figure 21.** a) Structure of rutile-type MnO_2 with oxygen vacancies. b) XRD patterns of different oxides. The symbols * and + denote Mn_3O_4 and MnOOH, respectively. From top to bottom: H_2/Ar-350-2h, Ar-350-2h, Air-350-2h, and pristine (c) and (d) HRTEM images of pristine β-MnO_2 (c) and β-MnO_2 heated in Ar (d), the insets show the FFT patterns. Reproduced with permission.[264]

**ADVANCED
SCIENCE NEWS**

www.advancedsciencenews.com

**ADVANCED
SUSTAINABLE
SYSTEMS**

www.advsustainsys.com

reported a hybrid material consisting of graphene-Co_3O_4 composite with a unique sandwich-architecture.[279] The obtained composite shows enhanced catalytic activities in both alkaline and neutral electrolytes. The onset potential towards the oxygen evolution reaction is 0.406 V (vs Ag/AgCl) in 1 M KOH solution, and 0.858 V (vs Ag/AgCl) in neutral phosphate buffer solution (PBS), respectively. The current density of 10 mA cm^{-2} has been achieved at the overpotential of 313 mV in 1 M KOH and 498 mV in PBS. The graphene-Co_3O_4 composite also exhibited an excellent stability in both alkaline and neutral electrolytes. In particular, no obvious current density decay was observed after 10 hours testing in alkaline solution and the morphology of the material was well maintained, which could be ascribed to the synergistic effect of combining Co_3O_4 and graphene. Owing to the excellent bifunctional catalytic performance in alkaline, Co_3O_4 can be found in many literatures concerning Zn-air batteries. Recently, Dai's group reported primary and rechargeable Zn-air batteries with novel CoO/CNT hybrid as ORR catalyst and Ni-Fe-layered double hydroxide (NiFe LDH) as OER catalyst for air cathode.[285] Surprisingly, these catalysts exhibited higher catalytic activity and durability in concentrated alkaline electrolytes than precious metal Pt and Ir catalysts. The primary Zn-air battery based on the CoO/CNT hybrid material catalyst demonstrated large discharge current densities with an unprecedented peak power density of ≈265 mW cm^{-2}. The ORR hybrid catalyst also showed high durability, which allowed the battery to run continuously and consistently by refueling the Zn anode and electrolyte periodically. The satisfying results indicate an ideal air catalyst for Zn-air fuel cells or Zn-air flow batteries for electrical vehicles. Among a handful of reports on rechargeable Zn-air batteries, this report successfully developed a Zn-air battery with low charge–discharge polarization of only ≈0.7 V and excellent cycling stability. Compared to aqueous systems, the application of Co_3O_4 in nonaqueous systems is relatively less reported, which is not the scope of our manuscript.

It should be noted that the metal-air battery system is still undergoing extensive investigation, chances are that some high performance cathode catalysts are yet to be found, especially in the nonaqueous aprotic Li-air battery system where the electrochemistry is quite different from that of the aqueous and solid-state systems. Other metal oxides such as NiO, CuO, Fe_xO_y also exhibit intrinsic activity toward oxygen electrochemistry. Bruce and co-workers used H_2O_2 decomposition reaction as selecting tool to screen some conventional oxygen electrocatalysts, such as Fe_2O_3, Fe_3O_4, NiO, CuO and mixed metal oxides $CoFe_2O_4$. The results showed that Fe_2O_3, NiO and $Li_{0.8}Sr_{0.2}MnO_4$ are not favorable for nonaqueous Li-air battery since the performance is undesirable. On the other hand, Fe_3O_4, CuO and $CoFe_2O_4$ exhibited good capacity retention, Co_3O_4 demonstrated the best compromise between discharge capacity and cycling performance.

5.2.2. Mixed Metal Oxides

In addition to single metal oxides, mixed metal oxides with spinel, perovskite and pyrochlore structure are also widely reported as cathode catalysts for metal-air batteries. Their interesting and unique electrochemical and physical properties were also reported to be promising electrode materials for FCs, LIBs and SCs. For catalytic use, the high electrochemical activities were acknowledged to be owing to the complex chemical compositions and the synergetic effects. Nanoparticle size and crystalline structure and be affected by the different constituents of mixed metal oxides. Furthermore, compared with single metal oxides, the introduction of multiple valence cations in mixed metal oxides can help to obtain the desirable electrochemical behavior of electrocatalysts by providing donor–acceptor chemisorption sites for the reversible adsorption of oxygen towards cathode oxygen reactions for metal-air batteries.[289–291]

5.2.2.1. Spinel-type Oxides: Spinel compounds can be described as AB_2X_4, where A represents a divalent metal ion in a tetrahedral site (e.g., Mn, Fe, Co and Ni), B represents a trivalent metal ion in an octahedral site (e.g., Al, Fe, Co and Mn), and X represents a chalcogen ion. Spinels can be classified as normal, inverted or random with respect to different crystal structure, which is, in the spinel structure, A and B site cations can occupy part or all the tetrahedral and octahedral sites, respectively.[292] Owing to the diversity of compositions, spinels exhibit a number of interesting properties which can be applied in many aspects, including magnetism, electronics and catalysis. For catalytic applications, mixed valence oxides of transition metals with a spinel structure display electrical conductivity or semi-conductivity, and thus can be directly used as cathode materials. The unique structure of mixed valance cations enables electron transfer with relatively low activation energies through a hopping process. Many researchers have reported a variety of spinels exhibiting ORR and OER catalytic activity in alkaline conditions. As an important class of metal oxides, spinels show very promising applications in metal-air batteries due to the high activity, low cost, simple preparation and high stability, the application of which in the alkaline solution and metal-air battery will be discussed briefly and separately.[293–319] In the alkaline solution, Xu et al. reported the application of $CoFe_2O_4$/graphene nanohybrid, which is is facilely synthesized via a two-step process, as an efficient bi-functional electrocatalyst for oxygen reduction reaction and oxygen evolution.[298] It is reported that at the same mass loading, the Tafel slope of $CoFe_2O_4$/graphene electrocatalyst for the ORR is comparable to that of the commercial Pt/C (20 wt% Pt on Vulcan XC-72, Johnson Matthey). The ORR on $CoFe_2O_4$/graphene mainly favors a direct 4e$^-$ reaction pathway. The $CoFe_2O_4$/graphene nanohybrid also affords high catalytic activity for the OER. The chronoamperometric tests show that $CoFe_2O_4$/graphene catalyst exhibits excellent stability for both the ORR and the OER, outperforming the commercial Pt/C. The high electrocatalytic activity and durability of $CoFe_2O_4$/graphene nanohybrid are attributed to the strong coupling between $CoFe_2O_4$ nanoparticles and graphene. While in another report, $NiCo_2O_4$ (NCO) spinel nanowire arrays were synthesized as a bifunctional catalyst for the oxygen reduction and evolution reaction.[303] The catalytic activity of spinel nanowire arrays for the ORR and the OER in 0.1 M KOH solution has been studied by using a rotating ring-diskelectrode (RRDE) technique. RRDE results show that the NCO spinel nanowire array catalyst exhibits excellent catalytic activity for the ORR. The ORR mainly favors a direct four electron pathway, which is close to the behavior of the Pt/C (20 wt% Pt on carbon) electrocatalyst under the same

**ADVANCED
SCIENCE NEWS**

www.advancedsciencenews.com

**ADVANCED
SUSTAINABLE
SYSTEMS**

www.advsustainsys.com

testing conditions. Anodic linear scanning voltammogram results show that the NCO spinel nanowire array catalyst is more active for the OER. The chonoamperometric and cyclic voltammogram results show that the NCO spinel nanowire array catalyst exhibits excellent stability and reversibility for the ORR and OER. In addition to the their application in the alkaline, various kinds of spine oxides are also applied in the metal-air battery. For example, the Shanmugam et al. has reported the application of hierarchical nanostructured $NiCo_2O_4$ as an efficient bifunctional non-precious metal catalysts for rechargeable zinc-air batteries.[306] In his report, the hierarchical nanostructured 1D-spinel $NiCo_2O_4$ materials showed a remarkable electrocatalytic activity towards oxygen reduction and evolution in an aqueous alkaline medim. The extraordinary bifunctional catalytic activity towards both ORR and OER was observed by the low overpotential (0.84 V) which is better than that of noble metal catalysts [Pt/C (1.16 V), Ru/C (1.01 V) and Ir/C (0.92 V)], making them promising cathode materials for metal–air batteries. Furthermore, the rechargeable zinc–air battery with NCO-A1 as a bifunctional electrocatalyst displays high activity and stability during battery discharge, charge, and cycling processes.

5.2.2.2. Perovskite-type Oxides: Another important class of transition metal oxide electrocatalysts is perovskite, with a chemical structure of AA′BB′O_3 where A, A′ represent rare-earth or alkaline-earth metal ions (e.g., La, Ca, Sr, etc.), and B, B′ represent transition metal ions (e.g., Co, Mn, Fe, etc.). Owing to their

excellent ORR catalytic abilities in both acid and alkaline media, perovskite oxides received extensive attention.[320–333] Generally speaking, A-site substitution mainly affects the ability of adsorbed oxygen, whereas B-site substitution influences the activity of adsorbed oxygen. Therefore, their properties can vary with a wide range with various replacements forming a wide variety family of perovskite oxides without disturbing the basic crystal structure. Their catalytic activity can be attributed to the ability of the transition metal cations to adopt different valance states, especially when they form redox couple within the potential of ORR and OER.

The first report in literature on perovskite electrocatalysts toward ORR was conducted by Bockris and Otagawa in the 1980s.[334] It was proposed that the ORR activity might be correlated with the number of d-electrons of transition metal cations. Up to now, a great deal of information with respect to the physical and solid-state chemical properties has been accumulated of this kind of interesting mixed metal oxide. However, there is still lack of fundamental understandings of the ORR mechanism and relation between material property and catalytic activity. In order to identify the material properties (descriptors) that govern their intrinsic ORR activities, Shao-Horn et al. investigated 15 type of perovskites by altering the A-site and B-site substitutions.[335] A previous proposed methodology of thin film rotating-disk electrode was introduced to allow a more accurate comparison of the ORR activities of different transition-metal oxides, which can enable well-defined
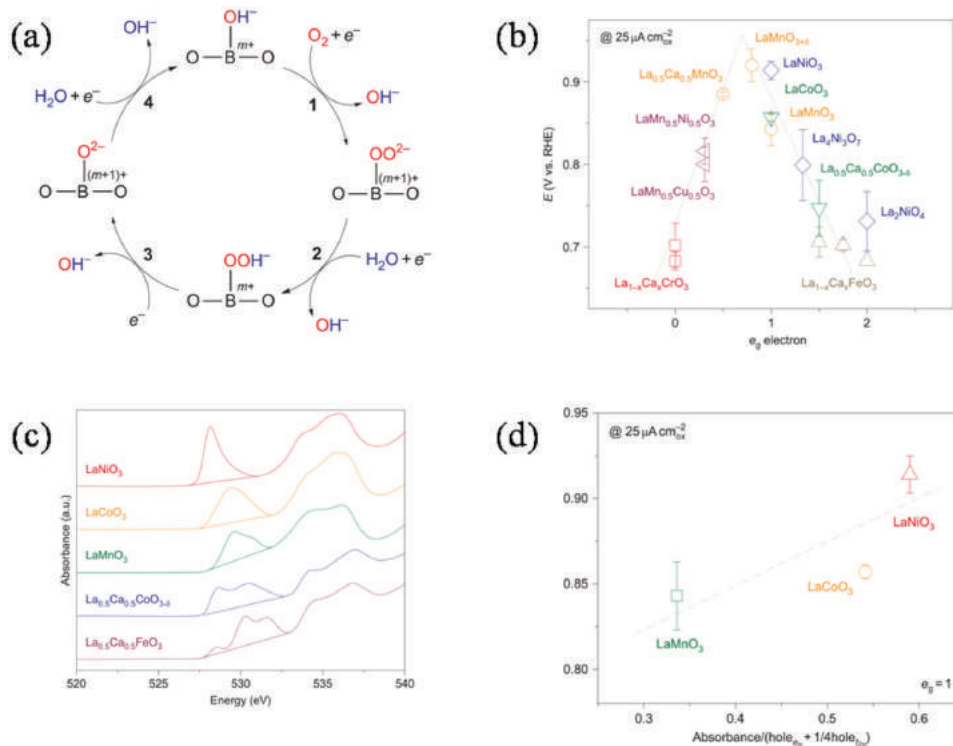
Figure 22. a) Proposed ORR mechanism on perovskite oxide catalysts. The ORR proceeds via four steps: 1) surface hydroxide displacement; 2) surface peroxide formation; 3) surface oxide formation; 4) surface hydroxide regeneration. b) Potentials at 25 $\mu A/cm_{ox}^2$ as a function of e_g orbital in perovskite oxides. c) O K-edge XAS of $La_{0.5}Ca_{0.5}FeO_3$, $La_{0.5}Ca_{0.5}CoO_{3-\delta}$, $LaMnO_3$, $LaCoO_3$ and LaNiO. d) Potentials at 25 $\mu A/cm_{ox}^2$ as a function of the B-O covalency with normalized absorbance at e_g-filling = 1. Reproduced with permission.[335] Copyright 2011, Nature Publishing Group.

ADVANCED
SCIENCE NEWS
www.advancedsciencenews.com

ADVANCED
SUSTAINABLE
SYSTEMS
www.advsustainsys.com

oxygen transport.[336] By using O K-edge X-ray absorption spectroscopy (XAS) analysis, it was reported that the primary descriptor that determine the ORR activity of the 15 perovskites examined in this literature is the extent of σ^*-antibonding (e_g) orbital filling of surface transition-metal cations, and it also involved in metal-oxygen covalent bonding. This hypothesis was further supported by increasing ORR activity with greater hybridization of the B—O (B-site-metal and oxygen) bond. As is shown in **Figure 22**a, the authors proposed an ORR mechanism on perovskite oxide catalysts to explain the ORR activity relation which relates to the rate-limiting mechanistic steps of the ORR where oxygen adsorption (B—O covalency) to form B-O$_2$ competes with the adsorption of hydroxide on the B-site. After three electrons are passed and three hydroxides produced, the B-OH site must be regenerated with water and another electron to continue the cycle. As for the case of LaFeO$_3$, the B-O$_2$ interaction was too weak when e_g was too full and thus O$_2$ adsorption cannot compete effectively with OH for the B-site. On the other hand, however, with too little e_g filing, as is the case of LaCrO$_3$, the B-O$_2$ interaction was too strong and thus further reduction was hindered. The result is a volcano curve, as is shown in Figure 22b, demonstrating an optimum activity when e_g is near unity. This optimum activity occurs with compounds like LaMnO$_3$ and LaNiO$_2$, which showed four orders of magnitude greater activity than that with high and low e_g B-sites. This quantitative result was supported by a number of studies and arguments at the molecular and electronic level, and suggested that tuning surface electronic features of nanoparticles can lead to high performance catalysts. The findings in this research differ from previous works in that it is quantitative and is based on an understanding of electronic structure, specifically the localized e_g electron in an orbital directed towards an O$_2$ molecule from the surface of the B cations, and explains the origins of the peak catalytic activities associated with high-spin and low-spin electrons.[337,338] This allows researchers to take advantage of the large number of possible electrocatalytic systems, including B site substitution and partial substitutions.

However, for most secondary metal-air batteries, the slow kinetics of OER greatly limit their efficiency. Later on, Shao-Horn expanded the research of the correlation surface cation e_g occupancy and high B-site oxygen covalency with the OER catalytic activity using the similar approach.[339] A same volcano curve of the OER performance (defined by the overpotentials at 25 μA/cm$_{ox}^2$ of OER current) was obtained by comparison of 10 perovskites with different occupancy of the e_g-symmetry electron of the transition metal (B in ABO$_3$). It was argued that the rate-determining step for the perovskites on the right branch of the volcano is the formation of the O—O bond in OOH adsorbate on B-site ions, whereas for the left branch, the deprotonation of the oxyhydroxide group to form peroxide ions might be rate-limiting. Having e_g filling close to unity experimentally facilitates these rate-determining steps efficiently and thereby leads to the highest OER activity. With the effective approach, researchers can create high performance bifunctional perovskite catalysts and electrodes for efficient, rechargeable metal-air batteries. A comparative first-principles calculation, including DFT functionals such as GGA, GGA+ U, and hybrid functional, were conducted to study the ORR activity on perovskite surface.[340] Since the kinetics of ORR on

each perovskite oxide surface differ significantly with different DFT methods, such comparative calculations can provide more reasonable observations. In addition to the intrinsic properties and different chemical compositions, the OER and ORR properties in alkaline media of different reaction planes were characterized using two-dimensional model electrodes.[341] Thin La$_{0.8}$Sr$_{0.2}$CoO$_3$ (001), (110), and (111) films were homogenously grown on SrTiO$_3$ (001), (110), and (111) substrates, respectively. With more oxygen vacancy formation, the (110) film was found to exhibit higher activity toward ORR and OER than the (001) or (111) films. Chen et al. prepared a series of calcium-manganese oxides (Ca-Mn-O) through thermal decomposition of carbonate solid-solution precursors and investigated their ORR performance.[342] Experimental and computational studies revealed that the catalytic properties were closely correlated with the surface Mn oxidation state and the crystallographic structures which affect the extent of O$_2$ activation. The current density and electron transfer number of the perovskite-type CaMnO$_3$, layered structured Ca$_2$Mn$_3$O$_8$, post-spinel CaMn$_2$O$_4$ and CaMn$_3$O$_6$ were comparable to those of the benchmark Pt/C, perovskite-type CaMnO$_3$ with open tunnels and multi-valances exhibited the highest activity, CaMn$_3$O$_6$ and CaMnO$_3$ exhibited superior OER performance and catalytic durability.

A subclass of perovskite oxides known as "double perovskites" was also investigated by researchers. It can be presented by a general formula A$_2$BB'O$_6$, where A is an alkaline-earth atom (e.g., Sr, Ba and Ca), B and B' are transition metal atoms. In the ideal structure of these transition metal oxides, a regular arrangement of corner-sharing BO$_6$ and B'O$_6$ octahedra alternating along the directions of the crystal can be observed. Since the properties of perovskites as electrocatalysts are generally determined by the nature, oxidation states and relative arrangement of B-sites cations, this interesting arrangement of altering different B and B' cations can be of great interest from the catalytic point of view.[343,344] Layered PrBaMn$_2$O$_{5+\delta}$ (H-PBM) was simply prepared by annealing pristine Pr$_{0.5}$Ba$_{0.5}$MnO$_3$-δin H$_2$.[343] And their oxygen reduction/evolution reaction activities were tested. Recently, Oscar et al. reported report on a class of oxygen-evolving catalysts based on iridium double perovskites which contain 32 wt% less iridium than IrO$_2$ and yet exhibit a more than threefold higher activity in acid media.[345] At that moment, the iridium double perovskites are the most active catalysts for oxygen evolution in acid media reported until now, to the best of their knowledge, and exhibit similar stability to IrO$_2$, which has provided a good guidance for further work.

Different perovskite oxides were reported in the application of metal-air batteries as effective catalysts.[346–359] For example, Liu group has reported the fabrication of the La$_{0.7}$(Sr$_{0.3-x}$Pd$_x$) MnO$_3$ (LSPM) perovskites with the substitution of Sr with Pd and its application in aluminum air battery.[346] While, both the (La$_{1-x}$Sr$_x$)$_{0.98}$MnO$_3$ perovskite with A-site deficiencies and La$_{1-x}$Ag$_x$MnO$_3$ (LAM) perovskites doped with Ag are reported to perform excellently in aluminum-air batteries.[347,348] Benefiting from the low cost, high electrochemical stability and high electronic/ionic conductivity, the perovskites can also sever an effective catalyst for Li-O$_2$ battery.[356] So far, some kinds of pervoskites, such as La$_{0.8}$Sr$_{0.2}$Mn$_{1-x}$Ni$_x$O$_3$, La$_{0.5}$Sr$_{0.5}$CoO$_{3-x}$, are widely applied in the Li-O$_2$ battery and have promoted the formation/decomposition of Li$_2$O$_2$ effectively.[351,356] As a typical

**ADVANCED
SCIENCE NEWS**

www.advancedsciencenews.com

**ADVANCED
SUSTAINABLE
SYSTEMS**

www.advsustainsys.com
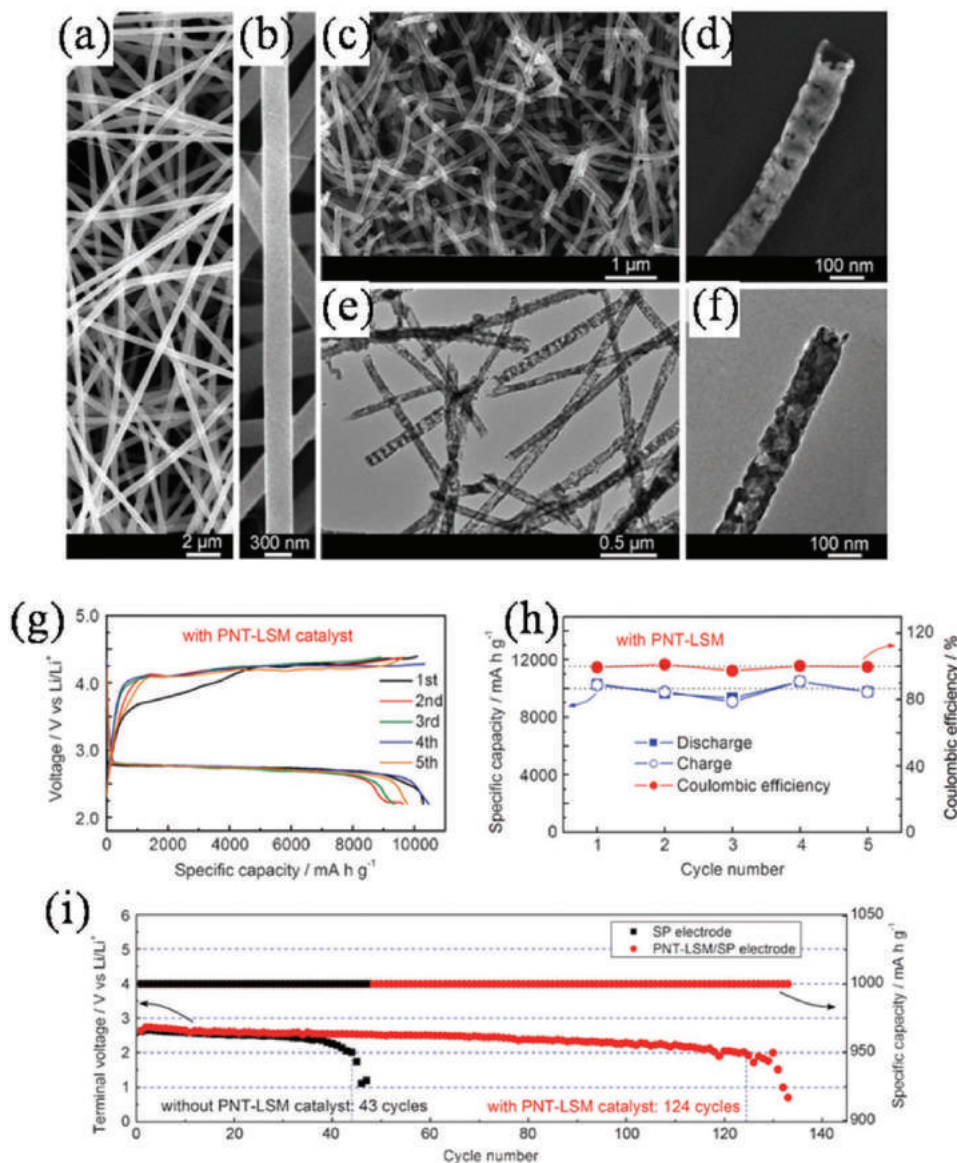
Figure 23. SEM images at different magnifications. (a) and (b) As-electrospun composite fibers. c, d) PNT-LSM after calcination at 650 °C for 3 h. e) Low-and (f) High-magnification TEM images of PNT-LSM. g) Cyclic performance, discharge and charge specific capacity, and (h) Coulombic efficiency of Li-O$_2$ cells with PNT-LSM catalyst at a current density of 0.025 mA cm^{-2}. i) Voltage of the terminal discharge vs the cycle number for Li-O$_2$ cells with and without PNT-LSM catalyst at 0.15 mA cm^{-2}. Reproduced with permission.[352]

example, our group also prepared perovskite based porous La$_{0.75}$Sr$_{0.25}$MnO$_3$ nanotubes (PNT-LSM) by using electrospinning technique followed by a heating process.[352] This strategy can realize a facile, effective, and scalable synthesis of PNT-LSM, which is also the first report in this area. As shown in **Figure 23**, the as-electrospun composite fibers have a smooth surface and ≈300 nm in diameter. After calcination at 650 °C for 3 h, an open tubular structure can be obtained with holes in the tube. The loose and porous structure can provide sufficient space for the deposition of discharge products, thus enhancing the discharge capacity. In addition, the porous PNT-LSM tubular can offer more abundant oxygen and electrolyte diffusion paths in the electrode, which can guarantee the

uniform distribution of O$_2$ and electrolyte inside the electrode. When firstly employed as electrocatalysts in a non-aqueous aprotic Li-O$_2$ cell, PNT-LSM significantly suppressed the ORR and especially OER overpotentials resulted in improved round-trip efficiency. Moreover, the synergistic effect of the high catalytic activity and the unique hollow channel structure of the PNT-LSM catalyst endowed the Li-O$_2$ cells with a high specific capacity, superior rate capability, and good cycling stability. The cells with PNT-LSM/SP electrode can be cycled at a capacity limit of 1000 mAh g^{-1} for over 124 cycles, which is among the best cycling performance of Li-O$_2$ cells. The facile and controllable method for scalable preparation opens up a promising path to prepare high performance metal-air catalysts. Most

**ADVANCED
SCIENCE NEWS**

www.advancedsciencenews.com

**ADVANCED
SUSTAINABLE
SYSTEMS**

www.advsustainsys.com

Figure 24. a) SEM images of 3DOM-LFO after calcination at 600 °C for 3 h. Inset is a magnified SEM image. b) Low-resolution and (c) higher resolution TEM images of 3DOM-LFO catalyst. d) SEM images of NP-LFO after calcination at 600 °C for 3 h. Inset is a magnified SEM image. e) Cyclic performance of Li-O_2 cells with 3DOM-LFO/KB electrodes at a current density of 0.025 mA cm^{-2}. f) Voltage on the terminal of discharge vs cycle number of the Li-O_2 cells with 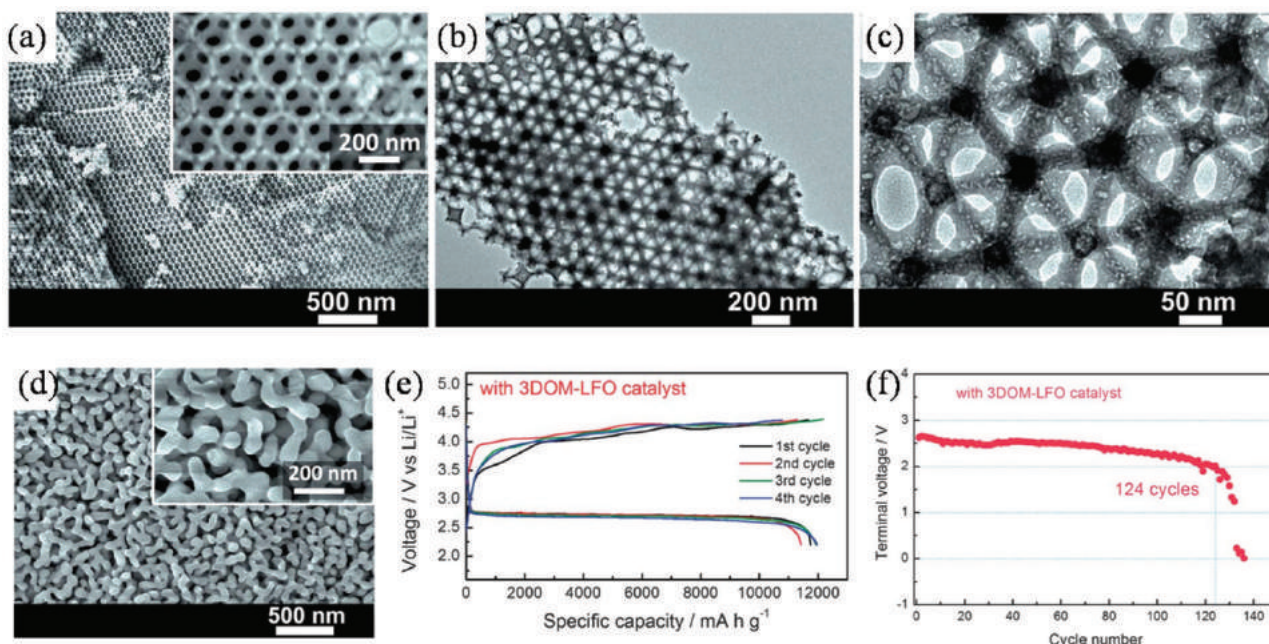3DOM- LFO/KB electrodes at a specific capacity limit of 1000 mA h g$_{carbon}$$^{-1}$. Reproduced with permission.[353] Copyright 2014, Royal Society of Chemistry.

recently, inspired by beehive, our group reported another 3D ordered macroporous LaFeO$_3$ (3DOM-LFO) based Li-O_2 battery.[353] As shown in **Figure 24**, such fine tuning of a beehive-like cathode nanostructure can ensure adequate space for the deposition of discharge products. The 3D ordered macroporous structure can also facilitate the transportation of reactants and electrolyte. In addition, the high catalytic performance of 3DOM-LFO toward ORR and OER can effectively lower the charge and discharge overpotentials. Thanks to the excellent properties of 3DOM-LFO, the Li-O_2 batteries demonstrated enhanced specific capacity, rate capability, and cycling stability.

5.2.2.3. Pyrochlore-type Oxides: Pyrochlore-type oxides are known for their excellent electrocatalytic activity toward ORR and OER in aqueous media.[360] They can be described by the chemical formula A$_2$B$_2$X$_6$O′$_{1-\delta}$, where A represents Pb or Bi, and B represents Ru or Ir. The crystal structure of pyrochlores can be viewed as a composite of two interwoven substructures, where corner-shared metal-oxygen octahedra (BO$_6$) generate a cage-like B$_2$O$_6$ framework that provides a conduction path for the electrons, resulting in the characteristics of a metallic oxide. At the same time, the A element is linearly connected to form A-O′-A linkages with special oxygen atoms (O′) that create corner-shared O′A$_4$ tetrahedra. Pyrochlores can exhibit high flexibility in stoichiometry and structure. For example, the special oxygen atoms (O′) can be partially or completely absent, resulting in up to 7% oxygen vacancies in the lattice when $\delta = 0.5$, or alternatively, the lattice can be fully oxygen filled to give the composition A$_2$B$_2$O$_7$. Some pyrochlores can exhibit the characteristics of a metallic oxide, single crystal conductivity such as Pb$_2$Ru$_2$O$_{6.5}$ can be as high as $2 \approx 5 \times 10^3$ S cm^{-1} at 300 K.[361] Furthermore, a portion of

the noble metal in the B-site can be replaced by the A-site cation, leading to an expanded pyrochlore A$_2$[B$_{2-x}$A$_x$]O$_{7-\delta}$, with x ranging from 0 to 1. Although partial substitution can result in decrease in the electronic conductivity, these modified oxides show excellent performance as bifunctional catalysts toward ORR and OER in strong alkaline media when B = Ru or Ir, and was already demonstrated in Zn-air cells.[362] Their high catalytic capability is believed to be originated from the variable-valent characteristics of the B cations and the oxygen vacancies.[363] Their catalytic activity can also be greatly enhanced by the cooperative effect from the efficient electron transportation to the reaction site and a good mass activity provided by the high surface area. Since the fundamental features of ORR and OER processes in aqueous and non-aqueous electrolytes share similarities, the interesting nature of pyrochlores suggests that these materials can be very promising candidates as metal-air catalysts. It should be noted that high catalytic performance toward OER is critical for the realization of secondary metal-air batteries with good round-trip efficiency, so that the anodic overpotential can be effectively lowered during charging. In addition, low charge overpotentials can avoid carbon corrosion and diminish electrolyte oxidation, which will be discussed in detail in the following sections.

Many successful demonstrations in metal-air batteries have proved the design of an electrocatalyst with high surface area and abundant surface defects is of great importance to the advancement of high performance metal-air batteries. As shown in **Figure 25**, the crystal structure of Pb$_2$Ru$_2$O$_{6.5}$ indicates the property of metallic conductivity from cage-like metal oxide octahedra (RuO$_6$) framework. In addition, the complete or partial absence of O′ in Pb-O′-Pb bridges will result in abundant surface defects which are catalytic active toward ORR and OER.
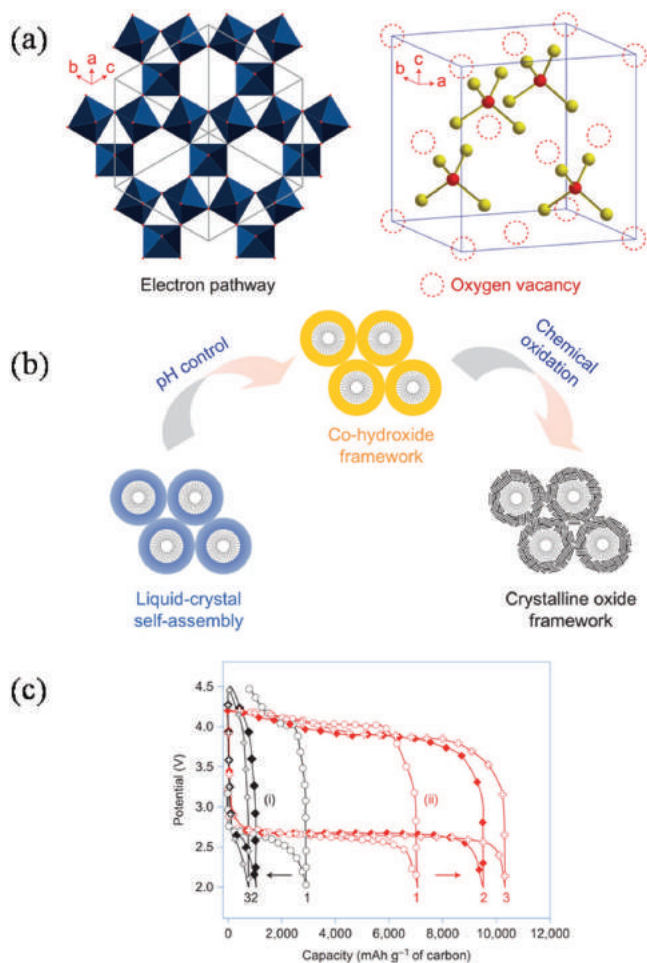
**ADVANCED
SCIENCE NEWS**

www.advancedsciencenews.com

**ADVANCED
SUSTAINABLE
SYSTEMS**

www.advsustainsys.com

Figure 25. a) Structure of the defect pyrochlore $A_2B_2O_{7-\delta}$ (δ = 0.5; A = Pb, Bi; B = Ru) showing oxygen vacancies and electron conduction paths via BO_6 octahedra that create metallic conductivity. b) Schematic illustration of the fabrication of the mesoporous pyrochlore oxide framework, using a surfactant template and chemical oxidation to condense the oxide framework to form a wall structure composed of aggregated nanocrystallites. c) Discharge-charge profiles of the first three cycles for carbon in $LiPF_6$/TEGDME (i, black) and mesoporous pyrochlore (ii, red), with cycle sweeps as indicated (current rate is 70 mA g^{-1} of carbon). Reproduced with permission.[364] Copyright 2012, American Chemical Society.

Based on this, Oh et al. developed a new strategy to synthesize mesoporous metallic oxide using liquid-crystal templating and subsequent oxidation by a chemical agent (Figure 25b).[364] The prepared pyrochlore showed high internal porosity with a surface area of up to 155 m^2 g^{-1}, which indicates increased catalytic sites. The mesoporous pyrochlore was subsequently applied in nonaqueous $Li-O_2$ batteries to characterize the electrocatalytic performance. As shown in Figure 30c, the $Li-O_2$ battery based on the prepared pyrochlore demonstrated a high reversible capacity of 10 000 mAh g^{-1} ($\approx$1000 mAh g^{-1} with respect to the total electrode weight including the peroxide product). The high performance can be attributed to the tailored properties, which include a high fraction of exposed oxygen vacancies, porosity that enables good diffusion to the active sites, and a nanoscale conductive network with metallic conductivity. This successful design

of a mesoporous metallic catalyst opens up a promising way to prepare high performance cathodes for metal-air batteries. Later, the same group reported the preparation of nanocrystalline and composition extended pyrochlore $Bi_2[Ru_{1.53}Bi_{0.47}]O_{7-\delta}$ (Bi/Ru = 1.61) (BiRO) and $Pb_2[Ru_{1.73}Pb_{0.27}]O_{6.5}$ (Pb/Ru = 1.31) (PbRO) by chemically oxidizing the metal (M = Bi or Pb, Ru) precursors with sodium hypochlorite in alkaline solution at low temperature.[365] This synthesis procedure can allow a greater degree of control over crystallite size. The expanded pyrochlore PdRO showed a substantial oxygen vacancy concentration, borderline metallic conductivity and a surface area of up to 66 m^2 g^{-1}, which indicate excellent catalytic behavior. The $Li-O_2$ cells based on PdRO demonstrated rechargeable capacities well over 10 000 mAh/g and significantly lowered anodic overpotentials. The excellent ORR and OER activity is facilitated by their high concentration of surface active sites afforded by the high surface area, intrinsic variable redox states, and facile electron transport owing to the metallic conductive character. The $Li-O_2$ cell was further modified by cooperating pyrochlore oxide with Au nanoparticles on the surface to gain better ORR activity, and the catalyst loading can be greatly reduced by homogenously coating the pyrochlore oxide onto the carbon surface.

5.2.3. Metal Nitrides and Carbides

Owing to the significant difference of electronegativity between metal and nitrogen atoms, there can be charge transfer in the nitrides which lead to the formation of catalytic active sites. In addition, transition metal nitrides possess good stability under both acidic/alkaline conditions and high electrochemical potentials, thus making them potential ORR electrocatalysts. For example, various nitride based ORR catalysts such as TiN, CuN, MoN, and Co_3N have been investigated in alkaline and acidic media.[366–379] TiN nanoparticles dispersed on Carbon black (CB) was achieved using an mpg-C_3N_4/CB composite as a template.[366] The good contact between TiN and CB enabled the composite as an efficient cathode catalyst for ORR. In addition, the synthesis procedure can be applied to the preparation of a variety of supported nano-nitride catalysts. Hierarchical TiN nanotube prepared by magnesiothermic reduction of titania replicas of ordinary filter paper was also reported to possess low charge-transfer resistance and superior electrochemical activity.[367] Chen et al. firstly reported cubic Cu_3N nanocrystals with tunable crystal size in organic solvents by a facile one-phase process.[373] Since the catalytic activity of catalysts are partly size- and shape-dependent, this size- and shape-controlled synthesis shows promising application for the preparation of non-noble ORR electrocatalysts.

Compared with other transition metal oxide catalysts, reports of the application of metal nitrides and carbides in metal-air batteries is relatively rare. However, great progress has been achieved by taking advantage of their good stability and catalytic activity.[175,200,380–385] Bruce et al. successfully used TiC-based cathode to prepare nonaqueous $Li-O_2$ cells.[175] Previous investigation have indicated that carbon can catalyze the decomposition of electrolyte during charge and discharge. Compared with carbon-based cathodes, the application of TiC greatly reduced side reactions at the electrolyte/cathode interface associated with

**ADVANCED
SCIENCE NEWS**
www.advancedsciencenews.com

**ADVANCED
SUSTAINABLE
SYSTEMS**
www.advsustainsys.com

electrode and electrolyte degradation. The detailed discussion will be presented in the next section. In another research, Kwak et al. reported the fabrication of molybdenum arbide nanoparticles (Mo_2C) dispersed on carbon nanotubes, which dramatically increase the electical efficiency up to 88% with a cycle life more than 100 cycles.[382] While, Zhou et al. has prepared ordered mesoporous TiC-C (OMTC) composites with large surface area (746.6 m^2 g^{-1}) and used it as catalysts for $Li-O_2$ battery.[384] The ordered mesoporous structure facilitates the electrolyte immersion and enhances Li^+ diffusion. TiC particles are homogenously distributed among the carbon framework to enhance the OER process and their intrinsic contact guarantees an efficient electron transfer process. The Li–O_2 battery with the OMTC electrode has a higher discharge plateau (ca. 60 mV) and a lower charge plateau (ca. 200 mV) than that of the bare SP electrode.

Currently, the reported metal-air batteries based on transition metal nitrides all demonstrated relatively low capacity, mainly due to the limited catalytic activity of catalysts. However, the highly stability and conductivity indicate their potential use as catalyst supports. Further optimization is needed to develop the full potential of this kind of interesting material.

5.3. Carbonaceous Materials

From the above discussions, the scarcity and high cost of noble metals is the major obstacle that hinders their large-scale development in metal-air batteries. Based on this, lowering the loadings of noble metal catalysts by exert their catalytic performance is a feasible solution, as demonstrated in section 5.1. However, the development of non-noble electrocatalysts is the ultimate goal to resolve the obstacle of the scarcity and high cost of noble metals. As one of the most affluent resource in the earth, carbonaceous materials have received tremendous attention in electrocatalysis owing to their favorable catalytic activity, high conductivity, large surface area, good stability, low weight and low cost. They were mainly investigated as metal-free oxygen catalysts or catalyst supports. Carbon materials can exist in a variety of forms with different physical, electrical and chemical properties. Carbon atoms can be sp^2 or sp^3 hybridized, forming a graphite or diamond structure, respectively. Carbon materials of sp^3 hybridized carbon with tetrahedral bonding are featured with low electric conductivity and compactness, which are unfavorable for catalytic use. The sp^2 hybridized carbon materials such as graphite, graphene, and carbon nanotubes exhibit high electric conductivity which are suitable for electrode applications. During the past few decades, oxygen catalytic activity of carbonaceous materials was well studied in aqueous solutions. Studies in non-aqueous metal-air batteries also demonstrate their potential applications. In general, carbon-based oxygen catalysts can be divided into nanostructured carbon, doped carbon, and metal/metal oxide-nanocarbon hybrid materials on an electrocatalytic base. In this section, carbonaceous catalysts are discussed accordingly.

5.3.1. Nanostructured Carbon

It should be noted that the catalytic performance of pristine nanocarbon materials for ORR and OER in aqueous solutions is not competitive to that in the nonaqueous electrolytes as they can provide enough catalytic activity for oxygen reactions. Their application as both catalyst supports and ORR catalysts is common in nonaqueous Li-air batteries. Benefitting from the excellent electronic conductivity, good ORR activity, ease of fabrication and low cost, the carbonaceous materials are widely used as cathode materials in $Li-O_2$ batteries. So far, various kinds of carbon materials, such as Super P, Ketjen black (KB) (normally EC 600JD and EC300JD), Vulcan XC-72, CNT, graphene etc. have been explored as cathode materials for $Li-O_2$ batteries.[386–414] In a traditional method, these carbonaceous powder is mixed with condcctive binder to produce cathodes. For example, Kim reported the application of graphene flakes as an air-cathode material for $Li-O_2$ battery.[406] While, Li et al. reported the useage of graphene/graphene-tube nanocomposites in $Li-O_2$ battery.[407] And Xin et al., reported the graphene/activated carbon composite material for oxygen electrodes in $Li-O_2$ batteries.[408] Early in 2011, a hierarchically porous graphene cathode, which was synthesized with a colloidal microemulsion approach, was reported Xiao et al.[409] Benefitting from the unique bimodal porous structure of electrode which consists of microporous channels facilitating rapid O_2 diffusion and the highly connected nanoscale pores providing a high density of reactive sites for $Li-O_2$ reactions, the $Li-O_2$ battery based on this cathode exhibits a desirable performance at that moment. In a similar case, Guo et al. synthesized an ordered hierarchical mesoporous/macroporous carbon.[410] Despite this improved performance with the help of porous sttructures, however, one common deficiency of these researches is the application of polymer binder. Generally, these porous carbon particles are closely aggregated by a binder in the cathode and such a tight aggregation unavoidably results in a low O_2-diffusion rate and a limited space for Li_2O_2 deposition, which consequently leads to low utilization of the carbon particles and leads further to a low capacity and low-rate capability of $Li-O_2$ batteries. In response, the construction of a porous cathode in an integrated manner holds great promise. As early as 2012, Wang et al. reported the construction of a graphene oxide gel-derived, free-standing, hierarchically porous carbon cathode in $Li-O_2$ battery.[412] In this research, free-standing, hierarchically porous carbon (FHPC) derived from graphene oxide (GO) gel in nickel foam without any additional binder is synthesized by a facile and effective in situ sol–gel method. Encouragingly, the $Li-O_2$ battery with this cathode exhibits a the capacity of 11060 mA h g^{-1} at a current density of 0.2 mA cm^{-2} and a high capacity of 2020 mA h g^{-1} at a current density of 2 mA cm^{-2}, which is the best performance reported at that moment. This excellent performance is attributed to the synergistic effect of the loose packing of the carbon, the hierarchical porous structure, and the high electronic conductivity of the Ni foam. Later on, Lim et al. has synthized a hierarchical-fibril CNT cathode by orthogonally plying individual sheets of aligned multiwalled nanotubes without any binder or solvent.[413] Benefiting from the facilated mass transfer of all reactants and the sufficient space for Li_2O_2 storage, the $Li-O_2$ battery with this cathode delivers capacities of ≈2100 and 1700 mAh g^{-1} even at current densities of 4000 and 5000 mA g^{-1}, respectively, after 20 cycles. Of note is that, it is the highest rate performance reported at that moment. Recently, Liu reported 3-D binder-

**ADVANCED
SCIENCE NEWS**
www.advancedsciencenews.com

**ADVANCED
SUSTAINABLE
SYSTEMS**
www.advsustainsys.com

free graphene foam as a cathode for Li-O$_2$ batteries.[414] In this study, a binder-free oxygen electrode consisting of a 3-D graphene structure on aluminum foam was directly used as the oxygen electrode in Li-O$_2$ batteries, delivering a high capacity of about 9×10^4 mA h g^{-1} (based on the weight of graphene) at the first full discharge using a current density of 100 mA g$_{graphene}^{-1}$. This performance is attributed to the 3-D porous structure of graphene foam providing both an abundance of available space for the deposition of discharge products and a high density of reactive sites for Li-O$_2$ reactions.

5.3.2. Doped Carbon

Pristine carbon materials have limited catalytic activity in aqueous electrolytes. A widely illustrated solution to enhance the catalytic activity is doping heteroatoms (such as N, B, S, and P). This doping process is effective in increasing the amount of structural defects at edge plane sites in the graphite carbon network, which induces active sites for ORR. Such process can be realized by heat treatment in a nitrogenous atmosphere, hydrothermal method, chemical vapor deposition (CVD), and so on. In particular, nitrogen has been proven as a very effective functional component or dopant to enhance ORR activity. Nitrogen can exist in the graphite network in graphitic, pyridinic and pyrrolic form. To develop metal-free carbon-based catalysts,

many researcher have demonstrated several approaches to produce nitrogen-doped Carbon nanomaterials.[415–419] As one of the typical examples, Gong et al. reported that vertically aligned nitrogen-doped carbon nanotubes (VA-NCNTs) can serve as metal-free catalysts which stimulate a four-electron ORR in alkaline solution (**Figure 26**a and b).[415] The VA-NCNTs demonstrated enhanced performance even outperform that of the Pt/C counterparts in catalytic activity, long-term stability, and tolerance to the crossover effect of CO poisoning (Figure 26c). This significant performance and a four-electron pathway can be attributed to the changes of nanostructure after the doping process. As shown in Figure 26d and e, the incorporation of electron-recepting nitrogen atoms in the conjugated nanotube carbon plane produce a relatively high positive charge density on adjacent carbon atoms, favoring parallel diatomic adsorption. N-CNTs derived from ethylenediamine precursor exhibited high activity toward ORR in alkaline solution and were studied as air cathode catalysts for zinc-air batteries.[416] Five different nitrogen containing aromatic precursors by injection CVD were prepared to produce N-CNTs.[417] Interestingly, it was found that the N incorporation in the corresponding N-CNTs product was dependent on the pre-existing C-N bond in the precursor, suggesting a controllable strategy to regulate the content and state of nitrogen. It also showed that over 60% carbon and nitrogen atoms could convert to N-CNTs for all the precursors, indicating the high efficiency and potential for scale-up of the injection
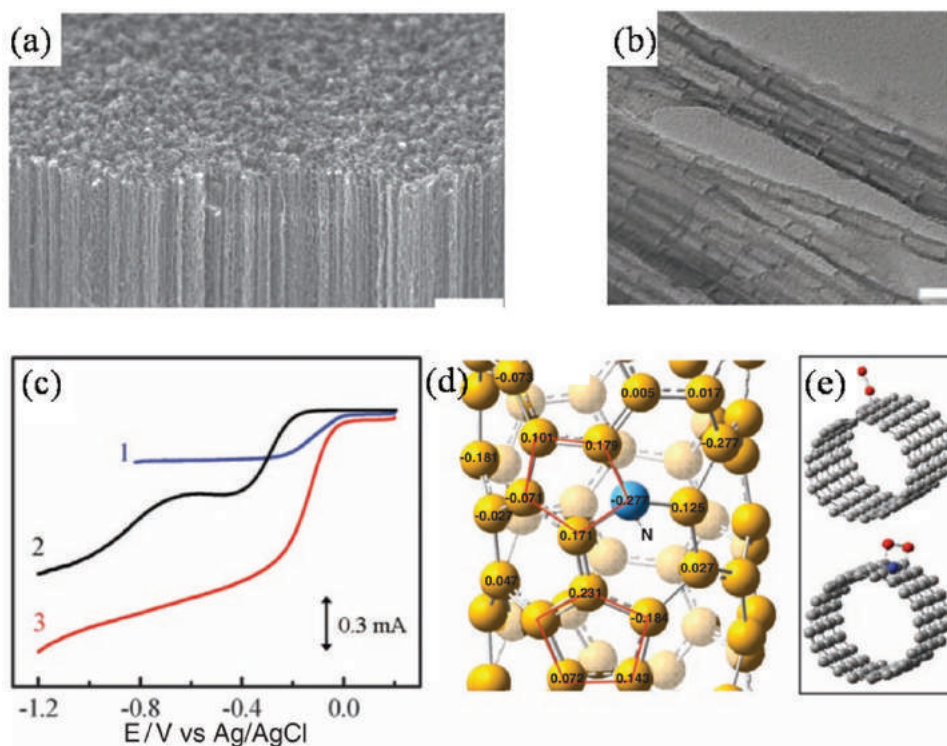
Figure 26. a) SEM image of the as-synthesized VA-NCNTs on a quartz substrate. b) TEM image of the electrochemically purified VANCNTs. c) RRDE voltammograms for oxygen reduction in air saturated 0.1 M KOH at the Pt-C/GC (curve 1), VA-CCNT/GC (curve 2), and VA-NCNT (curve 3) electrodes. d) Calculated charge density distribution for the NCNTs. e) Schematic representations of possible adsorption modes of an oxygen molecule at the CCNTs (top) and NCNTs (bottom). The C atoms around the pyrrolic-like nitrogen could possess much higher positive charges than do the C atoms around the pyridinic-like nitrogen. Reproduced with permission.[415] Copyright 2009, American Association for the Advancement of Science.

**ADVANCED
SCIENCE NEWS**
www.advancedsciencenews.com

**ADVANCED
SUSTAINABLE
SYSTEMS**
www.advsustainsys.com

CVD method. A one-step facile and method to produce graphene nanosheets with heterogeneously doped nitrogen atoms was reported by Chen and co-workers.[418] The uniquely large expansions and openings between the nanosheet layers resulting from this synthesis method can facilitate the diffusion of the electrolyte which lead to highly ORR activity. A Zn-air battery based on the doped graphene sheets also demonstrated comparable performance with that of the counterparts based on Pt/C. Nitrogen-doped graphene nanosheets were also reported to exhibit excellent performance in an aqueous Li-air battery using acid electrolyte.[419] The use of an acidic aqueous electrolyte in the air electrode side can increase the output voltage and also avoid poisoning by carbon dioxide gas in air. Experimental tests suggested that the presence of pyridine-type N with a large proportion of edge sites in the N-doped GNSs played a positive role in electrocatalysis for ORR under acidic conditions.

In addition to nitrogen, other elements such as B, P and S can also lead to enhanced activity for doped carbon materials.[420–423] Jiang et al. has performed a first-principles study of graphene, nitrogen-, boron-doped graphene, and codoped graphene as the potential catalysts in nonaqueous lithium-oxygen (Li-O$_2$) batteries.[420] In addition, phosphorus-doped OMCs (P-OMCs) were prepared by a simple metal-free nanocasting approach.[421] Interestingly, the activity of P-OMCs showed excellent ORR electrocatalytic activity with only a small amount of P-doping in alkaline solution. This great enhancement can be explained by the defects in carbon framework introduced by P-doping process which increased the electron delocalization due to the good electron donating properties of P. The above research demonstrates that carbon materials doped with elements with larger (N) or smaller (P, B) electronegativity than carbon can result in significant enhancement in ORR activity. It was also reported that graphene doped with the elements of similar electronegativity with carbon (such as sulfur and selenium) can also exhibit better catalytic activity.[423]

Inspired by the significant advance in catalytic activity for ORR by doping process, co-doping has recently developed to further enhance the activity.[424–431] It was found that after co-doping process, carbon materials show even higher activity than the corresponding single-atom-doped counterparts, which can be explained by the synergistic co-doping effect. For example, Qiao's group firstly reported a one-step synthesis of N and S dual-doped graphene (N-S-G).[424] The resulting N-S-G exhibited excellent activity comparable to that of commercial Pt/C and significant better performance than the solely doped graphene with N and S. Experimental data and DFT calculations revealed that the enhancement in catalytic activity was originated from the activation of C atoms brought by the redistribution of the spin and charge densities from the dual doping process. Further, N-S-G catalyst with large mesopores by using colloidal silica nanoparticle templates was prepared. The catalyst demonstrated long-term stability better than commercial Pt/C catalyst owing to the mesoporous nanostructure whit favorable ORR activity and mass transfer. This N-S-G shows great promise as low-cost catalyst for metal-air batteries. It should be noted that despite the significant enhancements in catalytic performance after co-doping process, a fundamental issues was raised concerning the distribution of doped heteroatoms in carbon frameworks. For instance, when B and N coexist in

sp^2 carbon, whether B and N are bonded together or located separately can lead to very different electronic structures, which result in distinct ORR activities. Zhao et al. reported that the bonded case cannot increase the catalytic activity because of the generation of chemically inert by-product hexagonal boron nitride (h-BN), while the separated case can greatly improve the ORR activity.[425] This study demonstrated the crucial role of the doping microstructure on ORR performance, which is of significance in exploring advanced carbonaceous electrocatalysts. Qiao's group also reported B and N dual-doped graphene by using a two-step doping strategy to avoid the formation of inert by-products.[426] Due to the synergistic effect of the well-defined doping sites, the resultant B,N-doped graphene exhibited comparable ORR performance with commercial Pt/C. These studies further opened up a variety of effective and low-cost approaches to produce high performance carbonaceous electrocatalysts.

Given the excellent ORR performance of doped carbon materials in alkaline electrolytes, it was expected that those materials can also provide catalytic advantage in nonaqueous systems. Some researchers have demonstrated the doping strategy is also effective in enhance the catalytic performance for carbon materials, but the fundamental study of reaction mechanisms is rare.[432–439] Shu et al. reported nitrogen-doped onion-like carbon as an efficient oxygen electrode for long-life Li-O$_2$ battery.[432] In another report, vertically aligned nitrogen-doped coral-like carbon nanofiber (VA-NCCF) array supported by stainless steel cloth was used as cathode for nonaqueous Li-O$_2$ battery.[433] As shown in **Figure 27**, the carbon fibers aligned normal to the substrate showing a zigzag-like morphology with many branches along the fiber axis, which provide high surface area and large free space between fibers. The slightly tangled Carbon fibers can also lead to good electric conductivities for both the in-plane and through-thickness directions. When applied as cathodes, this electrode design can not only facilitate electrolyte/reactant diffusion but also enhance electron transportation through the shortest pathway along the vertically aligned fiber length. As expected, the Li-O$_2$ battery based on the VA-NCCF electrode exhibited significant performance. A low overpotential of 0.3 V can be observed at the middle of the charge and discharge plateaus at a current density of 100 mA/g, and reasonably low overpotentials can still be observed at high rates (Figure 27d). An excellent and stable cycling performance was also obtained with 150 cycles at a specific capacity of 1000 mAh/g and current density of 500 mA g^{-1}. As demonstrated above, doped carbon nanomaterials show very promising performance in aqueous metal-air batteries. Although the fundamental catalytic mechanisms are not clear in nonaqueous systems, doped carbon catalysts also exhibited high catalytic activity as an alternative for noble metals.

5.3.3. Metal Oxide-Carbon Hybrid Materials

As discussed above, pristine carbon materials have relatively low activity in aqueous solutions, while noble metal catalysts show excellent activity both aqueous and nonaqueous electrolytes. The combination of those two materials are shown effective in lowing the loadings of noble metals and have shown significant performances in metal-air batteries.[440–448] For
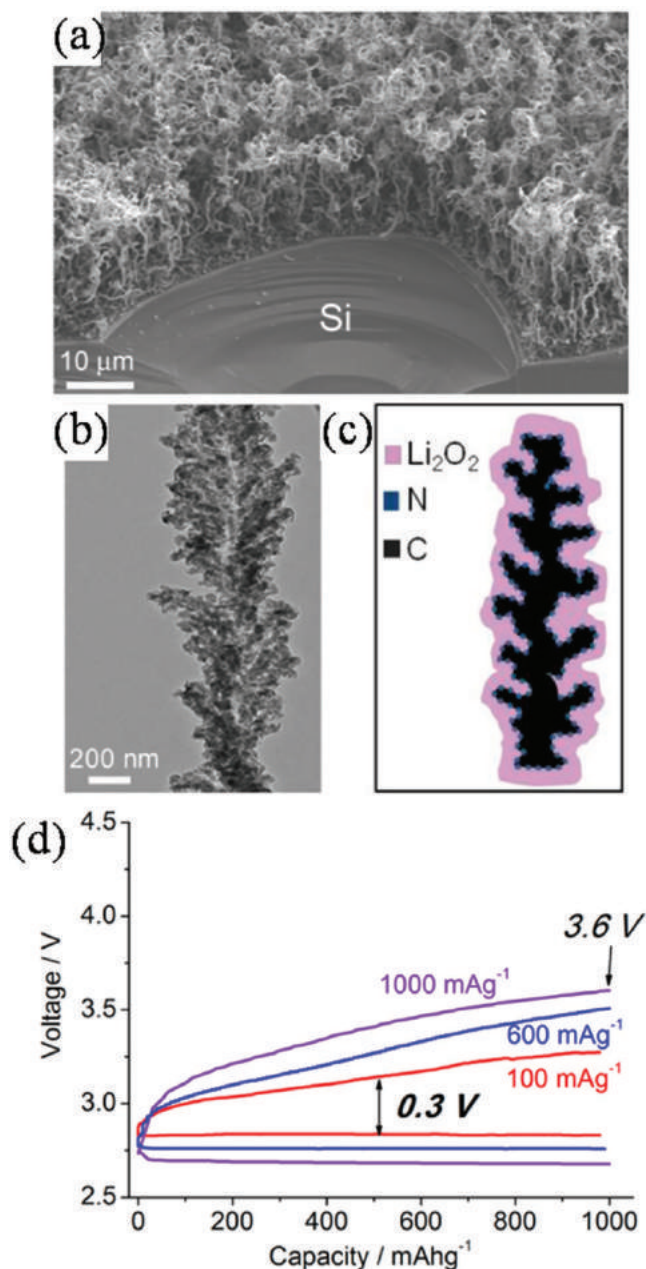
**ADVANCED
SCIENCE NEWS**

www.advancedsciencenews.com

**ADVANCED
SUSTAINABLE
SYSTEMS**

www.advsustainsys.com

Figure 27. a) SEM image of a VA-NCCF array grown on a piece of Si wafer by CVD. b) TEM image of an individual VA-NCCF. c) The sketch of Li_2O_2 grown on a coral-like carbon fiber. d) Rate performance of the VA-NCCF electrode at current densities of 100, 600, and 1000 mA g^{-1}. Reproduced with permission.[433] Copyright 2014, American Chemical Society.

example, Pt nanoparticles coated aligned MWNTs fabricated from CNT forest with a hierarchical micro-nano-mesh and well-ventilated structure were used as air cathodes for non-aqueous Li-air batteries.[441] The well aligned pore structure of the Pt-CNT fibrils not only facilitate facile accessibility of Li ions and oxygen but also provide good electrode/electrolyte interfaces which effectively expose catalysts to the discharge products, thereby providing ideal conditions for the catalytic reactions. The resulting Li-O$_2$ batteries exhibited significant low overpotentials compared with the counterparts based on pris-

tine CNT fibril electrode. In addition, remarkable cycling stability of over 100 full discharge/charge cycles was achieved at a high current rate of 2 A g^{-1}, further highlighting the advantages of this hierarchical Pt-CNT fibril air electrode. Tu et al. decorates the Au nanoparticles on the cracked carbon submicrometer tube arrays. The Li-O$_2$ battery with this cathode exhibits desirable performances.[444] Recently, Amine's group used an atomic layer deposition (ALD) method to produce Pd coatings on porous carbon support as an ORR catalyst.[446] This method can achieve highly uniform and conformal dispersed coatings ranging from subnanometer to a few nanometers in thickness, which is effective in lowing metal loadings while still retain the same catalytic activity. After the ALD process, the nanoporous of carbon support was well preserved, indicating a high surface area Pd layer with large density of catalytic active sites was obtained. The resulting nonaqueous Li-O$_2$ battery exhibited a high discharge voltage and capacity mainly due to the superior ORR activity of the catalyst. These studies have demonstrated various promising and effective approaches to reduce the loadings of noble metal catalysts while remain their high activity. However, the scarcity of noble metals is still a major obstacle hindering their large-scale applications. Transition metal oxides, on the other hand, show great potential applications as non-noble catalysts for air cathodes as mentioned in the last section. Nevertheless, their relative low electric conductivity reduces their overall catalytic performance. A feasible solution is to incorporate them with nanocarbon materials. The synergistic effect of the high conductivity and effective diffusion of reactants provided by the nanoc arbon support and the good ORR and OER catalytic activity of metal oxides can lead to superior performance.

Apart from the activity of electrocatalysts, the overall performance of air electrodes is mainly dependent on the structure and properties of catalyst support.[449–451] For air electrodes, carbon not only serves as a catalyst support and conductive pathways, but also helps to stabilize the triphase boundary and morphology which is essential to provide reaction sites for ORR. Benefitting from the excellent electronic condctivity and good catalytic activity, these metal oxides-carbon hybrid materials are also widely applied in the Na-O$_2$ battery.[452–461] Rosenberg and Hintennach reported the application of α-MnO$_2$ nanowires for Na-air batteries, which presented a large initial capacity of 2056 mAh g^{-1} but suffered 59% decrease in capacity after 2 cycles.[452] Chen and co-workers developed a porous CaMnO$_3$ microspheres, and tested it in Na-O$_2$ batteries.[460] The CaMnO$_3$/C electrode delivered a huge capacity of 9560 mAh g^{-1} at a current density of 100 mA g^{-1}, which was nearly 2.5 times of that of bare carbon black electrode. The Na-O$_2$ cell with CaMnO$_3$/C electrode maintained 80 cycles with a restricted cut-off capacity of 1000 mAh g^{-1}. This prolonged cycle life is 8 times longer than bare carbon black (around 10 cycles). On the other hand, Zhang et al. combined Pt particles on graphene nanosheets (GNSs) to fabricate nanostructured Pt@GNSs catalyst for Na-O$_2$ batteries.[461] The discharge capacities of the cells increased from 5413 to 7574 mAh g^{-1} after introducing Pt. The cell with Pt@GNSs catalyst was cycled for around10 cycles with a cut-off capacity of 1000 mAh g^{-1}.

In addition, some researchers have demonstrated that metal-air batteries based on metal oxides-carbon hybrid catalysts

**ADVANCED
SCIENCE NEWS**
www.advancedsciencenews.com

**ADVANCED
SUSTAINABLE
SYSTEMS**
www.advsustainsys.com

exhibit favorable performance. Most of the demonstrations of these hybrid catalysts in aqueous metal-air systems can find their application in Zn-air batteries.[462–467] For example, novel CoO/carbon nanotube hybrid oxygen reduction catalyst and Ni-Fe-layered double hydroxide oxygen evolution catalyst were synthesized as cathode for Zn-air batteries.[462] According to Li et al., the resulting primary Zn-air battery showed high discharge peak power density ≈265 mW cm^{-2}, current density ≈200 mA cm^{-2} at 1 V and energy density 4700 Wh kg^{-1}. Rechargeable Zn-air batteries in a tri-electrode configuration exhibited an unprecedented small charge–discharge voltage polarization of ≈0.70 V at 20 mA cm^{-2}, high reversibility and stability over long charge and discharge cycles. As for zinc-air battery, an efficient, durable and low cost catalyst is essential for a high performance metal-air battery. In this aspect, a composite bifunctional catalyst, Co_3O_4 nanoparticles-decorated carbon nanofibers (CNFs) is prepared.[465] The particles-on-fibers nanohybrid materials were derived from electrospun metal-ion containing polymer fibers followed by thermal carbonization and a post annealing process in air at a moderate temperature. Electrochemical studies suggest that the nanohybrid material effectively catalyzes oxygen reduction reaction via an ideal 4-electron transfer process and outperforms Pt/C in catalyzing oxygen evolution reactions. Accordingly, the prototype ZnABs exhibit a low discharge-charge voltage gap (e.g., 0.7 V, discharge–charge at 2 mA cm^{-2}) with higher stability and longer cycle life compared to their counterparts constructed using Pt/C in air-cathode. Importantly, the hybrid nanofiber mat readily serves as an integrated air-cathode without the need of any further modification. And such a design is expected to provide guidance for future catalyst design. In addition to the excellent performance in aqueous systems, these metal oxide-carbon hybrid also exhibits favorable catalytic activity in nonaqueous systems. Some researchers have demonstrated improved performance of metal oxide-carbon hybrids, especially in nonaqueous Li-air battery systems.[468–484] For example, Zhang et al. have prepared a three-dimensional (3D) graphene-Co_3O_4 electrode by a two-step method.[468] By growing the Co_3O_4 on the graphene strucure that was initially deposited on a Ni foam, a free-standing and binder-free monolithic electrode was obtained. When applied in the Li-O$_2$ battery, this composite structure exhibited enhanced performance with a specific capacity of 2453 mA h g^{-1} at 0.1 mA cm^{-2} and 62 stable cycles with 583 mA h g^{-1} (1000 mA h g$_{carbon}^{-1}$). The excellent electrochemical performance is associated with the unique architecture and superior catalytic activity of the 3D electrode. In additon, other kinds of materials including Co/CoO-graphene-carbonized melamine foam,[471] 3D nanoporous nitrogen-doped graphene with encapsulated RuO_2 nanoparticles,[473] RuO_2 nanoparticle-decorated buckypaper cathode,[477] carbon embedded α-MnO$_2$ @graphene nanosheet composite,[481] etc. have been reported. To be specific, recently, Salehi et al. reported the preparation of CNT-MnO$_2$ nanocomposite as a high rate cathode catalyst for the rechargeable Li-O$_2$ batteries.[480] Simultaneously, the performances of a series of CNT-MnO$_2$ nanocomposites containing different values of MnO$_2$ are also investigated. According to the authors, the s ynthesized CNT–60% MnO$_2$ compound had a capacity of about 4600 mA h/g$_{total\ cathode}$ at a current density of 1000 mA/g$_{total\ cathode}$. The battery fabricated

using the optimum nanocatalyst revealed over-voltages equal to 0.20 V and 0.87 V for discharge and charge, respectively, having a cycleability using the current density of 100 mA/g$_{total\ cathode}$.

It should be noted that the oxygen electrochemistry mechanisms in nonaqueous aprotic systems is still inclusive. For example, Nazar's group prepared Co_3O_4/rGO with Co_3O_4 nanocrystals covered all the surfaces of rGO to study the properties of Co_3O_4 catalyst independently. The rGO acted only as a conductive layer to support the high dispersion of Co_3O_4 nanocrystals.[485] It was found that the Li-O$_2$ batteries with Co_3O_4/rGO resulted in significant reduction of charge overpotentials and improved cycling performance. The authors argued that Co_3O_4/rGO acted as a promoter rather than a classic electron-transfer catalyst. The better performance was attributed to the enhanced surface transport of Li$_x$O$_2$ species, which was achieved by reduced binding energy in the electrochemical processes on discharge and charge. In another report, a first-principles approach is used to study the interactions between discharge products and δ-MnO$_2$ monolayers that serve as putative Li–air battery cathodes.[486] The adsorption energies of Li, O$_2$, and Li$_x$O$_y$ (x,y = 1,2) on MnO$_2$ are calculated. On the basis of an evaluation of the adsorption energies, it is found that the MnO$_2$ monolayer prefers to react with Li atoms rather than O$_2$ molecules to initiate LiO$_2$ formation. The incipient LiO$_2$ is expected to be strongly chemisorbed onto the MnO$_2$ layer. LiO$_2$ can be subsequently converted to Li$_2$O$_2$ and finally Li$_2$O via a sequence of lithiation or disproportionation reactions. Inspiringly, this study is expected to provide guidance for future research.

5.4. Metal-Nitrogen Complex

Another important class of non-noble metal electrocatalyst for ORR is Carbon-supported transitional metal-based nitrogen-containing materials (M-N$_x$/C, with M represents Fe, Co, Ni, Cu, Mn, etc., and x = 2 or 4, normally). Since the first report on the ORR catalytic active of M-N$_4$ macrocycle chelates such as cobalt phthalocyanines (Co-Pc) in 1964,[487] M-N$_x$/C materials have received intensive investigation as promising candidates to replace noble metal catalysts with high activity and stability for fuel cell cathodes. Until now, a series of M-N$_x$/C materials have been developed, transition metal porphyrins and their analogues have attracted particular attention.[488–513]

The ORR activity of these materials is directly related to the metal ion centers and encompassed ligands. During ORR, the charge transfer from the metal ion centers to the O$_2$ π^* orbital was believed to lead to the overall weakening of O-O bond, which consequently result in favorable ORR activity. Among the transition metal ion centers listed above, Fe and Co are mainly believed to display optimal overall ORR performance. In addition, the well-defined structures of the macrocycles and ligands can be facilely tailored by simple synthesis procedures, which allow for the further control over the ORR performances. For example, Chen's group synthesized iron phthalocyanine (Fe-Pc) based catalysts (**Figure 28**), and reported that significant improvements were observed for the Fe-SPc (as shown in Figure 28b and d) with respect to a comparable activity and better stability to that of commercial Pt/C catalyst in alkaline
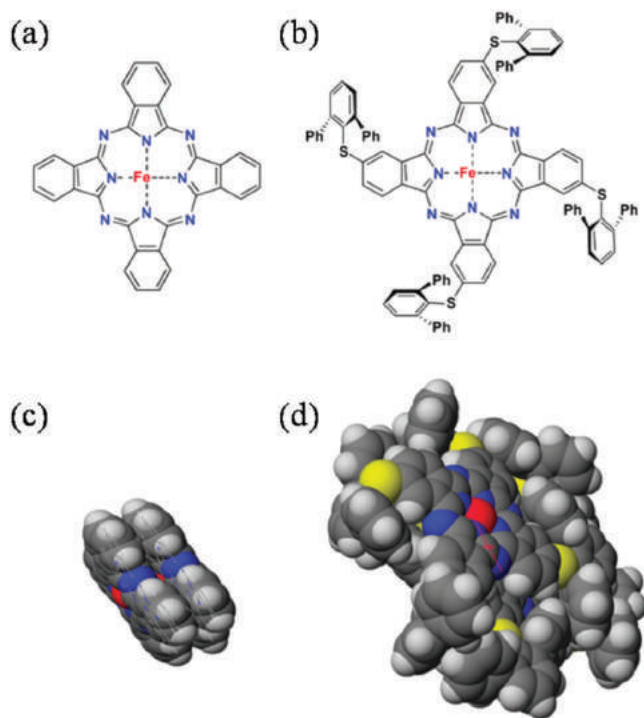
**ADVANCED
SCIENCE NEWS**
www.advancedsciencenews.com

**ADVANCED
SUSTAINABLE
SYSTEMS**
www.advsustainsys.com

Figure 28. a) Atomic structure of (A) Fe-Pc and (B) Fe-SPc and the space filling stacking model of (C) Fe-Pc (d_{Fe-Fe}: 4.119 Å) and (D) Fe-SPc (d_{Fe-Fe}: 6.945 Å); side view, same scale. Reproduced with permission.[489] Copyright 2010, American Chemical Society.

solutions.[489] The thioether groups were attached to the Pc macrocycles which can act as supplementary electro-donating sites to improve electron transfer. In addition, a high degree of steric hindrance can be obtained by the incorporation of bulky diphenyl thiophenol groups into the molecular structures, maintaining the isolation of catalytic active sites. That is to say, the incorporation of electron-donating functional groups along with the isolated active sites give rise to the ORR performance of the Fe-SPc. This work indicates that a careful design of molecular structures can lead to favorable ORR performances. Improved ORR activity was also observed after doping carbon supported cobalt polypyrrole (Co-PPy/C) with p-toluenesulfonic acid (TsOH).[490] The Co-PPy-TsOH/C demonstrated much higher current density and power density than Co-PPy/C when applied as cathode catalyst for fuel cells. This can be mainly attributed to the increase of N content after the doping process, the slight change in C content and micropores also made small contribution to the enhancement in ORR. Qiao et al. reported that metal addition and metal loadings could also affect the ORR activity of carbon supported Co-Pc in alkaline media.[491] DFT calculations on the dioxygen-binding abilities of substituted Co and Fe phthalocyanine, and porphyrin systems was investigated.[492] Results showed that the ability to bond dioxygen was determined by central metal ion, ligand and substituents. Generally speaking, the ORR activity of these materials is related to their ionization potential and dioxygen-binding ability. Higher ionization potential and larger dioxygen-binding energy are associated with better ORR activity. From experimental results and DFT calculations, Wang et al. indicated that

higher ORR kinetics can be obtained with lower the O_2 adsorption energy.[493]

A primary nonaqueous Li-O_2 battery utilizing carbon supported dilithium phthalocyanine (Li$_2$-Pc) was fabricated with a high discharge capacity, indicating the good ORR activity of Li$_2$-Pc.[494] Recently, Goodenough and co-workers designed a Li-O_2 battery utilizing organic-electrolyte-dissolved Fe-Pc as a shuttle to transport $(O_2)^-$ species and electrons between cathode surface and Li$_2O_2$.[495] As shown in **Figure 29**, Li$_2O_2$ was observed to grow and decompose without direct contact with carbon electrode when Fe-Pc catalyst was added. In distinct contrast, the Li$_2O_2$ was coated on the electrode surface of the Li-O_2 battery without Fe-Pc catalyst which would block the electrocatalytic surface, leading to inferior capacity and round-trip efficiency. Further, to prevent some possible side reaction of the dissolved Fe-Pc with Li metal anode, a SEI layer was proposed to block their direct contact. The synergy of a solid catalyst and solution-phase shuttle catalyst demonstrated in this work indicate a promising route to produce high capacity and reversibility Li-O_2 cells. Wang's group reported that metal-organic framework (MOF) can also lead to enhanced performance for nonaqueous Li-O_2 cells.[496] A mixed composite of MOF and Super P carbon was applied as active cathode materials. The well-defined micropores lined with open metal sites in MOF can effectively enhance oxygen binding while the mesoporous Super P can facilitate electrolyte transportation and deposition of discharge products. The resulting Li-O_2 battery demonstrated a higher capacity than that based on Super P alone. Considering the diversity of MOFs and the facility with respect to the variety of organic links and multi-metal building units, MOFs present promising application in metal-air batteries.

Metal-air batteries based on pyrolyzed metal macrocycle complex were relatively less reported.[514–517] Fe/N/C composite derived from pyrolyzation of a mixture of ion acetate, 1,10-phenanthroline and high surface area carbon black was firstly investigated as cathode catalyst for nonaqueous Li-O_2 cells.[514] **Figure 30**a is the discharge/charge curves of two Li-O_2 cells using α-MnO$_2$/XC-72 and Fe/N/C as cathode catalysts, respectively. The discharge curve of Li-O_2 cells with Fe/N/C showed a slight reduction in discharge overpotential, indicating better ORR performance in promoting the formation of Li$_2O_2$ than the α-MnO$_2$/XC-72 catalyst. More interestingly, compared with the cell with α-MnO$_2$/XC-72 catalyst, a significant lowered charge potential throughout the whole charging process can be observed of that utilizing Fe/N/C composite, which can be addressed by the enhanced OER activity. In addition, the side-by-side comparison of GC signals after charge process in Figure 30b show that only oxygen was released from the cell with Fe/N/C catalyst, whereas CO_2 was also detected except for O_2 from the cell with α-MnO$_2$/XC-72 catalyst indicating electrolyte decomposition. This can be ascribed to the well dispersed active sites throughout the conductive substrate with high surface density. The high interfacial contact with Li$_2O_2$ can provide effective electron and mass transport, thus lowering the overpotential during charge process. Chen's group also demonstrated that pyrolyzed nanofiber by electrospun a solution of polyacrylonitrile (PAN) and iron acetate can be applied as catalysts for nonaqueous Li-O_2 battery.[517] After pyrolysis, PAN formed into

**ADVANCED
SCIENCE NEWS**

www.advancedsciencenews.com

**ADVANCED
SUSTAINABLE
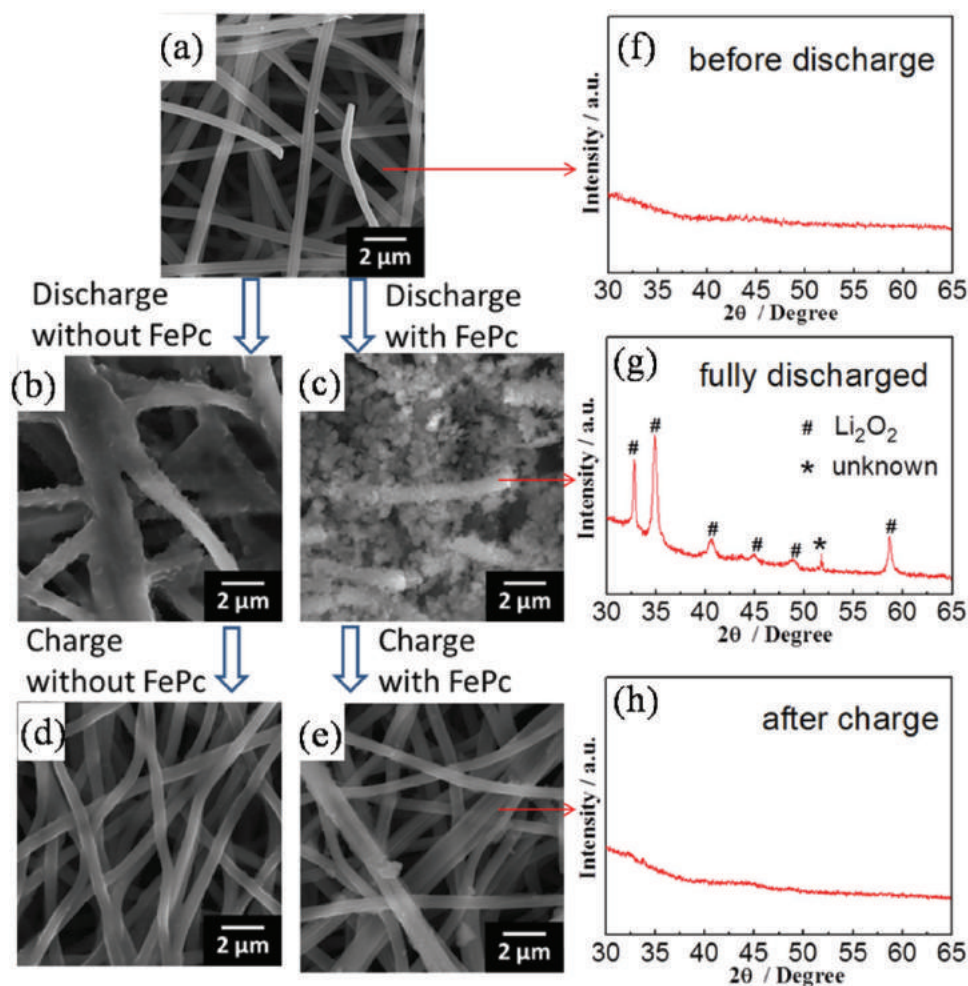SYSTEMS**

www.advsustainsys.com

Figure 29. a–e) SEM images of the CF cathodes (with Fe-N/C) before discharge (a), after discharge (b, d) and after charge (c,e) with Fe-Pc catalyst (d, e), and without Fe-Pc catalyst (b,c). f–h) XRD pattern of the CF cathode before discharge (f), after discharge (g), and after charge (h) with Fe-Pc dissolved in the TEGDME electrolyte. Reproduced with permission.[495]

porous nitrogen-containing carbon fibers which can provide excellent electron and mass transportation.

5.5. Conductive Polymers

Electrically conductive polymers (CPs), such as polyaniline (PANI), polypyrrole (PPy), polythiophen (PTh), poly(3-methyl) thiophen (PMeT), and poly(3,4-ethylenedioxythiophene) (PEDOT), present another alternative approach to replace noble metals as cathode electrocatalysts in metal-air batteries.[518–520] CPs usually display mixed metal and polymer like properties and have attracted certain attention due to their low cost, high electric conductivity, and distinct redox properties. Investigation of CPs as electrode catalysts was already conducted in their early stages, however, it was further hindered by their low conductivity, and inferior efficiency.[521–523] Recently, the development of chemical polymerization, such as vapor phase polymerization (VPP), have realized the fabrication of CPs with high conductivity, improved stability, and controllable morphology.[524–528] A PEDOT electro-active layer was coated on a

hydrophobic, porous membrane by VPP to prepare an three-phase interface air cathode, as shown in **Figure 31**a.[519] A Zn-air battery was then constructed based on the PEDOT air cathode utilizing a alkaline electrolyte. The catalytic mechanism of the PEDOT-based electrode was pointed out to involve a redox cycling process, where ORR is occurred when the PEDOT is in its reduced state. When O_2 is absorbed on the surface of the PEDOT, it rapidly oxidizes the PEDOT to the oxidized form where O_2 is reduced accordingly in this process. Owing to the high conductivity and stability, the Zn-air battery based on the PEDOT electrode exhibited a better performance with an open-circuit voltage of 1.44V than the similar battery based on the Pt/Goretex air electrode under the same testing conditions. By using quantum-chemical modeling calculations consistent with experimental results, it was reported that oxygen can be reduced when the CPs are in the reducing state.[521] On the other hand, it was also argued that the electrocatalytic activity of these polymers maybe attributed to the high electrochemically active nitrogen and sulfur content in their inherent structure. Owing to the strong electron withdrawing ability, nitrogen atoms with lone-pair electrons in conjugated π-bond
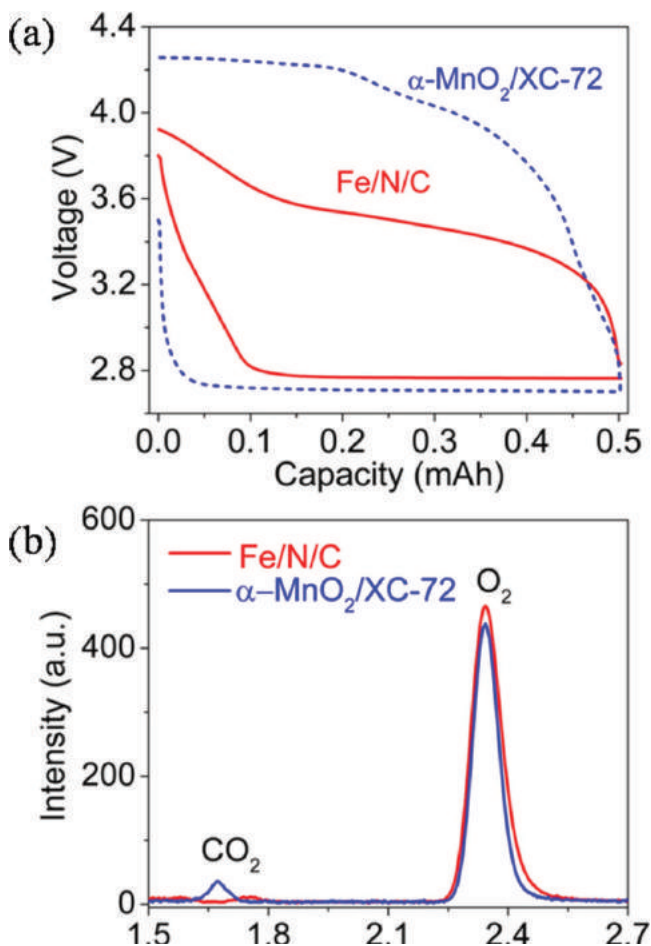
**ADVANCED
SCIENCE NEWS**
www.advancedsciencenews.com

**ADVANCED
SUSTAINABLE
SYSTEMS**
www.advsustainsys.com

Figure 30. a) Discharge/charge voltage profiles of Li-O_2 cells using α-MnO_2/XC-72 and Fe/N/C as cathode catalysts. b) Representative GC signals as a function of retention time for the gas effluents collected at the end of the charging processes. Reproduced with permission.[514] Copyright 2012, American Chemical Society.

structures, such as pyridinic-type nitrogen, are generally recognized as ORR catalytic active sites in CN_x materials.[529–532] A recent study reported a new CP with high and stable ORR catalytic activity, poly(bis-2,6-diaminopyridinesulfoxide) (PDPS).[528] The high content of nitrogen species (pyridinic and imine-type) which acted as ORR-active sites resulted in the high ORR activity of the PDPS.

A recent research reported that low cost and facile preparation of the water dispersed conducting PANI nanofibers doped with phosphate ester were firstly used to fabricate cathode for Li-O_2 battery.[533] Experimental test showed that the PANI nanofibers can actively catalyze the discharge reaction with good cycling stability. The Li-O_2 battery displayed an initial capacity of 3260 mAh g^{-1} at a current density of 0.05 mA cm^{-2}, then degraded to 2320 mAh g^{-1} during the first three charge/discharge cycles, the discharge capacity kept relatively stable in the subsequent 27 cycles, with 4% loss in capacity. This approach present a low cost and facile possibility to prepare high-capacity metal-air batteries. A nonaqueous Li-air battery based on a PPy nanotube air electrode was reported by Cui et al.[534] Owing to the high conductivity, stable chemical and electrochemical property, and 3-dimensional porous structure of PPy, the air electrode based on hydrophilic PPy nanotubes showed a higher reversible capacity, better round-trip efficiency, and improved cycling stability and rate performance than that of the carbon black-supported air electrode. The porous structure and hollow channels of the PPy nanotubes are beneficial to establish the triphase interfaces and also facilitate the O_2 diffusion and electrolyte distribution. In addition, the excellent performance of the PPy nanotubes can also be attributed to the possible bifunctional catalytic activity, which can commendably promote ORR and OER. The schematic illustration of the organic electrolyte and oxygen distribution and the discharge/charge process of the PPy nanotube electrode are also given in Figure 31b and c. At a current density of 0.1 mA cm^{-2}, the discharge voltage of the Li-O_2 battery based on PPy nanotube cathode is 300 mV higher than that of the carbon black
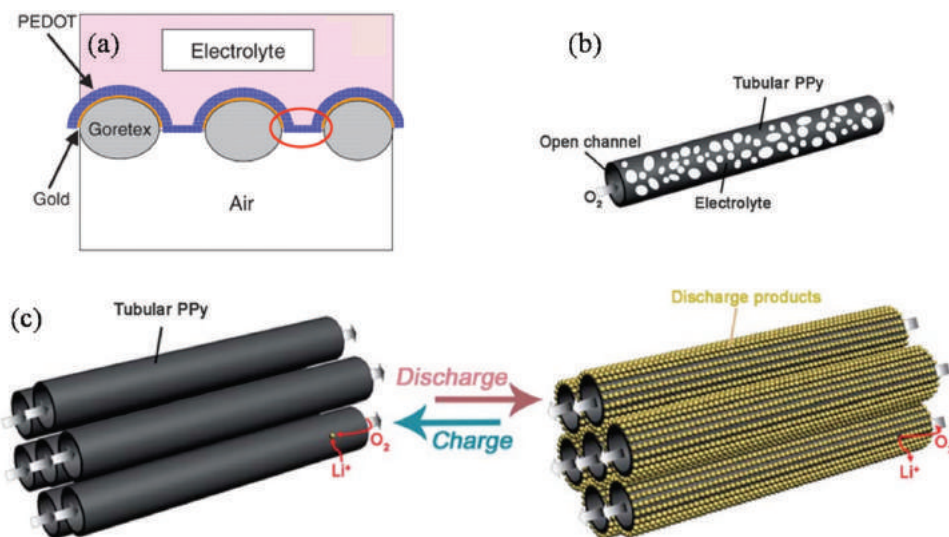

Figure 31. a) Schematic representation of the PEDOT/Goretex air electrode. Reproduced with permission.[519] Copyright 2003, Elsevier. b) The organic electrolyte and oxygen distributions on hydrophilic PPy nanotubes, and (c) the schematic discharge/charge process.[532]

**ADVANCED
SCIENCE NEWS**

www.advancedsciencenews.com

**ADVANCED
SUSTAINABLE
SYSTEMS**

www.advsustainsys.com

based counterparts, while the charge voltage is lower than that of carbon black by 600 mV.

In order to further improve the oxygen catalytic activity, incorporating transition metal complexes into the CP matrixes is also investigated by researchers to produce non-precious oxygen catalysts.[535–546] The fine dispersion of electrocatalyst particles within the matrixes of CP can allow homogeneous distribution of catalytic active sites which will result in better catalytic performance and stable performance within a wide range of pH. Reports have indicated that those composites may present a prospect to develop stable and efficient air cathodes.[547,548] It was firstly reported in 2006 by Bashyam and Zelenay with successful demonstration of a Co-PPy-C composite with high and stable ORR electrocatalytic activity in H_2-O_2 fuel cells, where carbon-supported polypyrrole was used to entrap cobalt to generate Co-N sites.[535] Experimental testing suggested that the excellent performance was originated from the CoN_x active sites formed by the strong interactions of Co sites with polypyrrole matrix. In addition to PPy, the incorporation of cobalt or nickel into CPs, such as PANI and PMet, were also investigated.[543,544] This research suggested that the Co-PPy-C composite exhibits the best ORR catalytic activity and stability among all the composites listed above. Furthermore, the effect of different doping anions on the catalytic activity of these complexes was investigated;[545] copper manganese oxide ($Cu_{1.4}Mn_{1.6}O_4$) was introduced with PPy which displayed ORR activity at low potentials.[546] Though no research was reported utilizing this kind of composite catalyst, these studies still bring up new possibilities to produce low-cost but high performance electrocatalysts for metal-air batteries.

Owing to the high content of nitrogen and sulfur, CPs can also be used as precursors to prepare $M-N_x/C$ catalysts through high temperature pyrolysis, where CPs act as both carbon and nitrogen/sulfur sources. Compared with the transition metal immobilized CPs, it was reported that heat treatment of these composites will lead to better ORR catalytic activity.[549] This enhancement in ORR activity can be attributed to the formation of pyrrolic and quaternary nitrogen during pyrolysis process with a shift of the reaction mechanism from two-electron dominant pathway to more efficient 4-electron dominant pathway. Yuasa et al. also investigated the effect of heat treatment temperature on the catalytic activity of Co-PPy-C.[550] The experimental results showed that a maximum in electrocatalytic activity can be obtained at a pyrolysis temperature of 700 °C, when ORR active sites Co-N_4 structures can be successfully maintained by immobilizing cobalt ions with carbon based PPy.

In conclusion, the investigation of CPs as air cathode catalysts or supporting materials can be split into three approaches: (i) directly utilizing the CPs as cathode catalysts, which was already reported by some researchers to fabricate rechargeable metal-air batteries; (ii) incorporating transition metal complexes into the CP matrixes; (iii) serving as precursors to prepare pyrolyzed $M-N_x/C$ catalysts. The latter two approaches have not yet been applied in the preparation of metal-air batteries, but was successful demonstrated in fuel cells with good catalytic activity and stable performance. The similarities that fuel cells share with metal-air batteries indicate new approaches to prepare cathode catalysts. Currently, reports of the application of CPs in metal-air batteries are relatively rare. These studies indicate

that CPs could be good candidates as catalysts and supports in reversible air cathodes, opening up a new path to develop high-performance metal-air batteries.

6. Separators

For metal-air batteries and other battery systems, separators have attracted less attention compared with the rest of cell components, yet they still play an important role in determining cell performance. Generally, for all battery systems, a separator basically function as a spacer to separate the anode and cathode, preventing electrical short circuit. A separator should also be electrically nonconductive, highly ionically conductive, good mechanical and dimensional stability, good chemical stability toward electrolyte corrosion, and easy configuration.[551] For metal-air batteries, a separator should also satisfy the requirement of stable operation with reduced oxygen species and at high potential during cycling and limited diffusion of oxygen to prevent parasitic reaction with the anodes.[184,551–557] In addition, the separator should also be highly porous and possess good wettability to sustain electrolyte and ease anode dendrite formation.

Unlike proton exchange membrane fuel cells that require high-cost proton transferring membranes (e.g., Nafion), only hydroxyl (aqueous) or metal ions (nonaqueous) are transferred in metal-air batteries. Until now, separators for metal air batteries are mostly microporous polyolefin membranes based on polyethylene, polypropylene, polyvinyl alcohol, polyethylene oxide and so on. A new Zn-air battery separator polysulfonium-1, poly(methylsufonio-1,4-phenylenethio-1,4-phenylene triflate) reported by Dewi et al. was found with high selectivity in preventing self-discharge caused by cation permeation from anode to cathode and increased the discharge capacity six times greater than that using commercial available polypropylene separators.[553] Wu et al. reported that sulfonation treatment has a positive effect on the enhancement of anionic conductivity in alkaline electrolytes.[554] A solid-state Zn-air battery based on this separator exhibited a power density of 38 mW cm^{-2} at 45 mA cm^{-2}, which is much higher than that based on the untreated one (20 mW cm^{-2} at 25 mA cm^{-2}). A nanoporous inorganic MCM-41 membrane with high surface area and pore volume density was also reported as a separator for Zn-air battery.[555] The hexagonally ordered, narrow pore structure of MCM-41 membrane was found to exhibit good adsorption and retention of electrolyte; the pores also served as effective channels for ion transport. When employed as a separator, a relative high power density of 32 mW cm^{-2} and volumetric energy density of 300 Wh l^{-1} were achieved of the Zn-air battery. Other nanoporous inorganic materials such as glass fiber membrane can also be found in many reports in the Li-air battery system, mainly owing to the excellent adsorption and retention of nonaqueous aprotic electrolytes provided by its porous structure, good ionic conductivity and low cost. As an important battery component, separators have been relatively studied in the fields of metal-air battery, especially the recently popular Li-air battery system. More work should be dedicated to this component to further improve overall performance of metal-air battery.

**ADVANCED
SCIENCE NEWS**
www.advancedsciencenews.com

**ADVANCED
SUSTAINABLE
SYSTEMS**
www.advsustainsys.com

7. Anodes

Unlike the widely used lithium-ion batteries that utilize Li-storage materials (e.g., graphite, metal oxides, etc.) as anodes, metal-air batteries currently use metal foils (e.g., Li, Na, Zn, Mg, Al, etc.) which are also known as metal anodes. During discharge, the metal anode is oxidized to release electrons and metal cations (M^+) and then reduced during charge. Among all the metal anodes, lithium metal possesses an ultrahigh specific energy of up to 3860 mAh g^{-1} and a low negative potential of -3.04 V (vs standard hydrogen electrode, SHE). For Li-air battery, the Li anode faces two major problems, that is, the formation of lithium dendrites and continuous growth of solid electrolyte interface (SEI) with the increase of cycle number. The former can cause internal short-circuit which lead to serious safety problems, while the growth of SEI consumes the Li anode and electrolyte which will cause low Coulombic efficiency and eventually irreversible anode failure.[558,559] One solution to this is the adoption of a protective solid-state lithium ion conductive layer on the surface of Li anode such as LiPON, LATP, and LAGP, as has been addressed in some reports.[57,560–563] Recently, Shui et al. found that only part of the lithium metal can be recovered during cycling while lithium hydroxide constantly accumulated on anode surface upon both discharge and charge processes in a nonaqueous Li-O$_2$ battery using 1 M LiCF$_3$SO$_3$-TEGDME as electrolyte, which will lead to high polarization and limited anode reversibility.[564] The formation of lithium hydroxide can be ascribed to the produced by electrolyte decomposition during discharge and charge. We note that the cell is tested in pure oxygen atmosphere, while for practical application the operating atmosphere is air which contains H$_2$O and may not be effectively blocked by the oxygen elective membrane. The use of a protective layer can be effective in protecting the Li anode from corrosion especially with the aqueous electrolyte and also the moisture in nonaqueous electrolyte. However, it should be noted that the ionic conductivity of these protective layers is still unfavorable which contributes to the polarization of a cell. Moreover, these protective layers were also found to have poor mechanical and chemical properties which may easily fracture and deteriorate during cell operation. Walker et al. reported that the use of a 1 M LiNO$_3$-DMA electrolyte contributes to the formation of a stable SEI on the Li anode surface.[565] The authors first investigated the stability of the solvent, DMA, the formation of soluble species which are electroactive above 3.4 V was observed resulting from the reaction of DMA with Li anode. On the contrary, these species were not detected after the addition of 1 M LiNO$_3$, which can be attributed to the formation of a stable SEI on Li anode and consequently inhibated the reaction with DMA. This phenomenon can be explained by the inertness of the amide core toward reduced oxygen species and the formation of a stable and protective SEI in the presence of nitrate anions which blocked the reaction of Li with DMA. Correspondingly, the
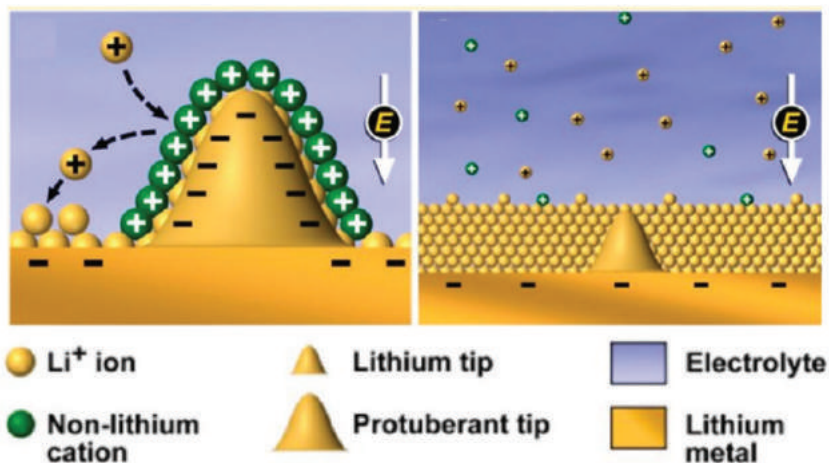

Figure 32. Schematic illustration of the proposed self-healing electrostatic shield mechanism. Reproduced with permission.[567] Copyright 2013, American Chemical Society.

Li-O$_2$ cell exhibited a stable cycling performance of over 80 cycles at 0.1 mA cm^{-2}.

Another issue is the formation of lithium dendrites which leads to potential safety hazards. Kang et al. have recently reported that a anodized aluminium oxide (AAO) membrane separator can be effective in suppress the surface roughening of Li anode.[566] The uniform ion transportation pathways provided by the porous AAO separator was found to facilitate the homogenous plating/stripping of lithium, which lead to a better anode reversibility. A novel mechanism to prevent lithium dendrite formation was proposed by Zhang's group.[567] The addition of a low concentration of some selected cations (e.g., Rb$^+$, or Cs$^+$) whose reduction potential is below that of Li$^+$ was found to form a positively charged electrostatic shield around the initial lithium tip of the protuberances during lithium deposition, as shown in **Figure 32**. This mechanism can further force the lithium to deposit on adjacent regions and thus prevent the formation of lithium dendrite. However, we note that this method may not be applicable in Li-air battery system due to the possible redox reaction of Rb$^+$ or Cs$^+$ with O$_2$, which can remove these cations from the electrolyte. Yet this concept may be extended to a broader research to discover a solution to the growth of lithium dendrite. Apart from the above proposed methods, a lithiated silicon-carbon composite anode to replace the commonly used Li metal anode was firstly reported by Scrosati's group as a metal-free anode.[568] Based on experimental data, the energy density of the reported Li$_x$Si-O$_2$ battery was estimated to 980 Wh kg^{-1}, assuming the operating discharge voltage is 2.4 V, which is more than two folds that of a state-of-the-art Li-ion battery. The replacement of a Li metal anode undoubtedly led to a compromise in the energy density and discharge voltage, the volume change of Si associated with lithiation and delithiation may also lead to limited cycle performance, yet this attempt can be effective in enhancing battery safety.

Other metal-air batteries such as Zn-air, Al-air, and Mg-air battery that utilize aqueous alkaline electrolytes, the corrosion of metal anode is the major cause accounting for the self-discharge. To the slow corrosion rate of metal anodes, various

**ADVANCED
SCIENCE NEWS**

www.advancedsciencenews.com

**ADVANCED
SUSTAINABLE
SYSTEMS**

www.advsustainsys.com

approaches have been proposed such as increase the purities of metal anodes, coating the anode surface, alloy with other metals, or add additives in the electrolytes.[569–573] For example, pure aluminium (99.999%), technical grade aluminium (99.8%) and the alloys with indium and tin were investigated as anodes for Al-air batteries using a NaCl-based electrolyte.[570] Experimental results showed that the Al-In alloy exhibited more favorable electrochemical properties such as minimal negative difference effect (NDE), hydrogen evolution rate, and a low anodic polarization. It should also be noted that aluminium can actively react with alkaline electrolyte, thus neutral electrolytes is commonly used to decrease heat generation. In addition to the modification of metal compositions to enhance the corrosion resistance, the fabrication of a protection film on the metal Li anode is also an effective strategy.[571] As reported by Qing et al., the stability of Li anode is protected effectively with the help of protection film. The Li-O_2 battery with the protected lithium anode has exhibited superior cycle stability-more than 100 stable cycles under a fixed capacity of 1000 mA h g^{-1} at a current density of 300 mA g^{-1}, which is more than three times that of the Li-O_2 battery with the pristine Li metal as an anode (31 cycles). Simultaneously, it is well acknowledged that the anode performance can be effectively enhanced by tailoring the morphology to increase the surface area.[574–576] As is the situation in Li-air battery, other metal-air batteries also suffer from the dendrite formation during cycling, which lead to safety hazards during operation.[577,578] Banik et al. reported that the addition of polyethylene glycol in the electrolyte can effectively suppress the formation of dendrite during the zinc electrodeposition.

To briefly summarize, metal-air battery anodes are relatively less investigated given that the performance enhancement of air electrodes is a more critical issues at the current stage of development of metal-air battery technologies. The challenges facing the anodes are associated with the corrosion and irreversible recovery and dendrite formation with the increase of cycle numbers. Further investigation is required to address these problems to achieve better electrochemical and safety performances for metal-air batteries.

8. Kinetics and Interfaces

The electrochemical performances of metal-air batteries are correlated with the kinetics which manifests in rate capability, energy density, round-trip efficiency, cycle life, overpotentials, and so on. The above reviewed research efforts are almost entirely associated with the enhancement of kinetics. For instance, the kinetics of ORR and OER can be influenced by dissolve and diffusion of oxygen, electrolyte viscosity, transportation of electrolytes and metal cations throughout the porous structure of air cathodes, catalytic activity of electrocatalysts, morphology and charge transport of discharge products, etc.[12,62–64,97–104,107–132,352,353,579–582] As reported by Read et al., the nature of electrolyte such as viscosity, oxygen solubility and diffusion properties affect greatly on the discharge performances.[12,62–64] In addition, the electrolyte should possess good wettability to guarantee favorable contact with the air cathode while not over-flood the porous structure to sustain the essen-

tial triphase interfaces for oxygen reduction. At the same time, the air cathode structure should be well-designed to facilitate fast transportation of oxygen and electrolyte. Furthermore, the addition of electrocatalysts in the cathode nanostructure has been proved effective in accelerating the proceedings of ORR and OER processes. For nonaqueous Li-air and Na-air batteries, the cathode structure should also accommodate the accumulation of solid discharge products as well as maintaining the continuous discharge process. A Li-air battery cathode structure design proposed by our group can serve as an efficient solution to this requirement.[186] Moreover, the control over the characteristics of the solid discharge products also plays an important part in determining the electrochemical kinetics which further influence discharge capacity, rate capability, round-trip efficiencies, and so on. For example, Li_2O_2 with a layered structure, poor crystallinity, and metal-like properties was found to facilitate the subsequent decomposition of Li_2O_2 at low potential on charge, which lead to relatively low energy loss.[48,192] Such structure might be resulted from the synergy of fast ORR kinetics and catalytic preferential deposition of Li_2O_2. This enhancement in OER process can be explained by the favorable interface properties resulting from the close and massive contact of Li_2O_2 with catalytic active sites and highly conductive cathode support that benefit the improvement of OER kinetics and the metal-like nature which favors the charge transport upon charging. Moreover, the lower the charge overpotentials can prevent potential degradation of electrolyte and carbon cathode, leading to more stable and prolonged cycling performance. While on the contrary, the decomposition of the more typical Li_2O_2 structure (e.g., toroidal-like particles) with a large particle size and small contact area with cathode surface can lead to high charge overpotentials and low round-trip efficiencies. Additionally, the introduction of soluble redox mediators which can serve as a medium for electron transportation at the electrolyte-Li_2O_2 interface was found to effectively catalyze the decomposition of Li_2O_2.[180–184] To briefly summarize, the goal to enhance the electrochemical performances of metal-air batteries depend largely on the improvement of kinetics and interfaces which should be combined with the research efforts on building more rational cathode structure with high catalytic activity, utilization of better electrolytes that favor fast dissolve and diffusion of oxygen, and construction of high-efficiency interfaces to lower energy barriers during electrochemical processes.

9. In situ Analyses of Discharged Product Characterization

In light of the researches mentioned above, intensive efforts have been devoted into improving the performances of metal-air battery, such as the construction of powerful electrodes, the selection of stable electrolyte and the application of effective catalyst etc. However, the development of these metal-air batteries, especially the aprotic Li-O_2 battery is restricted by many difficulties such as the poor rate capacity, low round-trip efficiency etc. To address these problems, the fundamental understanding of the oxygen reaction mechanisms during discharge and charge should be deepened, so as to help identify effective

**ADVANCED
SCIENCE NEWS**

www.advancedsciencenews.com

**ADVANCED
SUSTAINABLE
SYSTEMS**

www.advsustainsys.com

strategies to improve the performance of Li-O$_2$ battery, such as developing stable and reversible oxygen electrodes, application of stable electrolyte etc. In this aspect, various kinds of in situ analyses of discharged product characterization including in situ surface enhanced Raman spectroscopy (SERS) technique, FTIR, quantitative differential electrochemical mass spectrometry (DEMS) and XRD have been carried out.[583–587] In detail, Lu et al. has applied an in situ surface enhanced Raman spectroscopy (SERS) technique can gain significant insights into the reaction intermediates and products of the Li–O$_2$ redox chemistry.[583] And Read et al. has analyzed the decomposition process of the electrolyte with in situ FTIR technique.[586] In addition, in situ XRD technique was developed to provide a simple and straightforward analytical method for simultaneously attaining chemical and quantified information on Li$_2$O$_2$ (discharge product) and byproducts.[588] Benefitting from the identification of discharge product, the real-time acquisition of the Li$_2$O$_2$ XRD pattern allowed us to estimate the increasing and decreasing Li$_2$O$_2$ peak-area change, thus revealing the rates of formation and decomposition of solid-state Li$_2$O$_2$ during discharge and recharge, respectively. More recently, Wang et al. has revealed the reaction mechanisms of Li-O$_2$ batteries using environmental transmission electron microscopy.[589] In this research, the authors have imaged the product morphology evolution on a carbon nanotube (CNT) cathode of a working solid state Li-O$_2$ nanobattery and correlate these features with the electrochemical reaction at the electrode. They find that the oxygen-reduction reaction (ORR) on CNTs initially produces LiO$_2$, which subsequently disproportionates into Li$_2$O$_2$ and O$_2$. The release of O$_2$ creates a hollow nanostructure with Li$_2$O outer-shell and Li$_2$O$_2$ inner-shell surfaces. Their findings show that, in general, the way the released O$_2$ is accommodated is linked to lithium-ion diffusion and electron-transport paths across both spatial and temporal scales; in turn, this interplay governs the morphology of the discharging/charging products in Li-O$_2$ cells. In situ techniques provide a powerful approach for exploring the fundamental nanoscale processes, which impact the cell-level performance. Given the similarity in the cell chemistry between Li-O$_2$ battery and Na-O$_2$ battery, these techniques used in the Li-O$_2$ field can be applied in the Na-O$_2$ field, thus being able to push the development of Na-O$_2$ battery. At the same time, the advance in analyzing the discharged product with in situ technique will provide an improved understanding of the mechanisms of the ORR and OER in the metal–air batteries.

10. Challenges and Outlook

Metal-air batteries possess a huge advantage over other battery systems such as Li-ion, lead-acid, and Ni-HM batteries in that they are able to provide much higher specific energies. The semi-open structure can effectively reduce the battery weight, which lead to a high gravimetric energy density. Li-air battery can provide the highest theoretical specific energy amongst all metal-air batteries and also possesses some advantages over fuel cells including easy configuration and low cost. Such high energy output of metal-air batteries, if fully exploited, can serve as next-generation high performance and environmental benign power

sources for large-scale energy storage systems, mobile energy fields and aerospace industry. Thanks to the rapid research development on the preparation of nanomaterials and the corresponding characterization technology, metal-air batteries, especially Li-air battery have regained considerable research interests as they hold a key to the future success of the global energy consumption shift from fossil resources to renewable energies. To this end, this review is dedicated to provide a comprehensive and systematic summarization of the development and mechanism understandings of this promising and popular research area.

To date, there have already been some commercial applications of metal-air batteries as high energy density, low-cost and environmental benign power sources. For instance, Al-air batteries have been applied to power marine navigation beacons; Zn-air batteries are widely used in hearing-aids and can also be found in some railway signal lamps. Moreover, various attempts have been carried out explore their application in PEVs to replace currently used lithium-ion batteries. Despite the promising properties and some successful practical applications, metal-air batteries are still inferior in some aspects, hindering their large-scale utilization. For example, commercial metal-air batteries are currently deposable or mechanically rechargeable, while commercial lithium-ion batteries can be recharged at least for 1000 times in average. The semi-open structure can effectively simplify the configuration and lower cell weight and cost, yet such design can also lead to potential electrolyte leakage under sever vibrations, extruding or decompression conditions. An enclosed design can effectively solve this issue but require an additional air-supply system, complicating the battery configuration and thus losing the advantage over lithium-ion batteries. The high recycle cost of disused cells is also a challenge especially for compact metal-air batteries. In addition, the CO$_2$ and H$_2$O in air can interfere the desired electrochemical processes in metal-air batteries, whereas current membrane technology cannot effectively block those unwanted components while guarantee the fast penetration of O$_2$. To sum up, great potential and huge challenges coexist in this area.

For researchers, some basic issues should be overcame before their large-scale application. Aqueous metal-air batteries such as Zn-air, Al-air, and Mg-air battery mainly suffer from poor rechargeability, sluggish kinetics, and anode degradation. To this end, various ORR and OER electrocatalysts have been investigated to enhance the rechargeability and kinetics alloying or increase purity of anodes were also introduced to improve their corrosion resistance. Nevertheless, it should be noted that the concept of aqueous metal-air fuel cells have been proposed for quite a long time, yet the practical application of these batteries is incomparable to the worldwide commercial triumph of lithium-ion batteries.

For nonaqueous metal-air batteries especially Li-air battery, the challenges mainly lie in five aspects: (i) the lack of a fundamental understanding of the reaction mechanism associated with the nature of electrocatalysts and electrochemical processes of ORR and OER in nonaqueous aprotic electrolytes; (ii) the instability of electrolytes and carbon-based cathodes can lead to a series of parasitic reactions that largely reduce the cycling performances and capacity; (iii) low-cost and high efficient bifunctional electrocatalysts are required to increase kinetics to lower the overpotentials during discharge and charge and

**ADVANCED
SCIENCE NEWS**

www.advancedsciencenews.com

**ADVANCED
SUSTAINABLE
SYSTEMS**

www.advsustainsys.com

improve rate capability and cycling performances such as Coulombic and cycle efficiency and cycle life; (iv) rational structure designs of the air cathodes are needed to achieve full utilization of the porous nanostructure to increase specific capacity and further enhance the electrochemical kinetics; (v) the irreversible recovery of anodes during cycling also decreases cycle life and will lead to high polarization, furthermore, the formation of highly reactive lithium and sodium dendrites is also a safety issues that should be settled before commercialization.

To start with, a thorough understanding of the oxygen electrochemistry and catalytic mechanism is the first and most critical step toward the design of a high-performance Li-air battery. A combination of nanoscale modelling, theoretical and in situ experimental analysis is believed to provide more insights and deepen our mechanistic understanding of the oxygen electrochemistry in nonaqueous metal-air battery systems. Secondly, the instability of electrolytes (including organic solvents and salts) and carbon electrodes can cause the formation of by-products which in turn accelerates the proceed of parasitic reaction, leading to overwhelming degradation of electrolytes and electrodes rather than the formation and decomposition of expected discharge products, which ultimately decreases the cycling performances of metal-air batteries. Thirdly, a highly efficient electrocatalyst can remarkably increase the reaction kinetics, thus enhance the overall battery performance. Of the five classes of electrocatalysts discussed in section 5, noble metal and their alloys and oxides exhibit excellent catalytic activity and long-term stability, yet the high makes it impractical for their large-scale application in metal-air batteries. Pt, for instance, has been widely adopted as a benchmark to evaluate the performance of electrocatalysts. Comparatively, other classes of catalysts such as carbonaceous materials, transition metal oxides, metal-nitrogen compounds, and conductive polymers are less expensive but also have pros and cons. Nanostructured carbon such as CNTs and graphene show good electric conductivity but inferior catalytic activity. Doping with heteroatoms have been proposed to enhance their activity. Transition metal oxides are also widely investigated owing to their favorable and bifunctional activity. Composing with highly conductive carbon materials can alleviate the drawback of low conductivity. The properties of metal-nitrogen compounds and their derived $M-N_x/C$ can be easily tailored by controlling the metal centers and organic ligands, yet the preparation is relatively complicated and more investigation should be conducted no their utilization in organic electrolytes. Further, one should note the instability issue of carbon under high charge overpotentials when used in nonaqueous Li-air batteries. Moreover, the search for catalysts in organic electrolytes are initially adopted from the research in aqueous electrolytes which have been carried out for decades, more work should be done to discover more efficient electrocatalysts on the basis of a thorough understanding of the mechanism in nonaqueous environments. Fourthly, a rational cathode design will not only increase specific capacity through better utilization of the porous structure but also enhance electrochemistry kinetics by providing effective mass transportation pathways and exposing more catalytic active sites on optimized triphase interfaces. To date, a series of feasible cathode structure designs have been proposed, more improvements are believed to be achieved with the rapid development of materials and chemistry science. Finally, the anode have been rarely researched when numerous reports are concerning other aspects, yet the anode performance can also be a limiting factor of battery performance. The major problem facing the Li anode is dendrite formation and irreversible cycling. Considering the high activity of Li, the formation of dendrites may cause short circuits which poses serious safety hazards. Li metal anode is also found to gradually turn into LiOH as a result of a series of parasitic reactions of electrolyte and Carbon cathode, which in turn lead to high polarization and limited cycle number. It can be concluded that the improvement in battery performance require a systematic study on the fundamental mechanism and all battery components.

Currently, flexible and on-chip micro power sources have attracted considerable research and commercial interests in that they can meet the energy demand in versatile situations, which endows extensive applications in portable, wearable, and implantable smart electronic devices. Extensive efforts have been devoted to the research of suitable power sources, mainly focusing on supercapacitors and lithium-ion batteries, as reviewed by our group.[590] Metal-air batteries, on the other hand, can provide ultra-high energy output, which we believe can act as a promising candidate. The challenge here is the prevention of leakage of liquid electrolytes and replacement of less flexible mental anodes. Learning from the experience of the research in flexible supercapacitors and lithium-ion batteries, polymer electrolytes can be an effective solution to electrolyte leakage from the semi-open structure. However, no effective solution have been proposed so far to the replacement of metal anodes while maintaining relative high energy output.

Of all the challenges stated above, the acquisition of an insightful understanding on the mechanisms of oxygen electrochemistry during cycling is of vital importance, on which guidance we can develop more efficient and high performance electrocatalysts and air cathodes, more stable electrolytes and anodes. We believed that when fully developed, metal-air batteries, especially Li-air batteries, can exceed most current battery technologies with ultra-high energy density but at a much lower cost and less environmental compacts. It also believed that metal-air batteries will play an important role in building a petrol-independent and environmentally-friendly society.

Acknowledgements

Conflict of Interest

The authors declare no conflict of interest.

Keywords

**ADVANCED
SCIENCE NEWS**

www.advancedsciencenews.com

**ADVANCED
SUSTAINABLE
SYSTEMS**

www.advsustainsys.com

[1] M. Eberhard, M. Tarpenning, *The 21st Century Electric Car*, Tesla Motors, Palo Alto, CA, USA, **2006**.

[2] G. A. Nazri, G. Pistoia, *Lithium Batteries Science and Technology*, Kluwer Academic Publishers, Dordrecht, The Netherlands, **2004**.

[3] W. V. Schalkwijk, B. Scrosati, *Advances in Lithium-Ion Batteries*, Kluwer Academic Publishers, Dordrecht, The Netherlands, **2002**.

[4] D. Linden, *Handbook of Batteries and Fuel Cells*, McGraw-Hill, New York, **1984**.

[5] V. Etacheri, R. Marom, R. Elazari, G. Salitra, D. Aurbach, *Energy Environ. Sci.* **2011**, *4*, 3243.

[6] K. G. Gallagher, S. Goebel, T. Greszler, M. Mathias, W. Oelerich, D. Eroglu, V. Srinivasan, *Energy Environ. Sci.* **2014**, *7*, 1555.

[7] Fuel Cells, http://americanhistory.si.edu/fuelcells/alk/alk3.htm (accessed: January 2015).

[8] N. Yabuuchi, K. Kubota, M. Dahbi, S. Komaba, *Chem. Rev.* **2014**, *114*, 11636.

[9] Y. G. Li, H. J. Dai, *Chem. Soc. Rev.* **2014**, *43*, 5257.

[10] E. L. Littauer, K. C. Tsai, *J. Electrochem. Soc.* **1976**, *123*, 771.

[11] K. M. Abraham, Z. Jiang, *J. Electrochem. Soc.* **1996**, *143*, 1.

[12] J. Read, *J. Electrochem. Soc.* **2002**, *149*, A1190.

[13] T. Ogasawara, A. Debart, M. Holzapfel, P. Novak, P. G. Bruce, *J. Am. Chem. Soc.* **2006**, *128*, 1390.

[14] M. Armand, J. M. Tarascon, *Nature* **2008**, *451*, 652.

[15] Z. L. Wang, D. Xu, J. J. Xu, X. B. Zhang, *Chem. Soc. Rev.* **2014**, *43*, 7746.

[16] S. Wu, J. Tang, F. Li, X. Liu, Y. Yamauchi, M. Ishida, H. Zhou, *Adv. Funct. Mater.* **2016**, *26*, 3291.

[17] T. Liu, M. Leskes, W. Yu, A. J. Moore, L. Zhou, P. M. Bayley, G. Kim, C. P. Grey, *Science* **2015**, *350*, 53.

[18] H.-D. Lim, B. Lee, Y. Zheng, J. Hong, J. Kim, H. Gwon, Y. Ko, M. Lee, K. Cho, K. Kang, *Nat. Energy* **2016**, *1*, 16066.

[19] A. Kraytsberg, Y. Ein-Eli, *Nano Energy* **2013**, *2*, 468.

[20] P. G. Bruce, S. A. Freunberger, L. J. Hardwick, J. M. Tarascon, *Nat. Mater.* **2012**, *11*, 19.

[21] P. Hartmann, M. Heinemann, C. L. Bender, K. Graf, R.-P. Baumann, P. Adelhelm, C. Heiliger, J. R. Janek, *J. Phys. Chem. C* **2015**, *119*, 22778.

[22] J. L. Ma, J. B. Wen, J. H. X. Zhu, Q. N. Li, *J. Power Sources* **2015**, *293*, 1.

[23] A. L. Vignesh, M. Prabu, S. Shanmugam, *ACS Appl. Mater. Interfaces* **2016**, *8*, 6019.

[24] Y. Shao, F. Ding, J. Xiao, J. Zhang, W. Xu, S. Park, J. G. Zhang, Y. Wang, J. Liu, *Adv. Funct. Mater.* **2013**, *23*, 987.

[25] J. Lu, L. Li, J.-B. Park, Y.-K. Sun, F. Wu, K. Amine, *Chem. Rev.* **2014**, *114*, 5611.

[26] A. A. Franco, K.- H. Xue, *ECS J. Solid State Sci. Technol.* **2013**, *2*, M3084.

[27] Z. Guo, X. Dong, S. Yuan, Y. Wang, Y. Xia, *J. Power Sources* **2014**, *264*, 1.

[28] L. L. Zhang, Z. L. Wang, D. Xu, X. B. Zhang, L. M. Wang, *Int. J. Smart Nano Mater.* **2013**, *4*, 27.

[29] X. D. Ren, K. C. Lau, M. Z. Yu, X. X. Bi, E. Kreidler, L. A. Curtiss, Y. Y. Wu, *ACS Appl. Mater. Interfaces* **2014**, *6*, 19299.

[30] Y. C. Lu, B. M. Gallant, D. G. Kwabi, J. R. Harding, R. R. Mitchell, M. S. Whittingham, Y. Shao-Horn, *Energy Environ. Sci.* **2013**, *6*, 750.

[31] L. Shi, A. Xu, T. Zhao, *Phys. Chem. Chem. Phys.* **2015**, *17*, 29859.

[32] F. Li, H. Kitaura, H. Zhou, *Energy Environ. Sci.* **2013**, *6*, 2302.

[33] H. Zhou, *Energy Environ. Sci.* **2013**, *6*, 2256.

[34] N. Akhtar, W. Akhtar, *Int. J. Energy Res.* **2014**, *39*, 303.

[35] M. A. Rahman, X. Wang, C. Wen, *J. Appl. Electrochem.* **2013**, *44*, 5.

[36] F. Wang, C. S. Liang, D. L. Xu, H. Q. Cao, H. Y. Sun, Z. K. Luo, *Int. J. Inorg. Mater.* **2013**, *27*, 1233.

[37] X. X. Guo, S. T. Huang, N. Zhao, Z. H. Cui, W. G. Fan, C. L. Li, H. Li, *Int. J. Inorg. Mater.* **2014**, *29*, 113.

[38] D. Capsoni, M. Bini, S. Ferrari, E. Quartarone, P. Mustarelli, *J. Power Sources* **2012**, *220*, 253.

[39] K. P. Yao, M. Risch, S. Y. Sayed, Y.-L. Lee, J. R. Harding, A. Grimaud, N. Pour, Z. Xu, J. Zhou, A. Mansour, *Energy Environ. Sci.* **2015**, *8*, 2417.

[40] A. Kraytsberg, Y. Ein-Eli, *J. Power Sources* **2011**, *196*, 886.

[41] E. J. Yoo, H. S. Zhou, *RSC Adv.* **2014**, *4*, 13119.

[42] N. Garcia-Araez, P. Novák, *J. Solid State Electrochem.* **2013**, *17*, 1793.

[43] H. Ohmori, H. Iwai, K. Itakura, M. Saito, H. Yoshida, *J. Power. Sources* **2016**, *309*, 160.

[44] Y. Sun, *Nano Energy* **2013**, *2*, 801.

[45] J. Wang, Y. Li, X. Sun, *Nano Energy* **2013**, *2*, 443.

[46] L. Fan, H. M. Lu, J. Leng, *Eletro Acta* **2015**, *165*, 22.

[47] M. D. Bhatt, H. Geaney, M. Nolan, C. O'Dwyer, *Phys. Chem. Chem. Phys.* **2014**, *16*, 12093.

[48] S. I. Smedley, X. G. Zhang, *J. Power Sources* **2007**, *165*, 897.

[49] J. Y. Cheon, K. H. Kim, Y. J. Sa, S. H. Sahgong, Y. Hong, J. Woo, S.-D. Yim, H. Y. Jeong, Y. Kim, S. H. Joo, *Adv. Energy Mater.* **2016**, 1501794.

[50] D. R. Egan, C. Ponce de León, R. J. K. Wood, R. L. Jones, K. R. Stokes, F. C. Walsh, *J. Power Sources* **2013**, *236*, 293.

[51] E. I. Shkolnikov, A. Z. Zhuk, M. S. Vlaskin, *Renewable Sustainable Energy Rev.* **2011**, *15*, 4611.

[52] K.-Y. Zhou, G.-Y. Chen, J.-A. Liu, Z.-P. Zhang, P. Sun, W.-Z. Zhang, F. Niu, W.-X. Zhang, J.-C. Liang, *RSC Adv.* **2016**, *6*, 90069.

[53] T. Zhang, Z. Tao, J. Chen, *Mater. Horiz.* **2014**, *1*, 196.

[54] S. K. Das, S. Lau, L. Archer, *J. Mater. Chem. A* **2014**, *2*, 12623.

[55] G. Vardar, E. G. Nelson, J. G. Smith, J. Naruse, H. Hiramatsu, B. M. Bartlett, A. E. S. Sleightholme, D. J. Siegel, C. W. Monore, *Chem. Mater.* **2015**, *27*, 7564.

[56] T. Zhang, H. Zhou, *Angew. Chem. Int. Ed.* **2012**, *51*, 11062.

[57] T. Zhang, N. Imanishi, S. Hasegawa, A. Hirano, J. Xie, Y. Takeda, O. Yamamoto, N. Sammes, *J. Electrochem. Soc.* **2008**, *155*, A965.

[58] P. S. Ruvinskiy, A. Bonnefont, C. Pham-Huu, E. R. Savinova, *Langmuir* **2011**, *27*, 9018.

[59] A. Schneider, L. Colmenares, Y. E. Seidel, Z. Jusys, B. Wickman, B. Kasemo, R. Behm, *J. Phys. Chem. Chem. Phys.* **2008**, *10*, 1931.

[60] A. Ito, L. W. Zhao, S. Okada, J.-I. Yamaki, *J. Power Sources* **2011**, *196*, 8154.

[61] M. Jingling, W. Jiuba, Z. Hongxi, L. Quanan, *J. Power Sources* **2015**, *293*, 592.

[62] J. Read, K. Mutolo, M. Ervin, W. Behl, J. Wolfenstine, A. Driedger, D. Foster, *J. Electrochem. Soc.* **2003**, *150*, A1351.

[63] J. Read, *J. Electrochem. Soc.* **2006**, *153*, A96.

[64] S. Zhang, D. Foster, J. Read, *J. Power Sources* **2010**, *195*, 1235.

[65] C. O. Laoire, S. Mukerjee, K. M. Abraham, E. J. Plichta, M. A. Hendrickson, *J. Phys. Chem. C* **2009**, *113*, 20127.

[66] C. O. Laoire, S. Mukerjee, K. M. Abraham, E. J. Plichta, M. A. Hendrickson, *J. Phys. Chem. C* **2010**, *114*, 9178.

[67] C. J. Allen, J. Hwang, R. Kautz, S. Mukerjee, E. J. Plichta, M. A. Hendrickson, K. M. Abraham, *J. Phys. Chem. C* **2012**, *116*, 20755.

[68] A. C. Luntz, B. D. McCloskey, *Chem. Rev.* **2014**, *114*, 11721.

[69] Y. C. Lu, H. A. Gasteiger, Y. Shao-Horn, *Electrochem. Solid-State Lett.* **2011**, *14*, A70.

[70] Z. Peng, S. A. Freunberger, L. J. Hardwick, Y. Chen, V. Giordani, F. Barde, P. Novak, D. Graham, J. M. Tarascon, P. G. Bruce, *Angew. Chem. Int. Ed.* **2011**, *50*, 6351.

**ADVANCED
SCIENCE NEWS**

www.advancedsciencenews.com

**ADVANCED
SUSTAINABLE
SYSTEMS**

www.advsustainsys.com

[71] J. S. Hummelshoj, J. Blomqvist, S. Datta, T. Vegge, J. Rossmeisl, K. S. Thygesen, A. C. Luntz, K. W. Jacobsen, J. K. Norskov, *J. Chem. Phys.* **2010**, *132*, 071101.

[72] B. D. McCloskey, R. Scheffler, A. Speidel, G. Girishkumar, A. C. Luntz, *J. Phys. Chem. C* **2012**, *116*, 23897.

[73] Y. Zhang, X. M. Zhang, J. W. Wang, W. C. Mcke, Y. Xu, Z. Q. Peng, *J. Phys. Chem. C* **2016**, *120*, 3690.

[74] X. Guo, N. Zhao, *Adv. Energy Mater.* **2013**, *3*, 1413.

[75] P. Tan, Z. Wei, W. Shyy, T. S. Zhao, *Appl. Energy* **2013**, *109*, 275.

[76] K. C. Lau, J. Lu, X. Luo, L. A. Curtiss, K. Amine, *ChemPlusChem* **2015**, *80*, 336.

[77] R. Cao, E. D. Walter, W. Xu, E. N. Nasybulin, P. Bhattacharya, M. E. Bowden, M. H. Engelhard, J. G. Zhang, *ChemSusChem* **2014**, *7*, 2436.

[78] J. Z. Zhu, X. D. Ren, J. J. Liu, W. Q. Zhang, Z. Y. Wen, *ACS Catal.* **2015**, *5*, 73.

[79] B. D. Adams, C. Radtke, R. Black, M. L. Trudeau, K. Zaghib, L. F. Nazar, *Energy Environ. Sci.* **2013**, *6*, 1772.

[80] B. Horstmann, T. Danner, W. G. Bessler, *Energy Environ. Sci.* **2013**, *6*, 1299.

[81] H. Zheng, D. D. Xiao, X. Li, Y. Liu, Y. Wu, J. P. Wang, K. Jiang, C. Chen, L. Gu, X. L. Wei, Y.-S. Hu, Q. Chen, H. Li, *Nano Lett.* **2014**, *14*, 4245.

[82] J. Z. Zhu, F. Wang, B. Z. Wang, Y. W. Wang, J. J. Liu, W. Q. Zhang, Z. Y. Wen, *J. Am. Chem. Soc.* **2015**, *137*, 13572.

[83] B. D. Adams, R. Black, C. Radtke, Z. Williams, B. L. Mehdi, N. D. Browning, L. F. Nazar, *ACS Nano* **2014**, *8*, 12483.

[84] Y. C. Lu, Y. Shao-Horn, *J. Phys. Chem. Lett.* **2013**, *4*, 93.

[85] S. S. Sandhu, G. W. Brutchen, J. P. Fellner, *J. Power Sources* **2007**, *170*, 196.

[86] C. O. Laoire, S. Mukerjee, K. M. Abraham, E. J. Plichta, M. A. Hendrickson, *J. Phys. Chem. C* **2010**, *114*, 9178.

[87] C. J. Allen, J. Hwang, R. Kautz, S. Mukerjee, E. J. Plichta, M. A. Hendrickson, K. M. Abraham, *J. Phys. Chem. C* **2012**, *116*, 20755.

[88] B. M. Gallant, D. G. Kwabi, R. R. Mitchell, J. Zhou, C. V. Thompson, Y. Shao-Horn, *Energy Environ. Sci.* **2013**, *6*, 2518.

[89] Y. C. Lu, H. A. Gasteiger, Y. Shao-Horn, *Electrochem. Solid-State Lett.* **2011**, *14*, A70.

[90] B. D. McCloskey, D. S. Bethune, R. M. Shelby, G. Girishkumar, A. C. Luntz, *J. Phys. Chem. Lett.* **2011**, *2*, 1161.

[91] B. D. McCloskey, D. S. Bethune, R. M. Shelby, T. Mori, R. Scheffler, A. Speidel, M. Sherwood, A. C. Luntz, *J. Phys. Chem. Lett.* **2012**, *3*, 3043.

[92] J. Hong, H. D. Lim, M. Lee, S. W. Kim, H. Kim, S. T. Oh, G. C. Chung, K. Kang, *Chem. Mater.* **2012**, *24*, 2692.

[93] H.-K. Lim, H.-D. Lim, K.-Y. Park, D.-H. Seo, H. Gwon, J. Hong, W. A. Goddard, H. Kim III, K. Kang, *J. Am. Chem. Soc.* **2013**, *135*, 9733.

[94] D. Zhai, H. H. Wang, K. C. Lau, J. Gao, P. C. Redfern, F. Kang, B. Li, E. Indacochea, U. Das, H. H. Sun, H. J. Sun, K. Amine, L. A. Curtiss, *J. Phys. Chem. Lett.* **2014**, *5*, 2705.

[95] G. Yang, Y. Wang, Y. Ma, *J. Phys. Chem. Lett.* **2014**, *5*, 2516.

[96] N. B. Aetukuri, B. D. McCloskey, J. M. Garcia, L. E. Krupp, V. Viswanathan, A. C. Luntz, *Nat. Chem.* **2015**, *7*, 50.

[97] H. Cheng, K. Scott, *Appl. Catal. B* **2011**, *140*, 108.

[98] S. Meini, M. Piana, N. Tsiouvaras, A. Garsuch, H. A. Gasteiger, *Electrochem. Solid-State Lett.* **2012**, *15*, A45.

[99] J. Lu, Y. J. Lee, X. Y. Luo, K. C. Lau, M. Asadi, H.-H. Wang, S. Brombosz, J. Wen, D. Y. Zhai, Z. H. Chen, D. J. Miller, Y. S. Jeong, J.-B. Park, Z. Z. Fang, B. D. Kumar, A. S.-K hojin, Y.-K. Sun, L. A. Curtiss, K. Amine, *Nature* **2016**, *529*, 377.

[100] S. R. Gowda, A. Brunet, G. M. Wallraff, B. D. McCloskey, *J. Phys. Chem. Lett.* **2013**, *4*, 276.

[101] M. Mirzaeian, P. J. Hall, *J. Power Sources* **2010**, *195*, 6817.

[102] W. Xu, K. Xu, V. V. Viswanathan, S. A. Towne, J. S. Hardy, J. Xiao, Z. Nie, D. Hu, D. Wang, J. G. Zhang, *J. Power Sources* **2011**, *196*, 963.

[103] M. Mirzaeian, P. J. Hall, F. B. Sillars, I. Fletcher, M. M. Goldin, G. O. Shitta-bey, H. F. Jirandehi, *J. Electrochem. Soc.* **2012**, *160*, A25.

[104] J. B. Park, J. Hassoun, H. G. Jung, H. S. Kim, C. S. Yoon, I. H. Oh, B. Scrosati, Y. K. Sun, *Nano. Lett.* **2013**, *13*, 2971.

[105] X. Y. Lu, Y. Yin, L. Zhang, L. X. Xi, S. Oswald, J. W. Deng, *Nano Energy* **2016**, *30*, 69.

[106] J. R. Harding, Y. C. Lu, Y. Tsukada, Y. Shao-Horn, *Phys. Chem. Chem. Phys.* **2012**, *14*, 10540.

[107] R. R. Mitchell, B. M. Gallant, Y. Shao-Horn, C. V. Thompson, *J. Phys. Chem. Lett.* **2013**, *4*, 1060.

[108] B. Horstmann, B. Gallant, R. Mitchell, W. G. Bessler, Y. Shao-Horn, M. Z. Bazant, *J. Phys. Chem. Lett.* **2013**, *4*, 4217.

[109] S. Nakanishi, F. Mizuno, K. Nobuhara, T. Abe, H. Iba, *Carbon* **2012**, *50*, 4794.

[110] D. Zhai, H.-H. Wang, J. Yang, K. C. Lau, K. Li, K. Amine, L. A. Curtiss, *J. Am. Chem. Soc.* **2013**, *135*, 15364.

[111] L. Zhong, R. R. Mitchell, Y. Liu, B. M. Gallant, C. V. Thompson, J. Y. Huang, S. X. Mao, Y. Shao-Horn, *Nano Lett.* **2013**, *13*, 2209.

[112] H. Zheng, D. Xiao, X. Li, Y. Liu, Y. Wu, J. Wang, K. Jiang, C. Chen, L. Gu, X. Wei, Y. S. Hu, Q. Chen, H. Li, *Nano Lett.* **2014**, *14*, 4245.

[113] R. Wen, M. Hong, H. R. Byon, *J. Am. Chem. Soc.* **2013**, *135*, 10870.

[114] V. Viswanathan, K. S. Thygesen, J. S. Hummelshoj, J. K. Norskov, G. Girishkumar, B. D. McCloskey, A. C. Luntz, *J. Chem. Phys.* **2011**, *135*, 214704.

[115] M. Leskes, N. E. Drewett, L. J. Hardwick, P. G. Bruce, G. R. Goward, C. P. Grey, *Angew. Chem., Int. Ed.* **2012**, *51*, 8560.

[116] J. L. Shui, J. S. Okasinski, D. Zhao, J. D. Almer, D. J. Liu, *ChemSusChem* **2012**, *5*, 2421.

[117] M. D. Radin, J. F. Rodriguez, F. Tian, D. J. Siegel, *J. Am. Chem. Soc.* **2012**, *134*, 1093.

[118] M. D. Radin, F. Tian, D. J. Siegel, *J. Mater. Sci.* **2012**, *47*, 7564.

[119] K. C. Lau, R. S. Assary, P. Redfern, J. Greeley, L. A. Curtiss, *J. Phys. Chem. C* **2012**, *116*, 23890.

[120] L. Johnson, C. M. Li, Z. Liu, Y. H. Chen, S. A. Freunberger, P. C. Ashok, B. B. Praveen, K. Dholakia, J.-M. Tarascon, P. G. Bruce, *Nat. Chem.* **2014**, *6*, 1091.

[121] M. D. Radin, D. J. Siegel, *Energy Environ. Sci.* **2013**, *6*, 2370.

[122] J. M. Garcia-Lastra, J. S. G. Myrdal, R. Christensen, K. S. Thygesen, T. Vegge, *J. Phys. Chem. C* **2013**, *117*, 5568.

[123] J. B. Varley, V. Viswanathan, J. K. Nørskov, A. C. Luntz, *Energy Environ. Sci.* **2014**, *7*, 720.

[124] O. Gerbig, R. Merkle, J. Maier, *Adv. Mater.* **2013**, *25*, 3129.

[125] M. Leskes, N. E. Drewett, L. J. Hardwick, P. G. Bruce, G. R. Goward, C. P. Grey, *Angew. Chem. Int. Ed.* **2012**, *51*, 8560.

[126] Y. Wang, *Electrochim. Acta* **2012**, *75*, 239.

[127] W. Fan, Z. Cui, X. Guo, *J. Phys. Chem. C* **2013**, *117*, 2623.

[128] Y. Hu, X. Han, F. Cheng, Q. Zhao, Z. Hu, J. Chen, *Nanoscale* **2014**, *6*, 177.

[129] J. Nanda, H. Bilheux, S. Voisin, G. M. Veith, R. Archibald, L. Walker, S. Allu, N. J. Dudney, S. J. Pannala, *Phys. Chem. C* **2013**, *116*, 8401.

[130] H. Lim, E. Yilmaz, H. R. Byon, *J. Phys. Chem. Lett.* **2012**, *3*, 3210.

[131] X. W. Gao, Y. H. Chen, L. Johnson, P. G. Bruce, *Nat. Mat* **2016**, *15*, 882.

[132] Y. Hase, E. Ito, T. Shiga, F. Mizuno, H. Nishikoori, H. Iba, K. Takechi, *Chem. Commun.* **2013**, *49*, 8389.

[133] L. Li, S.-H. Chai, S. Dai, A. Manthiram, *Energy Environ. Sci.* **2014**, *7*, 2630.

[134] P. He, Y. Wang, H. Zhou, *Electrochem. Commun.* **2010**, *12*, 1686.

[135] Y. Wang, P. He, H. Zhou, *Energy Environ. Sci.* **2011**, *4*, 4994.

[136] P. He, Y. Wang, H. Zhou, *J. Power Sources* **2011**, *196*, 5611.

[137] L. Li, X. Zhao, Y. Fu, A. Manthiram, *Phys. Chem. Chem. Phys.* **2012**, *14*, 12737.

[138] P. Andrei, J. P. Zheng, M. Hendrickson, E. J. Plichta, *J. Electrochem. Soc.* **2012**, *159*, A770.

[139] T. Zhang, H. Zhou, *Nat. Commun.* **2013**, *4*, 1817.

[140] H. Kitaura, H. Zhou, *Energy Environ. Sci.* **2012**, *5*, 9077.

[141] H. Kitaura, H. Zhou, *Adv. Energy Mater.* **2012**, *2*, 889.

[142] X. Zhao, X. Li, Y. Gong, N. Xu, K. Romito, K. Huang, *Chem. Commun.* **2013**, *49*, 5357.

[143] B. Kumar, J. Kumar, *J. Electrochem. Soc.* **2010**, *157*, A611.

[144] P. Kichambare, S. Rodrigues, J. Kumar, *ACS Appl. Mater. Interfaces* **2012**, *4*, 49.

[145] H. Ye, J. Huang, J. J. Xu, A. Khalfan, S. G. Greenbaum, *J. Electrochem. Soc.* **2007**, *154*, A1048.

[146] T. Zhang, N. Imanishi, A. Hirano, Y. Takeda, O. Yamamoto, *Electrochem. Solid-State Lett.* **2011**, *14*, A45.

[147] D. Zhang, R. Li, T. Huang, A. Yu, *J. Power Sources* **2010**, *195*, 1202.

[148] J. Y. Sun, N. Zhao, Y. Q. Li, X. X. Guo, X. F. Feng, X. S. Liu, Z. Liu, G. L. Cui, H. Zeng, L. Gu, H. Li, *Sci Rep.* **2017**, *7*, 41217.

[149] W. Xu, J. Xiao, D. Wang, J. Zhang, J. G. Zhang, *J. Electrochem. Soc.* **2009**, *157*, A219.

[150] V. S. Bryantsev, *Theor. Chem. Acc.* **2012**, *131*, 1250.

[151] S. S. Zhang, J. Read, *J. Power Sources* **2011**, *196*, 2867.

[152] S. S. Zhang, K. Xu, J. Read, *J. Power Sources* **2011**, *196*, 3906.

[153] S. A. Freunberger, Y. Chen, Z. Peng, J. M. Griffin, L. J. Hardwick, F. Barde, P. Novak, P. G. Bruce, *J. Am. Chem. Soc.* **2011**, *133*, 8040.

[154] V. S. Bryantsev, M. Blanco, *J. Phys. Chem. Lett.* **2011**, *2*, 379.

[155] T. Laino, A. Curioni, *Chem. Eur. J.* **2012**, *18*, 3510.

[156] R. Younesi, M. Hahlin, F. Björefors, P. Johansson, K. Edström, *Chem. Mater.* **2013**, *25*, 77.

[157] J. Xiao, J. Hu, D. Wang, D. Hu, W. Xu, G. L. Graff, Z. Nie, J. Liu, J. G. Zhang, *J. Power Sources* **2011**, *196*, 5674.

[158] A. K. Thapa, T. Ishihara, *J. Power Sources* **2011**, *196*, 7016.

[159] H. Wang, K. Xie, *Electrochim. Acta* **2012**, *64*, 29.

[160] J. Herranz, A. Garsuch, H. A. Gasteiger, *J. Phys. Chem. C* **2012**, *116*, 19084.

[161] G. M. Veith, N. J. Dudney, J. Howe, J. Nanda, *J. Phys. Chem. C* **2011**, *115*, 14325.

[162] W. Xu, V. V. Viswanathan, D. Wang, S. A. Towne, J. Xiao, Z. Nie, D. Hu, J. G. Zhang, *J. Power Sources* **2011**, *196*, 3894.

[163] Z. C. Zhang, J. Lu, R. S. Assary, P. Du, H. H. Wang, Y. K. Sun, Y. Qin, K. C. Lau, J. Greeley, P. C. Redfern, H. Iddir, L. A. Curtiss, K. Amine, *J. Phys. Chem. C* **2011**, *155*, 25535.

[164] S. A. Freunberger, Y. Chen, N. E. Drewett, L. J. Hardwick, F. Barde, P. G. Bruce, *Angew. Chem. Int. Ed.* **2011**, *50*, 8609.

[165] G. M. Veith, J. Nanda, L. H. Delmau, N. J. Dudney, *J. Phys. Chem. Lett.* **2012**, *3*, 1242.

[166] J. Xie, X. H. Yao, I. P. Madden, D.-E. Jiang, L.-Y. Chou, C.-K. sung, D. W. Wang, *J. Am. Chem. Soc.* **2014**, *136*, 8903.

[167] K. R. Ryan, L. Trahey, B. J. Ingram, A. K. Burrell, *J. Phys. Chem. C* **2012**, *116*, 19724.

[168] H. D. Lim, K. Y. Park, H. Gwon, J. Hong, H. Kim, K. Kang, *Chem. Commun.* **2012**, *48*, 8374.

[169] V. S. Bryantsev, F. Faglioni, *J. Phys. Chem. A* **2012**, *116*, 7128.

[170] B. M. Gallant, R. R. Mitchell, D. G. Kwabi, J. Zhou, L. Zuin, C. V. Thompson, Y. Shao-Horn, *J. Phys. Chem. C* **2012**, *116*, 20800.

[171] W. Xu, J. Xiao, D. Y. Wang, J. Zhang, J. G. Zhang, *Electrochem. Solid-State Lett.* **2010**, *13*, A48.

[172] O. Crowther, B. Meyer, M. Salomon, *Electrochem. Solid-State Lett.* **2011**, *14*, A113.

[173] D. Xu, Z. L. Wang, J. J. Xu, L. L. Zhang, X. B. Zhang, *Chem. Commun.* **2012**, *48*, 6948.

[174] Z. Peng, S. A. Freunberger, Y. Chen, P. G. Bruce, *Science* **2012**, *337*, 563.

[175] M. M. Ottakam Thotiyl, S. A. Freunberger, Z. Peng, Y. Chen, Z. Liu, P. G. Bruce, *Nat. Mater.* **2013**, *12*, 1050.

[176] D. G. Kwabi, T. P. Batcho, C. V. Amanchukwu, N. Ortiz-Vitoriano, P. Hammond, C. V. Thompson, Y. Shao-Horn, *J. Phys. Chem. Lett.* **2014**, *5*, 2850.

[177] Y. Chen, S. A. Freunberger, Z. Peng, F. Barde, P. G. Bruce, *J. Am. Chem. Soc.* **2012**, *134*, 7952.

[178] F. Bardé, Y. Chen, L. Johnson, S. Schaltin, J. Fransaer, P. G. Bruce, *J. Phys. Chem. C* **2014**, *118*, 18892.

[179] Y. Chen, S. A. Freunberger, Z. Peng, O. Fontaine, P. G. Bruce, *Nat. Chem.* **2013**, *5*, 489.

[180] H. D. Lim, H. Song, J. Kim, H. Gwon, Y. Bae, K. Y. Park, J. Hong, H. Kim, T. Kim, Y. H. Kim, X. Lepro, R. Ovalle-Robles, R. H. Baughman, K. Kang, *Angew. Chem. Int. Ed.* **2014**, *53*, 39263931.

[181] B. J. Bergner, A. Schurmann, K. Peppler, A. Garsuch, J. Janek, *J. Am. Chem. Soc.* **2014**, *136*, 15054.

[182] D. Sun, Y. Shen, W. Zhang, L. Yu, Z. Q. Yi, W. Yin, D. Wang, Y. H. Huang, J. Wang, D. Wang, J. B. Goodenough, *J. Am. Chem. Soc.* **2014**, *136*, 8941.

[183] Z. J. Liang, Y.-C. Lu, *J. Am. Chem. Soc.* **2016**, *138*, 7574.

[184] X. W. Gao, Y. H. Chen, L. Johnson, P. G. Bruce, *Nat. Mater.* **2016**, *15*, 882.

[185] D. Y. Kim, M. W. Kim, D. W. Kim, J. D. Suk, J. J. Park, O. O. Park, Y. K. Kang, *Carbon* **2016**, *100*, 265.

[186] J. J. Xu, Z. L. Wang, D. Xu, L. L. Zhang, X. B. Zhang, *Nat. Commun.* **2013**, *4*, 2438.

[187] D. Oh, J. Qi, Y. C. Lu, Y. Zhang, Y. Shao-Horn, A. M. Belcher, *Nat. Commun.* **2013**, *4*, 2756.

[188] M. M. Ottakam Thotiyl, S. A. Freunberger, Z. Peng, P. G. Bruce, *J. Am. Chem. Soc.* **2013**, *135*, 494.

[189] R. Black, S. H. Oh, J. H. Lee, T. Yim, B. Adams, L. F. Nazar, *J. Am. Chem. Soc.* **2012**, *134*, 2902.

[190] D. M. Itkis, D. A. Semenenko, E. Y. Kataev, A. I. Belova, V. S. Neudachina, A. P. Sirotina, M. Havecker, D. Teschner, A. Knop-Gericke, P. Dudin, A. Barinov, E. A. Goodilin, Y. Shao-Horn, L. V. Yashina, *Nano. Lett.* **2013**, *13*, 4697.

[191] W. Zhou, J. Li, H. Nie, Y. Zhang, X. Xi, H. Zhang, *Electrochim. Acta* **2014**, *138*, 410.

[192] J. Lu, Y. Lei, K. C. Lau, X. Luo, P. Du, J. Wen, R. S. Assary, U. Das, D. J. Miller, J. W. Elam, H. M. Albishri, D. A. El-Hady, Y. K. Sun, L. A. Curtiss, K. Amine, *Nat. Commun.* **2013**, *4*, 2383.

[193] S. J. Kang, T. Mori, S. Narizuka, W. Wilcke, H. C. Kim, *Nat. Commun.* **2014**, *5*, 3937.

[194] Z. Jian, P. Liu, F. Li, P. He, X. Guo, M. Chen, H. Zhou, *Angew. Chem. Int. Ed.* **2014**, *53*, 442.

[195] J. Xie, X. Yao, Q. Cheng, I. P. Madden, P. Dornath, C. C. Chang, W. Fan, D. Wang, *Angew. Chem. Int. Ed.* **2014**, *54*, 4299.

[196] J. Xie, X. Yao, I. P. Madden, D. E. Jiang, L. Y. Chou, C. K. Tsung, D. Wang, *J. Am. Chem. Soc.* **2014**, *136*, 8903.

[197] F. J. Li, D.-M. Tang, T. Zhang, K. M. Liao, P. He, D. Golberg, A. Yamada, H. S. Zhou, *Adv. Energy Mater.* **2015**, *1500294*.

[198] X. P. Han, F. Y. Cheng, C. C. Chen, F. J. Li, J. Chen, *Inorg. Chem. Front.* **2016**, *3*, 866.

[199] W.- B. Luo, X.-W. Gao, D.-Q. Shi, S.-L. Chou, J.-Z. Wang, H.-K. Liu, *Small* **2016**, *12*, 3031.

[200] B. G. Kim, C. S. Jo, J. H. Shin, Y. D. Mun, J. W. Lee, J. W. Choi, *ACS Nano* **2017**, *11*, 1736.

[201] S. D. Song, W. Xu, J. M. Zheng, L. L. Luo, M. H. Engelhard, M. E. Bowden, B. Liu, C.-M. Wang, J.-G. Zhang, *Nano Lett.* **2017**, *17*, 1417.

[202] C. Cao, Y. C. Yan, H. Zhang, J. Xie, S. C. Zhang, B. Pan, G. S. Cao, X. B. Zhao, *ACS Appl. Mater. Interfaces* **2016**, *8*, 31653.

**ADVANCED
SCIENCE NEWS**

www.advancedsciencenews.com

**ADVANCED
SUSTAINABLE
SYSTEMS**

www.advsustainsys.com

[203] J.-W. Jung, H.-G. Im, D. W. Lee, S. M. Yu, J.-H. Jang, K. R. Yoon, Y. H. Kim, J. B. Goodenough, J. H. Jin, I.-D. Kim, B.-S. Bae, *ACS Energy Lett.* **2017**, *2*, 673.

[204] W.-B. Luo, T. V. Pham, H.-P. Guo, H.-K. Liu, S.-X. Dou, *ACS Nano* **2017**, *11*, 1747.

[205] A. Riaz, K.-N. Jung, W. Y. Chang, K.-H. Shin, J.-W. Lee, *ACS Appl. Mater. Interfaces* **2014**, *6*, 17815.

[206] J. G. Cao, S. Y. Liu, J. Xie, S. C. Zhang, G. S. Cao, X. B. Zhao, *ACS Catal.* **2015**, *5*, 241.

[207] C. Shen, Z. Y. Wen, F. Wang, T. Wu, X. W. Wu, *ACS Catal.* **2016**, *6*, 4149.

[208] J. Z. Zhu, F. Wang, B. Z. Wang, Y. W. Wang, J. J. Liu, W. Q. Zhang, Z. Y. Wen, *J. Am. Chem. Soc.* **2015**, *137*, 13572.

[209] X. Huang, H. Yu, H. Tan, J. Zhu, W. Zhang, C. Wang, J. Zhang, Y. Wang, Y. Lv, Z. Zeng, D. Liu, J. Ding, Q. Zhang, M. Srinivasan, P. M. Ajayan, H. H. Hng, Q. Yan, *Adv. Funct. Mater.* **2014**, *24*, 6516.

[210] S. Ma, Y. Wu, J. Wang, Y. Zhang, Y. Zhang, X. Yan, Y. Wei, P. Liu, J. Wang, K. Jiang, S. Fan, Y. Xu, Z. Peng, *Nano Lett.* **2015**, *15*, 8084.

[211] J. Liu, R. Younesi, T. Gustafsson, K. Edstrom, J. Zhu, *Nano Energy* **2014**, *10*, 19.

[212] V. R. Chitturi, M. Ara, W. Fawaz, K. Y. S. Ng, L. M. R. Arava, *ACS Catal.* **2016**, *6*, 7088.

[213] B. Sun, P. Munroe, G. Wang, *Sci Rep* **2013**, *3*, 2247.

[214] S. Tong, M. Zheng, Y. Lu, Z. Lin, X. Zhang, P. He, H. Zhou, *Chem. Commun.* **2015**, *51*, 7302.

[215] X. D. Lin, Y. Cao, S. Cai, J. Fan, Y. Li, Q.-H. Wu, M. Zheng, Q. Dong, *J. Mater. Chem. A* **2016**, *4*, 7788.

[216] D. Su, D. H. Seo, Y. Ju, Z. J. Han, K. Ostrikov, S. Dou, H.-J. Ahn, Z. Peng, G. Wang, *NPG Asia Materials* **2016**, *8*, e286.

[217] H.-G. Jung, Y. S. Jeong, J.-B. Park, Y.-K. Sun, B. Scrosati, Y. J. Lee, *ACS Nano* **2013**, *7*, 3532.

[218] E. Yilmaz, C. Yogi, K. Yamanaka, T. Ohta, H. R. Byon, *Nano Lett.* **2013**, *13*, 4679.

[219] P. Bhattacharya, E. N. Nasybulin, M. H. Engelhard, L. Kovarik, M. E. Bowden, X. S. Li, D. J. Gaspar, W. Xu, J.-G. Zhang, *Adv. Funct. Mater.* **2014**, *24*, 7510.

[220] Y. Yang, W. Liu, Y. Wang, X. Wang, L. Xiao, J. Lu, L. Zhuang, *Phys. Chem. Chem. Phys.* **2014**, *16*, 20618.

[221] W.-B. Luo, X.-W. Gao, S.-L. Chou, J.-Z. Wang, H.-K. Liu, *Adv. Mater.* **2015**, *27*, 6862.

[222] Y.-J. Kang, S. C. Jung, H. J. Kim, Y.-K. Han, S. H. Oh, *Nano Energy* **2016**, *27*, 1.

[223] L. Leng, J. Li, X. Zeng, H. Song, T. Shu, H. Wang, S. Liao, *J. Power Sources* **2017**, *337*, 173.

[224] W. B. Luo, T. V. Pham, H.-P. Guo, H.-K. Liu, S.-X. Dou, *ACS Nano* **2017**, *11*, 1747.

[225] C. Zhao, C. Yu, M. N. Banis, Q. Sun, M. Zhang, X. Li, Y. Liu, Y. Zhao, H. Huang, S. Li, X. Han, B. Xiao, Z. Song, R. Li, J. Qiu, X. Sun, *Nano Energy* **2017**, *34*, 399.

[226] H. Yadegari, M. N. Banis, A. Lushington, Q. Sun, R. Li, T.-K. Sham, X. Sun, *Energy Environ. Sci.* **2017**, *10*, 286.

[227] W. Fan, X. Guo, D. Xiao, L. Gu, *J. Phys. Chem. C* **2014**, *118*, 7344.

[228] S. Kumar, C. Selvaraj, N. Munichandraiah, L. G. Scanlonb, *RSC Adv.* **2013**, *3*, 21706.

[229] M. Marinaro, U. Piek, S. K. E. Moorthy, J. Bernhard, U. Kaiser, M. Wohlfahrt-Mehrens, L. Jorissen, *Electrochem. Commun.* **2013**, *37*, 53.

[230] A. K. Thapa, T. H. Shin, S. Ida, G. U. Sumanasekera, M. K. Sunkara, T. Ishihara, *J. Power Sources* **2012**, *220*, 211.

[231] Y. Xu, W. A. Shelton, *J. Chem. Phys.* **2010**, *133*, 024703.

[232] Y.-C. Lu, H. A. Gasteiger, E. Crumlin, R. McGuire, Y. Shao-Horn, *J. Electrochem. Soc.* **2010**, *157*, A1016.

[233] Y.-C. Lu, H. A. Gasteiger, M. C. Parent, V. Chiloyan, Y. Shao-Horn, *Electrochem. Solid-State Lett.* **2010**, *13*, A69.

[234] Y. C. Lu, Z. Xu, H. A. Gasteiger, S. Chen, K. Hamad-Schifferli, Y. Shao-Horn, *J. Am. Chem. Soc.* **2010**, *132*, 12170.

[235] Y. C. Lu, H. A. Gasteiger, Y. Shao-Horn, *J. Am. Chem. Soc.* **2011**, *133*, 19048.

[236] Y.-C. Lu, D. G. Kwabi, K. P. C. Yao, J. R. Harding, J. Zhou, L. Zuin, Y. Shao-Horn, *Energy Environ. Sci.* **2011**, *4*, 2999.

[237] S. J. Ye, D. Y. Kim, D. W. Kim, O. O. Park, Y. K. Kang, *J. Mater. Chem. A* **2016**, *4*, 578.

[238] K. R. Yoon, G. Y. Lee, J.-W. Jung, N.-H. Kim, S. O. Kim, I.-D. Kim, *Nano Lett.* **2016**, *16*, 2076.

[239] T. Zhang, N. Imanishi, Y. Shimonishi, A. Hirano, Y. Takeda, O. Yamamoto, N. Sammes, *Chem Commun.* **2010**, *46*, 1661.

[240] A. Ishihara, Y. Ohgi, K. Matsuzawa, S. Mitsushima, K. Ota, *Electrochim. Acta* **2010**, *55*, 8005.

[241] A. Débart, A. J. Paterson, J. Bao, P. G. Bruce, *Angew. Chem., Int. Ed.* **2008**, *47*, 4521.

[242] R. Cao, J.-S. Lee, M. Liu, J. Cho, *Adv. Energy Mater.* **2012**, *2*, 816.

[243] P. Zółtowski, D. M. Dražić, L. Vorkapić, *J. Appl. Electrochem.* **1973**, *3*, 271.

[244] X. F. Hu, J. B. Wang, Z. F. Li, J. Q. Wang, D. H. Gregory, J. Chen, *Nano Lett.* **2017**, *17*, 2073.

[245] J. W. Deng, L. F. Chen, Y. Y. Sun, M. H. Ma, L. Fu, *Carbon* **2015**, *92*, 177.

[246] H. Q. Wang, J. Chen, S.-J. Hu, X.-H. Zhang, X.-P. Fan, J. Du, Y.-G. Huang, Q.-Y. Li, *RSC Adv.* **2015**, *5*, 72495.

[247] S. Y. Liu, Y. G. Zhu, J. Xie, Y. Huo, H. Y. Yang, T. J. Zhu, G. S. Cao, X. B. Zhao, S. C. Zhang, *Adv. Energy Mater.* **2014**, *4*, 1301960.

[248] S. Chen, G. X. Liu, H. Yadegari, H. H. Wang, S. Z. Qiao, *J. Mater. Chem. A* **2015**, *3*, 2559.

[249] X. F. Hu, F. G. Cheng, N. Zhang, X. P. Han, J. Chen, *Small* **2015**, *11*, 5545.

[250] X. Y. Lu, W. P. Si, X. L. Sun, B. Liu, L. Zhang, C. L. Yan, O. G. Schmidt, *Nano Energy* **2016**, *19*, 428.

[251] L. L. Zhang, F. F. Zhang, G. Huang, J. W. Wang, X. C. Du, Y. L. Qin, L. M. Wang, *J. Power. Sources* **2014**, *261*, 311.

[252] X. Y. Lu, W. P. Si, X. L. Sun, J. W. Deng, L. X. Xi, B. Liu, C. L. Yan, O. G. Schmidt, *J. Power. Sources* **2015**, *295*, 197.

[253] Y.-F. Xu, Y. Chen, G.-L. Xu, X. R. Zhang, Z. H. Chen, J.-T. Li, L. Huang, K. Amine, S.-G. Sun, *Nano Energy* **2016**, *28*, 63.

[254] Z. H. Wei, T. S. Zhao, X. B. P. Tan, *J. Power. Sources* **2016**, *306*, 724.

[255] Y. Meng, W. Song, H. Huang, Z. Ren, S.-Y. Chen, S. L. Suib, *J. Am. Chem. Soc.* **2014**, *136*, 11452.

[256] G. Q. Wang, L. L. Huang, W. Huang, J. Xie, G. H. Du, S. C. Zhang, P. Zhu, G. Cao, X. B. Zhao, *Nanoscale* **2015**, *7*, 20614.

[257] N. N. Xu, Y. Y. Liu, X. Zhang, X. M. Li, A. J. Li, J. L. Qiao, J. J. Zhang, *Sci. Rep.* **2016**, *6*, 33590.

[258] Y. Qin, J. Lu, P. Du, Z. Chen, Y. Ren, T. Wu, J. T. Miller, J. Wen, D. J. Miller, Z. Zhang, K. Amine, *Energy Environ. Sci.* **2013**, *6*, 519.

[259] Z. X. Yang, J. Lv, H. D. Pang, W. H. Yan, K. Qian, T. L. Guo, Z. P. Guo, *Sci. Rep.* **2015**, *5*, 17473.

[260] X. F. Hu, F. Y. Cheng, X. P. Han, T. Zhang, J. Chen, *Small* **2015**, *18*, 809.

[261] J. Wang, L. L. Liu, C. M. Subramaniyam, S. Chou, H. K. Liu, J. Z. Wang, *J. Appl Electrochem.* **2016**, *46*, 869.

[262] X. F. Hu, F. Y. Cheng, N. Zhang, X. P. Han, J. Chen, *Small* **2015**, *4*, 5545.

[263] F. Wang, Z. Y. Wen, X. W. Wu, *Small* **2016**, *16*, 6749.

[264] F. Cheng, T. Zhang, Y. Zhang, J. Du, X. Han, J. Chen, *Angew. Chem. Int. Ed.* **2013**, *52*, 2474.

[265] H. Q. Wang, J. Chen, S.-J. Hu, X.-H. Zhang, X.-P. Fan, J. Du, Y.-G. Huang, Q.-Y. Li, *RSC Adv.* **2015**, *5*, 72495.

[266] Y.-F. Xu, Y. Chen, G.-L. Xu, X. R. Zhang, Z. H. Chen, J.-T. Li, L. Huang, K. Amine, S.-G. Sun, *Nano Energy* **2016**, *28*, 63.

[267] N. N. Xu, Y. Y. Liu, X. Zhang, X. M. Li, A. J. Li, J. L. Qiao, J. J. Zhang, *Sci Rep.* **2016**, *6*, 33590.

[268] D. A. Tompsett, S. C. Parker, P. G. Bruce, M. S. Islam, *Chem. Mater.* **2013**, *25*, 536.

[269] E. M. Benbow, S. P. Kelly, L. Zhao, J. W. Reutenauer, S. L. Suib, *J. Phys. Chem. C* **2012**, *115*, 22009.

[270] O. Oloniyo, S. Kumar, K. Scott, *J. Electron. Mater.* **2012**, *41*, 921.

[271] M. S. El-Deab, T. Ohsaka, *Angew. Chem. Int. Ed.* **2006**, *45*, 5963.

[272] I. Roche, E. Chaînet, M. Chatenet, J. Vondrák, *J. Phys. Chem. C* **2007**, *111*, 1434.

[273] M. S. El-Deab, T. Ohsaka, *Electrochim. Acta* **2007**, *52*, 2166.

[274] I. Roche, K. Scott, *J. Appl. Electrochem.* **2008**, *39*, 197.

[275] S. K. Bikkarolla, F. J. Yu, W. Z. Zhou, P. Joseph, P. Cumpson, P. Papakonstantinou, *J. Mater. Chem. A* **2014**, *2*, 14493.

[276] Y. L. Wang, L. Zhu, X. Yang, E. Shao, X. Y. Deng, N. Liu, M. H. Wu, *J. Mater. Chem. A* **2015**, *3*, 2934.

[277] F. Švegl, B. Orel, I. Grabec-Švegl, V. Kaučič, *Electrochim. Acta* **2000**, *45*, 4359.

[278] J. Xu, P. Gao, T. S. Zhao, *Energy Environ. Sci.* **2012**, *5*, 5333.

[279] Y. F. Zhao, S. Q. Chem, B. Sun, D. W. Su, X. D. Huang, H. Liu, Y. M. Yan, K. Sun, G. X. Wang, *Sci Rep* **2015**, *5*, 7629.

[280] J. Ming, Y. Wu, J. B. Park, J. K. Lee, F. Zhao, Y. K. Sun, *Nanoscale* **2013**, *5*, 10390.

[281] J. Zhu, X. Ren, J. Liu, W. Zhang, Z. Wen, *ACS Cata.* **2015**, *5*, 73.

[282] Q.-Z. Xu, Y.-Z. Su, H. Wu, H. Cheng, Y.-P. Guo, N. Li, Z.-Q. Liu, *Current Nanoscience* **2015**, *11*, 107.

[283] M. Tahir, N. Mahmood, X. X. Zhang, T. Mahmood, F. K. Butt, I. Aslam, M. Tanveer, F. Idrees, S. Khalid, I. Shakir, Y. Yan, J. J. Zou, C. B. Cao, Y. L. Hou, *Nano Research* **2015**, *8*, 3725.

[284] D. Pletcher, X. Li, S. W. T. Price, A. E. Russell, T. Sonmez, S. J. Thompson, *Electreochimica Acta* **2016**, *188*, 286.

[285] Y. Li, M. Gong, Y. Liang, J. Feng, J. E. Kim, H. Wang, G. Hong, B. Zhang, H. Dai, *Nat. Commun.* **2013**, *4*, 1805.

[286] B. Li, X. M. Ge, F. W. T. Goh, T. S. A. Hor, D. S. Geng, G. J. Du, Z. L. Liu, J. Zhang, X. G. Liu, Y. Zong, *Nanoscale* **2015**, *7*, 1830.

[287] D. U. Lee, J. Scott, H. W. Park, S. Abureden, J.-Y. Choi, Z. W. Chen, *Electrochem. Commun.* **2014**, *43*, 109.

[288] Y. B. Yang, W. Yin, S. Wu, X. D. Yang, W. Xia, Y. Shen, Y. H. Huang, A. Cao, Q. Yuan, *ACS Nano* **2016**, *10*, 1240.

[289] V. Giordani, S. A. Freunberger, P. G. Bruce, J.-M. Tarascon, D. Larcher, *Electrochem. Solid-State Lett.* **2010**, *13*, A180.

[290] R. Gao, Z. Y. Li, X. L. Zhang, J. C. Zhang, Z. B. Hu, X. F. Liu, *ACS Catal.* **2016**, *6*, 400.

[291] C. Yuan, H. B. Wu, Y. Xie, X. W. Lou, *Angew. Chem. Int. Ed.* **2014**, *53*, 1488.

[292] H. Zhu, S. Zhang, Y. X. Huang, L. Wu, S. Sun, *Nano Lett.* **2013**, *13*, 2947.

[293] E. Rios, G. Poillerat, J. F. Koenig, J. L. Gautier, P. Chartier, *Thin Solid Films* **1995**, *264*, 18.

[294] X. B. He, F. X. Yin, S. Yuan, N. Liu, X. F. Huang, *ChemElectroChem* **2016**, *3*, 1107.

[295] Y. J. Xu, W. Y. Bian, J. Wu, J.-H. Tian, R. Z. Yang, *Electrochimica Acta* **2015**, *151*, 276.

[296] A. Tan, M. V. Reddy, S. Adams, *Ionics* **2017**, https://doi.org/10.1007/s11581-016-1913-9.

[297] F. Cheng, J. Shen, B. Peng, Y. Pan, Z. Tao, J. Chen, *Nat. Chem.* **2011**, *3*, 79.

[298] W. Y. Bian, Z. R. Yang, P. Strasser, R. Z. Yang, *J. Power Sources* **2014**, *250*, 196.

[299] Y. Cheng, S. Dou, J.-P. Veder, S. Y. Wang, M. Saunders, S. P. Jiang, *ACS Appl. Mater. Interfaces* **2017**, *9*, 8121.

[300] W. H. Guo, X. X. Ma, X. L. Zhang, Y. Q. Zhang, D. L. Yu, X. Q. He, *RSC Adv.* **2016**, *6*, 96436.

[301] R. Miao, J. K. He, S. J. Sahoo, Z. Luo, W. Zhong, S.-Y. Chen, C. Guilld, T. Jafari, B. Dutta, S. A. Cetegen, M. C. Wang, S. P. Alpay, S. L. Suib, *ACS Catal.* **2017**, *7*, 819.

[302] P. F. Li, W. Sun, Q. L. Yu, P. Yang, J. H. Qiao, Z. H. Wang, D. Rooney, K. Sun, *Solid State Ionics* **2016**, *289*, 17.

[303] C. Jin, F. L. Lu, X. C. Cao, Z. R. Yang, R. Z. Yang, *J. Mater. Chem. A* **2013**, *1*, 12170.

[304] H. J. Shi, G. H. Zhao, *Phys. Chem. C* **2014** *118*, 25939.

[305] W. N. Yan, W. Y. Bian, C. Jin, J.-H. Tian, R. Z. Yang, *Electrochimica Acta* **2015**, *177*, 65.

[306] M. Prabu, K. Ketpang, S. Shanmugam, *Nanoscale* **2014**, *6*, 3173.

[307] J. Li, Y. Li, K. Guo, L. L. Zou, Q. H. Huang, Z. Q. Zou, H. Yang, *Int. J. Electrochem. Sci.* **2016**, *11*, 3227.

[308] W. N. Yan, Z. R. Yang, W. Y. Bian, R. Z. Yang, *Carbon* **2015**, *92*, 74.

[309] H. Cheng, Y.-Z. Su, P.-Y. Kuang, G.-F. Chen, Z.-Q. Liu, *J. Mater. Chem. A* **2015**, *3*, 19314.

[310] J. Zhang, L. J. Wang, L. L. Xu, X. M. Ge, X. Zhao, M. Lai, Z. L. Liu, W. Chen, *Nanoscale* **2014**, *6*, 9043.

[311] G. T. Fu, Z. Y. Liu, J. F. Zhang, J. Y. Wu, L. Xu, D. M. Sun, J. B. Zhang, Y. Tang, P. Chen, *Nano Research* **2016**, *9*, 2110.

[312] J. Zhang, L. J. Wang, L. L. Xu, X. M. Ge, X. Zhao, M. Lai, Z. L. Liu, W. Chen, *Nanoscale* **2015**, *7*, 720.

[313] L. Y. Li, L. Shen, P. Nie, G. Pang, J. Wang, H. Q. Li, S. Y. Dong, X. G. Zhang, *J. Mater. Chem. A* **2015**, *3*, 24309.

[314] J. G. Kim, Y. M. Kim, Y. Noh, W. B. Kim, *ChemSusChem* **2015**, *8*, 1752.

[315] P. Li, H. C. Zeng, *Adv. Funct. Mater.* **2017**, 1606325, https://doi.org/10.1002/adfm.201606325.

[316] M. A.-Mamun, X. Su, H. Zhang, H. Yin, P. Liu, H. Yang, D. Wang, Z. Tang, Y. Wang, H. J. Zhao, *Small* **2017**, *12*, 2886.

[317] F. Niu, N. Wang, J. Yue, L. Chen, J. Yang, Y. Qian, *Electrochimica Acta* **2016**, *208*, 148.

[318] B. Sun, X. Huang, S. Chen, Y. Zhao, J. Zhang, P. Munroe, G. Wang, *J. Mater. Chem. A* **2014**, *2*, 12053.

[319] X. Lin, Y. Shang, T. Huang, A. Yu, *Nanoscale* **2014**, *6*, 9043.

[320] J. G. Lee, J. Hwang, H. J. Hwang, O. S. Jeon, J. Jang, O. Kwon, Y. Lee, B. C. Han, Y.-G. Shui, *J. Am. Chem. Soc.* **2016**, *138*, 3541.

[321] S. Gupta, W. Kellogg, H. Xu, X. Liu, J. Cho, G. Wu, *Chemistry – An Asian Journal* **2016**, *11*, 10.

[322] J. T. Mefford, X. Rong, A. M. Abakumov, W. G. Hardin, S. Dai, A. M. Kolpak, K. P. Johnston, K. J. Stevenson, *Nat. Commun* **2015**, *7*, 11053.

[323] B.-Q. Li, C. Tang, H.-F. Wang, X.-L. Zhu, Q. Zhang, *Sci. Adv.* **2016**, *2*, 1.

[324] B. Shin, S. Choi, Y. Tak, *Int. J. Electrochem. Sci.* **2016**, *11*, 5900.

[325] M. Sakthivel, S. Bhandari, J.-F. Drillet, *ECS Electrochemistry Letters* **2015**, *4*, A56.

[326] M.-S. Ekrami-Kakhki, Z. Yavari, J. Saffari, S. A. Ekrami-Kakhki, *Journal of Electrical Engineering* **2016**, *4*, 88.

[327] Y. Wang, Z. B. Yang, F. L. Lu, C. Jin, J. Wu, M. Shen, R. Z. Yang, F. L. Chen, *RSC Adv.* **2015**, *5*, 974.

[328] Y. L. Zhu, W. Zhou, Z.-G. Chen, Y. Chen, C. Su, M. O. Tade, Z. P. Shao, *Angew. Chem. Int. Ed.* **2015**, *54*, 3897.

[329] H. W. Park, D. U. Lee, P. Y. Zamani, M. H. Seo, L. F. Nazar, Z. W. Chen, *Nano Energy* **2014**, *10*, 192.

[330] H. Ohkuma, I. Uechi, N. Imanishi, A. Hirano, Y. Takeda, O. Yamamoto, *J. Power Sources* **2013**, *223*, 319.

[331] Y. L. Zhu, W. Zhou, J. Sunarso, Y. J. Zhong, Z. P. Shao, *Adv. Funct. Mater.* **2016**, *26*, 5862.

[332] A. I. D. Sa, C. M. Rangel, M. E. M. Jorge, *J. Solid State Electrochem.* **2016**, *20*, 1713.

[333] H. Y. Zhu, P. F. Zhang, S. Dai, *ACS Catal.* **2015**, *5*, 6370.

[334] J. O'M. Bockris, T. Otagawa, *J. Electrochem. Soc.* **1984**, *131*, 290.

[335] J. Suntivich, H. A. Gasteiger, N. Yabuuchi, H. Nakanishi, J. B. Goodenough, Y. Shao-Horn, *Nat. Chem.* **2011**, *3*, 546.

[336] J. Suntivich, H. A. Gasteiger, N. Yabuuchi, Y. Shao-Horn, *J. Electrochem. Soc.* **2010**, *157*, B1263.

**ADVANCED
SCIENCE NEWS**

www.advancedsciencenews.com

**ADVANCED
SUSTAINABLE
SYSTEMS**

www.advsustainsys.com

[337] R. F. Savinell, *Nat. Chem.* **2011**, *3*, 501.

[338] J. B. Goodenough, B. L. Cushing, *Handbook of Fuel Cells – Fundamentals*, Wiley, Hoboken, NJ, USA, **2003**, 520.

[339] J. Suntivich, K. J. May, H. A. Gasteiger, J. B. Goodenough, Y. Shao-Horn, *Science* **2011**, *334*, 1383.

[340] Y. Wang, H.-P. Cheng, *J. Phys. Chem. C* **2013**, *117*, 2106.

[341] M. Komo, A. Hagiwara, S. Taminato, M. Hirayama, R. Kanno, *Electrochem.* **2012**, *80*, 834.

[342] X. Han, T. Zhang, J. Du, F. Cheng, J. Chen, *Chem. Sci.* **2013**, *4*, 368.

[343] D. J. Chen, J. Wang, Z. B. Zhang, Z. P. Shao, F. Ciucci, *Chem. Commun.* **2016**, *52*, 10739.

[344] S. Sengodan, S. Choi, A. Jun, T. H. Shin, Y.-W. Ju, H. Y. Jeong, J. Shin, J. T. S. Irvine, G. Kim, *Nat Mat.* **2014**, *14*, 205.

[345] O. Diaz-Morales, S. Raaijiman, R. Kortlever, P. J. Kooyman, T. Wezendonk, J. Gascon, W. T. Fu, M. T. M. Koper, *Nat. Commun* **2016**, *7*, 12363.

[346] Y. J. Xue, S. S. Sun, Q. Wang, H. Miao, S. H. Li, Z. P. Liu, *Electrochimica Acta* **2017**, *230*, 418.

[347] Y. J. Xue, H. Miao, S. S. Sun, Q. Wang, S. H. Li, Z. Q. Liu, *J. Power Sources* **2017**, *342*, 192.

[348] Y. J. Xue, H. Miao, S. S. Sun, Q. Wang, S. H. Li, Z. P. Liu, *RSC Adv.* **2017**, *7*, 5214.

[349] X. Han, Y. Hu, J. Yang, F. Cheng, J. Chen, *Chem. Commun.* **2014**, *50*, 1497.

[350] R. S. Kalubarme, H. S. Jadhav, C.-N. Park, K.-N. Jung, K.-H. Shin, C.-J. Park, *J. Mater. Chem. A* **2014**, *2*, 13024.

[351] Z. D. Wang, Y. You, J. Yuan, Y.-X. Yin, Y.-T. Li, S. Xin, D. W. Zhang, *ACS Appl. Mater. Interfaces* **2016**, *8*, 6520.

[352] J.-J. Xu, D. Xu, Z.-L. Wang, H.-G. Wang, L.-L. Zhang, X.-B. Zhang, *Angew. Chem. Int. Ed.* **2013**, *52*, 3887.

[353] J.-J. Xu, Z.-L. Wang, D. Xu, F.-Z. Meng, X.-B. Zhang, *Energy Environ. Sci.* **2014**, *7*, 2213.

[354] S. Velraj, J. H. Zhu, *J. Power Sources* **2013**, *227*, 48.

[355] F. Moureaux, P. Stevens, G. Toussaint, M. Chatenet, *J. Power Sources* **2013**, *229*, 123.

[356] G. X. Liu, H. B. Chen, L. Xia, S. Q. Wang, L.-X. Ding, D. D. Li, K. Xiao, S. Dai, H. H. Wang, *ACS Appl. Mater. Interfaces* **2015**, *7*, 22478.

[357] Z. Z. Du, P. Yang, L. Wang, Y. H. Lu, J. B. Goodenough, J. Zhang, D. W. Zhang, *J. Power Sources* **2014**, *265*, 91.

[358] G. H. Li, M. A. Mezaal, R. Zhang, K. Zhang, W. Liu, L. X. Lei, *Int. J. Electrochem. Sci.* **2015**, *10*, 8412.

[359] C. Jin, Z. Yang, X. C. Cao, F. L. Lu, R. Z. Yang, *Int. J. Hydrogen Energy* **2014**, *39*, 2526.

[360] D. U. Lee, B. J. Kim, Z. Chen, *J. Mater. Chem. A* **2013**, *1*, 4754.

[361] J. L. Gautier, J. F. Marco, M. Gracia, J. R. Gancedo, V. de la Garza Guadarrama, H. Nguyen-Cong, P. Chartier, *Electrochim. Acta* **2002**, *48*, 119.

[362] L. Zhang, S. Zhang, K. Zhang, G. Xu, X. He, S. Dong, Z. Liu, C. Huang, L. Gu, G. Cui, *Chem. Commun.* **2013**, *49*, 3540.

[363] J. Haenen, W. Visscher, E. Barendrecht, *J. Electroanal. Chem.* **1986**, *208*, 323.

[364] J. Landon, E. Demeter, N. İnoğlu, C. Keturakis, I. E. Wachs, R. Vasić, A. I. Frenkel, J. R. Kitchin, *ACS Catal.* **2012**, *2*, 1793.

[365] J. Du, Y. Pan, T. Zhang, X. Han, F. Cheng, J. Chen, *J. Mater. Chem.* **2012**, *22*, 15812.

[366] V. Nikolova, P. Iliev, K. Petrov, T. Vitanov, E. Zhecheva, R. Stoyanova, I. Valov, D. Stoychev, *J. Power Sources* **2008**, *185*, 727.

[367] J. Ponce, J.-L. Rehspringer, G. Poillerat, J. L. Gautier, *Electrochim. Acta* **2001**, *46*, 3373.

[368] V. Anandan, R. Kudla, A. Drews, J. Adams, M. Karulkar, *ECS Trans.* **2012**, *46*, 167.

[369] S.-W Woo, K. Dokk, K. Kanamura, *J. Power Sources*, **2008**, *185*, 1589.

[370] D. U. Lee, B. J. Kim, Z. Chen, *J. Mater. Chem. A* **2013**, *1*, 4754.

[371] J. L. Gautier, J. F. Marco, M. Gracia, J. R. Gancedo, V. de la Garza Guadarra, H. Nguyen-Cong, P. Chartier, *Electrochim. Acta* **2002**, *48*, 119.

[372] L. Zhang, S. Zhang, K. Zhang, G. Xu, X. He, S. Dong, Z. Liu, C. Huang, L. Gu, G. Cui, *Chem. Commun.* **2013**, *49*, 3540.

[373] J. Haenen, W. Visscher, E. Barendrecht, *J. Electroanal. Chem.* **1986**, *208*, 323.

[374] J. Landon, E. Demeter, N. no lu, C. Keturakis, I. E. Wachs, R. Vasić, A. I. Frenkel, J. R. Kitchin, *ACS Catal.* **2012**, *2*, 1793.

[375] J. Du, Y. Pan, T. Zhang, X. Han, F. Cheng, J. Chen, *J. Mater. Chem.* **2012**, *22*, 15812.

[376] V. Nikolova, P. Iliev, K. Petrov, T. Vitanov, E. Zhecheva, R. Stoyanova, I. Valov, D. Stoychev, *J. Power Sources* **2008**, *185*, 727.

[377] J. Ponce, J.-L. Rehspringer, G. Poillerat, J. L. Gautier, *Electrochim. Acta* **2001**, *46*, 3373.

[378] V. Anandan, R. Kudla, A. Drews, J. Adams, M. Karulkar, *ECS Trans.* **2012**, *46*, 167.

[379] V. Neburchilov, H. Wang, J. J. Martin, W. Qu, *J. Power Sources*, **2010**, *195*, 1271.

[380] Y. Lu, H. X. Ang, Q. Y. Yan, E. Fong, *Chem. Mater.* **2016**, *28*, 574.

[381] F. Li, R. Ohnishi, Y. Yamada, J. Kubota, K. Domen, A. Yamada, H. Zhou, *Chem. Commun.* **2013**, *48*, 1175.

[382] W.-J. kwak, K. C. Lau, C.-D. Shin, K. Amine, L. A. Curtiss, Y.-K. Sun, *ACS Nano* **2015**, *9*, 4129.

[383] K. Zhang, L. Zhang, X. Chen, X. He, X. Wang, S. Dong, P. Han, C. Zhang, S. Wang, L. Gu, G. Cui, *J. Phys. Chem. C* **2013**, *117*, 858.

[384] F. L. Qiu, P. He, J. Jiang, X. P. Zhang, S. F. Tong, H. S. Zhou, *Chem. Commun.* **2016**, *52*, 2713.

[385] J. Park, Y.-S. Jun, W.-R. Lee, J. A. Gerbec, K. A. See, G. D. Stucky, *Chem. Mater.* **2013**, *25*, 3677.

[386] J. Xiao, D. H. Wang, W. Xu, D. Y. Wang, R. E. Williford, J. Liu, J. G. Zhang, *J. Electrochem. Soc.* **2010**, *157*, A487.

[387] S. D. Beattie, D. M. Manolescu, S. L. Blair, *J. Electrochem. Soc.* **2009**, *156*, A44.

[388] C. K. Park, S. B. Park, S. Y. Lee, H. Lee, H. Jang, W. I. Cho, *Bull. Korean Chem. Soc.* **2010**, *31*, 3221.

[389] S. Meini, M. Piana, H. Beyer, J. Schwa mmlein, H. A. Gasteiger, *J. Electrochem. Soc.* **2012**, *159*, A2135.

[390] J. Zeng, J. R. Nair, Q. Chen, C. Francia, S. Bodoardo, N. Penazzi, *ChemElectroChem* **2014**, *1*, 1382.

[391] N. Ding, S. W. Chien, T. S. A. Hor, R. Lum, Y. Zong, Z. Liu, *J. Mater. Chem. A* **2014**, *2*, 12433.

[392] Q. Li, P. Xu, W. Gao, S. G. Ma, G. Zhang, R. G. Cao, J. Cho, H.-L. Wang, G. Wu, *Adv. Mater.* **2014**, *26*, 1378.

[393] X. Xin, K. Ito, L. Kubo, *Carbon* **2016**, *99*, 67.

[394] D. Y. Kim, M. Kim, D. W. Kim, J. D. Suk, J. J. Park, O. O. Park, Y. K. Kang, *Carbon* **2016**, *100*, 265.

[395] X. Zhong, B. Papandrea, Y. X. Xu, Z. Y. Lin, H. Zhang, Y. Liu, Y. Huang, X. F. Duan, *Nano research* **2017**, *10*, 472.

[396] L. Xu, J. Ma, B. H. Li, F. Y. Kang, *J. Power Sources* **2014**, *255*, 187.

[397] J. B. Park, J. Lee, C. S. Yoon, Y. K. Sun, *ACS Appl. Mater. Interfaces* **2013**, *5*, 13426.

[398] Z. Guo, D. Zhou, X. Dong, Z. Qiu, Y. Wang, Y. Xia, *Adv. Mater.* **2013**, *25*, 5668.

[399] N. Zhao, C. Li, X. Guo, *Phys. Chem. Chem. Phys.* **2014**, *16*, 15646.

[400] T. H. Yoon, Y. J. Park, *RSC Adv.* **2014**, *34*, 17434.

[401] H. Woo, J. Kang, J. Kim, C. Kim, S. H. Nam, B. W. Park, *Electron. Mater. Lett.* **2016**, *12*, 551.

[402] C. Y. Xu, J. Dai, X. G. Teng, Y. M. Zhu, *ChemCatChem* **2016**, *8*, 3725.

[403] Z. Ma, X. X. Yuan, L. Li, Z.-F. Ma, D. P. Wilkinson, L. Zhang, J. J. Zhang, *Energy Environ. Sci.* **2015**, *8*, 2144.

[404] W. Zhou, H. Z. Zhang, H. J. Nie, Y. W. Ma, Y. N. Zhang, H. M. Zhang, *ACS Appl. Mater. Interfaces* **2015**, *7*, 3389.

[405] B. Sun, X. Huang, S. Chen, P. Munroe, G. Wang, *Nano Lett.* **2014**, *14*, 3145.

[406] S. Y. Kim, H.-T. Lee, K.-B. Kim, *Phys. Chem. Chem. Phys.* **2013**, *15*, 20262.

[407] Q. Li, P. Xu, W. Gao, S. G. Ma, G. Q. Zhang, R. G. Cao, J. Cho, H.-L. Wang, G. Wu, *Adv. Mater.* **2014**, *26*, 1378.

[408] X. Xin, K. Ito, L. Kubo, *Carbon* **2016**, *99*, 67.

[409] J. Xiao, D. Mei, X. Li, W. Xu, D. Wang, G. L. Graff, W. D. Bennett, Z. Nie, L. V. Saraf, I. A. Aksay, J. Liu, J. G. Zhang, *Nano Lett.* **2011**, *11*, 5071.

[410] Z. Y. Guo, D. D. Zhou, X. L. Dong, Z. J. Qiu, Y. G. Wang, Y. Y. Xia, *Adv. Mater.* **2013**, *25*, 5668.

[411] Y. Chen, F. Li, D.-M. Tang, Z. Jian, C. Liu, D. Golberg, A. Yamada, H. Zhou, *J. Mater. Chem. A* **2013**, *1*, 13076.

[412] Z.-L. Wang, D. Xu, J.-J. Xu, L.-L. Zhang, X.-B. Zhang, *Adv. Funct. Mater* **2012**, *22*, 3699.

[413] H. D. Lim, K. Y. Park, H. Song, E. Y. Jang, H. Gwon, J. Kim, Y. H. Kim, M. D. Lima, R. Ovalle Robles, X. Lepro, R. H. Baughman, K. Kang, *Adv. Mater.* **2013**, *25*, 1348.

[414] C. J. Liu, R. Younesi, C.-W. Tai, M. Valvo, K. Edstrom, T. Gustafsson, J. F. Zhu, *J. Mater. Chem. A.* **2016**, *4*, 9767.

[415] K. Gong, F. Du, Z. Xia, M. Durstock, L. Dai, *Science* **2009**, *323*, 760.

[416] S. Zhu, Z. Chen, B. Li, D. Higgins, H. Wang, H. Li, Z. Chen, *Electrochim. Acta* **2011**, *56*, 5080.

[417] G. Jian, Y. Zhao, Q. Wu, L. Yang, X. Wang, Z. Hu, *J. Phys. Chem. C* **2013**, *117*, 7811.

[418] D. U. Lee, H. W. Park, D. Higgins, L. Nazar, Z. Chen, *J. Electrochem. Soc.* **2013**, *160*, F910.

[419] M. He, P. Zhang, L. Liu, B. Liu, S. Xu, *Electrochimica Acta* **2016**, *191*, 90.

[420] H. R. Jiang, T. S. Zhao, L. Shi, P. Tan, L. An, *J. Phys. Chem. C* **2016**, *120*, 6612.

[421] D.-S. Yang, D. Bhattacharjya, S. Inamdar, J. Park, J.-S. Yu, *J. Am. Chem. Soc.* **2012**, *134*, 16127.

[422] C. Zhang, N. Mahmood, H. Yin, F. Liu, Y. Hou, *Adv. Mater.* **2013**, *25*, 4932.

[423] Z. Yang, Z. Yao, G. F. Li, G. Y. Fang, H. G. Nie, Z. Liu, X. M. Zhou, X. Chen, S. M. Huang, *ACS Nano* **2012**, *6*, 205.

[424] J. Liang, Y. Jiao, M. Jaroniec, S. Z. Qiao, *Angew. Chem. Int. Ed.* **2012**, *51*, 11496.

[425] Y. Zhao, L. Yang, S. Chen, X. Wang, Y. Ma, Q. Wu, Y. Jiang, W. Qian, Z. J. Hu, *J. Am. Chem. Soc.* **2013**, *135*, 1201.

[426] Y. Zheng, Y. Jiao, L. Ge, M. Jaroniec, S. Z. Qiao, *Angew. Chem. Int. Ed.* **2013**, *52*, 3110.

[427] F. Wu, Y. Xing, L. Li, J. Qian, W. J. Qu, J. G. Wen, D. Miller, Y. S. Ye, R. J. Chen, K. Amine, J. Lu, *ACS Appl. Mater. Interfaces* **2016**, *8*, 23635.

[428] S. Wang, L. Zhang, Z. Xia, A. Roy, D. W. Chang, J.-B. Baek, L. Dai, *Angew. Chem. Int. Ed.* **2012**, *51*, 4209.

[429] S. Zhao, J. Liu, C. Li, W. Ji, M. Yang, H. Huang, Y. Liu, Z. Kang, *ACS Appl. Mater. Interfaces* **2014**, *6*, 22297.

[430] X. Ma, G. Ning, C. Qi, C. Xu, J. Gao, *ACS Appl. Mater. Interfaces* **2014**, *6*, 14415.

[431] M. Favaro, L. Ferrighi, G. Fazio, L. Colazzo, C. Di Valentin, C. Durante, F. Sedona, A. Gennaro, S. Agnoli, G. Granozzi, *ACS Cata.* **2015**, *5*, 129.

[432] C. Z. Shu, Y. M. Lin, D. S. Su, *J. Mater. Chem. A* **2016**, *4*, 2128.

[433] J. L. Shui, F. Du, C. M. Xue, Q. Li, L. M. Dai, *ACS Nano* **2014**, *8*, 3015.

[434] W. Zhou, H. Z. Zhang, H. J. Nie, Y. W. Ma, Y. N. Zhang, H. M. Zhang, *ACS Appl. Mater. Interfaces* **2015**, *7*, 3389.

[435] J. T. Zhang, L. Dai, *ACS Catal.* **2015**, *5*, 7244.

[436] J. L. Shui, Y. Lin, J. W. Connell, J. T. Xu, X. L. Fan, L. M. Dai, *ACS Energy Lett.* **2016**, *1*, 260.

[437] F. Wu, Y. Xing, L. Li, J. Qian, W. J. Qu, J. G. Wen, D. Miller, Y. S. Ye, R. Chen, K. Amine, J. Lu, *ACS Appl. Mater. Interfaces* **2016**, *8*, 23635.

[438] J.-H. Kim, A. G. Kannan, H.-S. Woo, D.-G. Jin, W. K. Kim, K. H. Ryu, D.-W. Kim, *J. Mater. Chem. A* **2015**, *3*, 18456.

[439] W. Meng, S. W. Liu, S. Wen, X. Qin, *RSC Adv.* **2015**, *5*, 52206.

[440] F. Wu, Y. Xing, X. Q. Zeng, Y. F. Yuan, X. Y. Zhang, R. S.-Yassar, J. G. Wen, D. J. Miller, L. Li, R. J. Chen, J. Lu, K. Amine, *Adv. Funct. Mater.* **2016**, *26*, 7626.

[441] H.-D. Lim, H. Song, H. Gwon, K.-Y. Park, J. Kim, Y. Bae, H. Kim, S.-K. Jung, T. Kim, Y. H. Kim, X. Lepró, R. Ovalle-Robles, R. H. Baughman, K. Kang, *Energy Environ. Sci.* **2013**, *6*, 3570.

[442] J. Wang, L. L. Liu, S. L. Chou, H. K. Liu, J. Z. Wang, *J. Mater. Chem. A* , *5*, 1462.

[443] X. Guo, B. Sun, J. Q. Zhang, H. Liu, G. X. Wang, *J. Mater. Chem. A* **2016**, *4*, 9774.

[444] F. F. Tu, J. P. Hu, J. Xie, G. S. Cao, S. C. Zhang, S. Y. A. Yang, X. B. Zhao, H. Y. Yang, *Adv. Funct. Mater.* **2016**, *26*, 7725.

[445] W. Zhou, Y. Cheng, X. F. Yang, B. S. Wu, H. J. Nie, H. Z. Zhang, H. M. Zhang, *J. Mater. Chem. A* **2015**, *3*, 14556.

[446] J. Lu, Y. Lei, K. C. Lau, X. Y. Luo, P. Du, J. G. Wen, R. S. Assary, U. Das, D. J. Miller, J. W. Elam, H. M. Albishri, D. A. E.-Hady, Y.-K. Sun, L. A. Curtiss, K. Amine, *Nat. Commun.* **2013**, *4*, 2383.

[447] G. Q. Wang, F. F. Tu, J. Xie, G. H. Du, S. C. Zhang, G. S. Cao, X. B. Zhao, *Adv. Sci.* **2016**, *3*, 1500339.

[448] J. Li, Y. Zhao, M. Zou, C. Wu, Z. G. Huang, L. Guan, *ACS Appl. Mater. Interfaces* **2014**, *6*, 12479.

[449] Z. Y. Guo, D. D. Zhou, H. J. Liu, X. L. Dong, S. Y. Yuan, A. S. Yu, Y. G. Wang, Y. Y. Y. Xia, *J. Power Sources* **2015**, *276*, 18.

[450] C. Y. Jung, T. S. Zhao, L. Zeng, P. Tan, *J. Power Sources* **2016**, *331*, 82.

[451] G. J. Sohn, H. J. Choi, I. Y. Jeon, D. W. Chang, L. Dai, J. B. Baek, *ACS Nano* **2012**, *6*, 6345.

[452] S. Rosenberg, A. Hintennach, *J. Power Sources* **2015**, *274*, 1043.

[453] J.-L. Ma, F.-L. Meng, D. Xu, X.-B. Zhang, *Energy Storage Materials* **2017**, *6*, 1.

[454] Z. Khan, S. Park, S. M. Hwang, J. Yang, Y. Lee, H.-K. Song, Y. Kim, H. Ko, *NPG Asia Materials* **2016**, *8*, e294.

[455] M. Shang, Y. Liu, J. Xia, S. M. Zhang, J. H. Yang, *Ceramics International* **2017**, *43*, 3218.

[456] E. Peled, D. Golognitsky, H. Mazor, M. Goor, S. Avshalomov, *J. Power Sources* **2011**, *196*, 6835.

[457] N. Li, D. Xu, D. Bao, J. Ma, X. Zhang, *Chinese J. Catalysis* **2016**, *37*, 1172.

[458] W.-W. Yin, Z.-W. Fu, *Chem. Commun.* **2017**, *53*, 1522.

[459] M. Shang, Y. Liu, S. Zhang, J. H. Yang, *Ceramics International.* **2017**, *43*, 3218.

[460] Y. X. Hu, X. P. Han, Q. Zhao, J. Du, F. Cheng, J. Chen, *J. Mater. Chem. A* **2015**, *3*, 3320.

[461] S. Zhang, Z. Wen, K. Rui, C. Shen, Y. Lu, J. Yang, *J. Mater. Chem. A* **2015**, *3*, 2568.

[462] Y. G. Li, M. Gong, Y. Y. Liang, J. Feng, J.-E. Kim, H. L. Wang, G. S. Hong, B. Zhang, H. J. Dai, *Nat. Commun* **2013**, *4*, 1805.

[463] Y. G. Li, H. J. Dai, *Chem. Soc. Rev.* **2014**, *43*, 5257.

[464] J. T. Zhang, Z. H. Zhao, Z. H. Xia, L. M. Dai, *Nature Nanotechnol.* **2015**, *10*, 444.

[465] B. Li, X. M. Ge, F. W. T. Goh, T. S. Andy Hor, D. S. Geng, G. J. Du, Z. L. Liu, J. Zhang, X. G. Liu, Y. Zong, *Nanoscale* **2015**, *7*, 1830.

[466] J. H. Song, C. Z. Zhu, S. F. Fu, Y. Song, D. Du, Y. H. Lin, *J. Mater. Chem. A* **2016**, *4*, 4864.

[467] M. F. Wang, T. Qian, J. Q. Zhou, C. L. Yan, *ACS Appl. Mater. Interfaces* **2017**, *9*, 5213.

[468] J. k. Zhang, P. F. Li, Z. H. Wang, J. S. Qiao, D. Rooney, W. Sun, K. N. Sun, *J. Mater. Chem. A* **2015**, *3*, 1504.

**ADVANCED
SCIENCE NEWS**

www.advancedsciencenews.com

**ADVANCED
SUSTAINABLE
SYSTEMS**

www.advsustainsys.com

[469] S. F. Wang, Y. J. Sha, Y. L. Zhu, X. M. Xu, Z. P. Shao, *J. Mater. Chem. A* **2015**, *3*, 16132.

[470] J. Zhang, Z. Y. Lyu, F. Zhang, L. J. Wang, P. Xiao, K. D. Yuan, M. Lai, W. Chen, *J. Mater. Chem. A* **2016**, *4*, 6350.

[471] P. Zhang, R. T. Wang, M. He, J. W. Lang, S. Xu, X. B. Yan, *Adv. Funct. Mater.* **2016**, *26*, 1354.

[472] D. Oh, J. F. Qi, B. H. Han, G. Zhang, T. J. Carney, J. Ohmura, Y. Zhang, Y. Shao-Horn, A. M. Belcher, *Nano Lett.* **2014**, *14*, 4837.

[473] X. W. Guo, P. Liu, J. H. Han, Y. Ito, A. Hirata, T. Fujita, M. Chen, *Adv. Mater.* **2015**, *27*, 6137.

[474] J. G. Kim, Y. M. Kim, Y. Noh, W. B. Kim, *Green Chem Environ.* **2015**, *8*, 1752.

[475] S. Liu, Y. Zhu, J. Xie, Y. Huo, H. Y. Yang, T. Zhu, G. Cao, X. Zhao, S. Zhang, *Adv. Energy Mater.* **2014**, *4*, 9.

[476] P. Tan, W. Shyy, T. S. Zhao, X. B. Zhu, Z. H. Wei, *J. Mater. Chem. A* **2015**, *3*, 19042.

[477] Y.-F. Xu, Y. Chen, G.-L. Xu, X.-R. Zhang, Z. H. Chen, J.-T. Li, L. Huang, K. Amine, S.-G. Sun, *Nano Energy* **2016**, *28*, 63.

[478] Z. Zhang, L. Su, M. Yang, M. Hu, J. Bao, J. Wei, Z. Zhou, *Chem. Commun.* **2014**, *50*, 776.

[479] B. Liu, P. F. Yan, W. Xu, J. M. Zheng, Y. He, L. Luo, M. E. Bowden, C.-M. Wang, J.-G. Zhang, *Nano Lett.* **2016**, *16*, 4932.

[480] M. Salehi, Z. Shariatinia, *Electrochim. Acta* **2016**, *188*, 428.

[481] Y. Cao, M.-S. Zheng, S. Cai, X. D. Lin, C. Yang, W. Q. Hu, Q.-F. Dong, *J. Mater. Chem. A* **2014**, *2*, 18736.

[482] K. Guo, Y. Li, T. Yuan, X. W. Dong, X. W. Li, H. Yang, *J. Solid. State. Electrochemistry* **2015**, *19*, 821.

[483] X. Y. Lu, L. Zhang, X. L. Sun, W. P. Si, C. L. Yan, O. G. Schmidt, *J. Mater. Chem. A* **2016**, *4*, 4155.

[484] M. Wu, J. Y. Jo, S. H. Choi, Y. K. Kang, H.-K. Jung, *RSC Adv.* **2015**, *5*, 24175.

[485] R. Black, J. H. Lee, B. Adams, C. A. Mims, L. F. Nazar, *Angew. Chem. Int. Ed.* **2013**, *52*, 392.

[486] Z. X. Liu, L. R. D. Jesus, S. B. Banerjee, P. P. Mukherjee, *ACS Appl. Mater. Interfaces* **2016**, *8*, 23028.

[487] R. Jasinski, *Nature* **1964**, *201*, 1212.

[488] D. S. Su, G. Sun, *Angew. Chem. Int. Ed.* **2011**, *50*, 11570.

[489] W. Li, A. Yu, D. C. Higgins, B. G. Llanos, Z. Chen, *J. Am. Chem. Soc.* **2010**, *132*, 17056.

[490] X. Yuan, X. Zeng, H. J. Zhang, Z. F. Ma, C. Y. Wang, *J. Am. Chem. Soc.* **2010**, *132*, 1754.

[491] L. Ding, X. Dai, R. Lin, H. Wang, J. Qiao, *J. Electrochem. Soc.* **2012**, *159*, F577.

[492] Z. Shi, J. Zhang, *J. Phys. Chem. C* **2007**, *111*, 7084.

[493] R. Chen, H. Li, D. Chu, G. Wang, *J. Phys. Chem. C* **2009**, *113*, 20689.

[494] D. Sun, Y. Shen, W. Zhang, L. Yu, Z. Yi, W. Yin, D. Wang, Y. Huang, J. Wang, D. Wang, J. B. Goodenough, *J. Am. Chem. Soc.* **2014**, *136*, 8941.

[495] D. Wu, Z. Guo, X. Yin, Q. Pang, B. Tu, L. Zhang, Y. G. Wang, Q. Li, *Adv. Mater.* **2014**, *26*, 3258.

[496] C. Selvaraj, N. Munichandraiah, L. G. Scanlon, *J. Porphyrins Phthalocyanines* **2012**, *16*, 255.

[497] K. M. Kadish, L. Fremond, Z. Ou, J. Shao, C. Shi, F. C. Anson, F. Burdet, C. P. Gros, J. M. Barbe, R. Guilard, *J. Am. Chem. Soc.* **2005**, *127*, 5625.

[498] C. Song, L. Zhang, J. Zhang, D. P. Wilkinson, R. Baker, *Fuel Cells* **2007**, *7*, 9.

[499] D. Das, Y. M. Lee, K. Ohkubo, W. Nam, K. D. Karlin, S. Fukuzumi, *J. Am. Chem. Soc.* **2013**, *135*, 4018.

[500] S. Kakuda, R. L. Peterson, K. Ohkubo, K. D. Karlin, S. Fukuzumi, *J. Am. Chem. Soc.* **2013**, *135*, 6513.

[501] C. Shi, F. C. Anson, *Inorg. Chem.* **1990**, *29*, 4298.

[502] B. Steiger, F. C. Anson, *Inorg. Chem.* **1997**, *36*, 4238.

[503] C. Shi, B. Steiger, M. Yuasa, F. C. Anson, *Inorg. Chem.* **1997**, *36*, 4294.

[504] E. Song, C. Shi, F. C. Anson, *Langmuir* **1998**, *14*, 4315.

[505] G. I. Cárdenas-Jirón, *J. Phys. Chem. A* **2002**, *106*, 3202.

[506] M. P. Somashekarappa, J. Keshavayya, B. S. Sherigara, *Spectrochim. Acta, Part A* **2003**, *59*, 883.

[507] J. Chen, W. Zhang, D. Officer, G. F. Swiegers, G. G. Wallace, *Chem. Commun.* **2007**, *32*, 3353.

[508] J. Li, R. L. Lord, B. C. Noll, M. H. Baik, C. E. Schulz, W. R. Scheidt, *Angew. Chem., Int. Ed.* **2008**, *47*, 10144.

[509] R. Baker, D. P. Wilkinson, J. Zhang, *Electrochim. Acta* **2008**, *53*, 6906.

[510] C. Zhang, R. Hao, H. Yin, F. Liu, Y. Hou, *Nanoscale* **2012**, *4*, 7326.

[511] G. Dong, M. Huang, L. Guan, *Phys. Chem. Chem. Phys.* **2012**, *14*, 2557.

[512] I. Kruusenberg, L. Matisen, Q. Shah, A. M. Kannan, K. Tammeveski, *Int. J. Hydrogen Energy* **2012**, *37*, 4406.

[513] H. Tang, H. Yin, J. Wang, N. Yang, D. Wang, Z. Tang, *Angew. Chem. Int. Ed.* **2013**, *52*, 5585.

[514] J. L. Shui, N. K. Karan, M. Balasubramanian, S. Y. Li, D. J. Liu, *J. Am. Chem. Soc.* **2012**, *134*, 16654.

[515] J. Wu, H. W. Park, A. Yu, D. Higgins, Z. Chen, *J. Phys. Chem. C* **2012**, *116*, 9427.

[516] A. Li Zhu, H. Wang, W. Qu, X. Li, Z. Jong, H. Li, *J. Power Sources* **2010**, *195*, 5587.

[517] Z. Chen, J. Y. Choi, H. Wang, H. Li, Z. Chen, *J. Power Sources* **2011**, *196*, 3673.

[518] Y. Zhao, K. Watanabe, K. Hashimoto, *J. Mater. Chem.* **2012**, *22*, 12263.

[519] U. Rammelt, P. T. Nguyen, W. Plieth, *Electrochim. Acta* **2003**, *48*, 1257.

[520] Z. W. Chen, D. Higgins, A. P. Yu, L. Zhang, J. J. Zhang, *Energy Environ. Sci.* **2011**, *4*, 3167.

[521] V. G. Khomenko, V. Z. Barsukov, A. S. Katashinskii, *Electrochim. Acta* **2005**, *50*, 1675.

[522] D. M. de Leeuw, P. A. Kraakman, P. F. G. Bongaerts, C. M. J. Mutsaers, D. B. M. Klaassen, *Synth. Met.* **1994**, *66*, 263.

[523] V. G. Khomenko, V. Z. Barsukov, A. S. Katashinskii, *Electrochim. Acta* **2005**, *50*, 1675.

[524] B. Winther-Jensen, K. West, *Macromolecules* **2004**, *37*, 4538.

[525] B. Winther-Jensen, M. Forsyth, K. West, J. W. Andreasen, G. Wallace, D. R. MacFarlane, *Org. Electron.* **2007**, *8*, 796.

[526] S. R. Sivakkumar, W. J. Kim, J.-A. Choi, D. R. MacFarlane, M. Forsyth, D.-W. Kim,. *J. Power Sources* **2007**, *171*, 1062.

[527] P. M. Bayley, B. Winther-Jensen, D. R. MacFarlane, N. M. Rocher, M. Forsyth, *React. Funct. Polym.* **2008**, *68*, 1119.

[528] P. Subramanian, N. B. Clark, L. Spiccia, D. R. MacFarlane, B. Winther-Jensen, C. Forsyth, *Synth. Met.* **2008**, *158*, 704.

[529] B. Winther-Jensen, O. Winther-Jensen, M. Forsyth, D. R. Macfarlane, *Science* **2008**, *321*, 671.

[530] S. Wang, D. Yu, L. Dai, *J. Am. Chem. Soc.* **2011**, *133*, 5182.

[531] F. Jaouen, E. Proietti, M. Lefevre, R. Chenitz, J.-P. Dodelet, G. Wu, H. T. Chung, C. M. Johnston, P. Zelenay, *Energy Environ. Sci.* **2011**, *4*, 114.

[532] C. V. Rao, C. R. Cabrera, Y. Ishikawa, *J. Phys. Chem. Lett.* **2010**, *1*, 2622.

[533] M. Salehi, Z. Shariatinia, *Electrochimica Acta* **2016**, *188*, 428.

[534] Q. Lu, Q. Zhao, H. Zhang, J. Li, X. Wang, F. Wang, *ACS Macro Lett.* **2013**, *2*, 92.

[535] Y. Cui, Z. Wen, X. Liang, Y. Lu, J. Jin, M. Wu, X. Wu, *Energy Environ. Sci.* **2012**, *5*, 7893.

[536] T. Hirayama, T. Manako, H. e-J. Imai, *Surf. Sci. Nanotechnol.* **2008**, *6*, 237.

[537] A. C. Marschilok, S. Zhu, C. C. Milleville, S. H. Lee, E. S. Takeuchi, K. J. Takeuchi, *J. Electrochem. Soc.* **2011**, *158*, A223.

[538] W. M. Zhang, J. Chen, P. Wagner, G. F. Swiegers, G. G. Wallace, *Electrochem. Commun.* **2008**, *10*, 519.

[539] Q. Zhou, C. M. Li, J. Li, J. T. Lu, *J. Phys. Chem. C* **2008**, *112*, 18578.

[540] S. Wang, D. Yu, L. Dai, D. W. Chang, J.-B. Baek, *ACS Nano* **2011**, *5*, 6202.

[541] R. Sulub, W. Martinez-Millan, M. A. Smit, *Int. J. Electrochem. Sci.* **2009**, *4*, 1015.

[542] A. L. Mohana Reddy, N. Rajalakshmi, S. Ramaprabhu, *Carbon* **2008**, *46*, 2.

[543] W. M. Millán, M. Smit, A. J. Appl. *Polym. Sci.* **2009**, *112*, 2959.

[544] W. Martinezmillan, T. Toledanothompson, L. Arriaga, M. Smit, *Int. J. Hydrogen Energy* **2009**, *34*, 694.

[545] H. Nguyen Cong, K. El Abbassi, J. L. Gautier, P. Chartier, *Electrochim. Acta* **2005**, *50*, 1369.

[546] Y. Shao, H. Nguyencong, *Solid State Ionics* **2007**, *178*, 1385.

[547] H. Nguyen-Cong, V. de la Garza Guadarrama, J. L. Gautier, P. Chartier, *Electrochim. Acta* **2003**, *48*, 2389.

[548] R. N. Singh, B. Lal, M. Malviya, *Electrochim. Acta* **2004**, *49*, 4605.

[549] K. Lee, L. Zhang, H. Lui, R. Hui, Z. Shi, J. Zhang, *Electrochim. Acta* **2009**, *54*, 4704.

[550] M. Yuasa, A. Yamaguchi, H. Itsuki, K. Tanaka, M. Yamamoto, K. Oyaizu, *Chem. Mater.* **2005**, *17*, 4278.

[551] P. Arora, Z. Zhang, *Chem. Rev.* **2004**, *104*, 4419.

[552] M. A. Rahman, X. Wang, C. Wen, *J. Electrochem. Soc.* **2013**, *160*, A1759.

[553] E. L. Dewi, K. Oyaizu, H. Nishide, E. Tsuchida, *J. Power Sources* **2003**, *115*, 149.

[554] G. M. Wu, S. J. Lin, J. H. You, C. C. Yang, *Mater. Chem. Phys.* **2008**, *112*, 798.

[555] H. Saputra, R. Othman, A. G. E. Sutjipto, R. Muhida, *J. Membr. Sci.* **2011**, *367*, 152.

[556] P. Sapkota, H. Kim, *J. Ind. Eng. Chem.* **2010**, *16*, 39.

[557] L. Puech, C. Cantau, P. Vinatier, G. Toussaint, P. Stevens, *J. Power Sources* **2012**, *214*, 330.

[558] I. C. Jang, Y. Hidaka, T. Ishihara, *J. Power Sources* **2013**, *244*, 606.

[559] J. Tan, E. M. Ryan, *ECS Transactions* **2013**, *3*, 35.

[560] N. Imanishi, S. Hasegawa, T. Zhang, A. Hirano, Y. Takeda, O. Yamamoto, *J. Power Sources* **2008**, *135*, 1392.

[561] L. Puech, C. Cantau, P. Vinatier, G. Toussaint, P. Stevens, *J. Power Sources* **2012**, *214*, 330.

[562] G. Yu. Aleshin, D. A. Semenenko, A. I. Belova, T. K. Zakharchenko, D. M. Itkis, E. A. Goodilin, Y. D. Tretyakov, *Solid State Ionics* **2011**, *184*, 62.

[563] S. J. Visco, V. Y. Nimon, A. Petrov, K. Pridatko, N. Goncharenko, E. Nimon, L. De Jonghe, Y. M. Volfkovich, D. A. Bograchev, *J. Solid State Electrochem.* **2014**, *18*, 1443.

[564] J. L. Shui, J. S. Okasinski, P. Kenesei, H. A. Dobbs, D. Zhao, J. D. Almer, D. J. Liu, *Nat. Commun.* **2013**, *4*, 2255.

[565] W. Walker, V. Giordani, J. Uddin, V. S. Bryantsev, G. V. Chase, D. Addison, *J. Am. Chem. Soc.* **2013**, *135*, 2076.

[566] S. J. Kang, T. Mori, J. Suk, D. W. Kim, Y. Kang, W. Wilcke, H. C. Kim, *J. Mater. Chem. A* **2014**, *2*, 9970.

[567] F. Ding, W. Xu, G. L. Graff, J. Zhang, M. L. Sushko, X. Chen, Y. Shao, M. H. Engelhard, Z. Nie, J. Xiao, X. Liu, P. V. Sushko, J. Liu, J. G. Zhang, *J. Am. Chem. Soc.* **2013**, *135*, 4450.

[568] J. Hassoun, H. G. Jung, D. J. Lee, J. B. Park, K. Amine, Y. K. Sun, B. Scrosati, *Nano. Lett.* **2012**, *12*, 5775.

[569] Y. Li, H. Dai, *Chem. Soc. Rev.* **2014**, *43*, 5257.

[570] I. V. A. N. A. Smoljko, S. Gudić, N. Kuzmanić, M. Kliškić, *J. Appl. Electrochem.* **2012**, *42*, 969.

[571] Q.-C. Liu, J.-J. Xu, S. Yuan, Z.-W. Chang, D. Xu, Y.-B. Yin, L. Li, H.-X. Zhong, Y.-S. Jiang, J.-M. Yan, X.-B. Zhang, *Adv. Mater.* **2015**, *27*, 5241.

[572] Y. Lv, M. Liu, Y. Xu, D. Cao, J. Feng, *J. Power Sources* **2013**, *225*, 124.

[573] S. M. Lee, Y. J. Kim, S. W. Eom, N. S. Choi, K. W. Kim, S. B. Cho, *J. Power Sources* **2013**, *227*, 117.

[574] C. C. Yang, S. J. Lin, *J. Power Sources* **2012**, *112*, 174.

[575] N. Shaigan, W. Qu, T. Takeda, *ECS Trans.* **2010**, *28*, 35.

[576] X. G. Zhang, *J. Power Sources* **2006**, *163*, 591.

[577] K. L. Wang, P. C. Pei, Z. Ma, H. C. Chen, H. C. Xu, D. F. Chen, X. Z. Wang, *J. Mater. Chem. A* **2015**, *3*, 22648.

[578] S. G. Higashi, S. W. Lee, J. S. Lee, K. Takechi, Y. Cui, *Nat. Commun* **2016**, *7*, 11801.

[579] Y. L. Zhang, X. M. Zhang, J. W. Wang, W. C. Mckee, Y. Xu, Z. Q. Peng, *J. Phys. Chem. C* **2016**, *120*, 3690.

[580] H. R. Jiang, T. S. Zhao, L. S. P. Tan, L. An, *J. Phys. Chem. C* **2016**, *120*, 6612.

[581] D. Y. Zhai, K. C. Lau, H.-H. Wang, J. G. Wen, D. J. Miller, J. Lu, F. Y. Kang, B. H. Li, W. G. Yang, J. Gao, E. Indacochea, L. A. Curtiss, *Nano Lett.* **2015**, *15*, 1041.

[582] C. Z. Yang, R. A. Wong, M. Hong, K. Yamanaka, T. Ohta, *Nano Lett.* **2016**, *16*, 2969.

[583] Y. C. Lu, H. A. Gasteiger, E. Crumlin, R. McGuire, Y. Shao-Horn, *J. Electrochem. Soc.* **2010**, *157*, A1016.

[584] B. D. McCloskey, D. S. Bethune, R. M. Shelby, G. Girishkumar, A. C. Luntz, *J. Phys. Chem. Lett.* **2011**, *2*, 1161.

[585] B. D. McCloskey, R. Scheffler, A. Speidel, D. S. Bethune, R. M. Shelby, A. C. Luntz, *J. Am. Chem. Soc.* **2011**, *133*, 18038.

[586] S. S. Zhang, D. Foster, J. Read, *J. Power Sources* **2010**, *195*, 1235.

[587] C. O. Laoire, S. Mukerjee, E. J. Plichta, M. A. Hendrickson, K. M. Abraham, *J. Electrochem. Soc.* **2011**, *158*, A302.

[588] H. Lim, E. Yilmaz, H. R. Byon, *J. Phys. Chem. Lett.* **2012**, *3*, 3210.

[589] L. Luo, B. Liu, S. Song, W. Xu, J.-G. Zhang, C. Wang, *Nat. Nanotechnol.* **2017**, *12*, 535.

[590] L. Li, Z. Wu, S. Yuan, X.-B. Zhang, *Energy Environ. Sci.* **2014**, *7*, 2101.